

# Asteroseismology of the fast-rotating high-amplitude $\delta$ Scuti star V2367 Cygni

J. Daszyńska-Daszkiewicz<sup>\*</sup>, W. Szewczuk, P. Walczak

*Instytut Astronomiczny, Uniwersytet Wrocławski, Kopernika 11, 51-622 Wrocław, Poland*

Accepted XXX. Received YYY; in original form ZZZ

## ABSTRACT

We present the comprehensive analysis of the high-amplitude  $\delta$  Sct star V2367 Cygni. Firstly, we perform the frequency analysis for the whole available set of the *Kepler* and *TESS* photometry. Most of the frequency peaks are harmonics or combinations of the three known independent frequencies with the highest amplitudes, i.e.,  $\nu_1 = 5.66106 \text{ d}^{-1}$ ,  $\nu_2 = 7.14898 \text{ d}^{-1}$  and  $\nu_3 = 7.77557 \text{ d}^{-1}$ . The total number of independent frequencies is 26 and 25 from the *Kepler* and *TESS* light curve, respectively. Then, using the *UBVRI* time-series photometry, we unambiguously identify the dominant frequency  $\nu_1$  as the radial mode, whereas in the case of frequencies  $\nu_2$  and  $\nu_3$  the most probable mode degrees are  $\ell = 0$  or  $\ell = 2$ . However, only the frequency  $\nu_2$  can be associated with a radial mode, and only if higher order effects of rotation are taken into account. Including the rotational mode coupling, we constructed complex seismic models of V2367 Cyg, which fit  $\nu_1$  and  $\nu_2$  as radial modes, and reproduce the amplitude of bolometric flux variations (the parameter  $f$ ) for the dominant mode. The empirical values of  $f$  are derived from the *UBVRI* amplitudes and phases. We rely on the Bayesian analysis based on Monte Carlo simulations to derive constraints on evolutionary stage, mass, rotation, overshooting from the convective core and efficiency of convective transport in the envelope. Our seismic analysis clearly indicates that V2367 Cyg is in a post-MS phase of evolution. This is the first extensive seismic modelling that takes into account the effect of rotational coupling between pulsation modes.

**Key words:** stars: evolution – stars: oscillation – stars:rotation – Physical Data and Processes: opacity, convection – stars: individual: V2367 Cygni

## 1 INTRODUCTION

Asteroseismology has already become a mature and well-developed branch of modern astrophysics, widely used to obtain constraints on the internal structure of various types of stars. The most recent excellent reviews by Aerts (2021) and Kurtz (2022) summarize roughly the results obtained to date. Obviously, there are still many uncertainties in stellar modelling and the uniqueness of a seismic model depends on the number of observables we have at our disposal. The greatest uncertainties concern processes described by free parameters, i.e., primarily the efficiency of convection in the outer layers and all mixing processes like diffusion, convective zone boundary mixing or rotationally induced mixing. Another difficulty arises from the effects of rotation, both on the equilibrium model as well as on stellar pulsations. Moreover, in the case of some pulsating stars including  $\delta$  Scuti variables, the main obstacle to the use of asteroseismic methods is the mode identification. This is because, with some exceptions (Bedding et al. 2020), we do not observe regular patterns in the oscillation spectra of  $\delta$  Sct pulsators

and more sophisticated methods of the mode identification must be applied. The most commonly used and effective methods are based on photometric amplitudes and phases, which were proposed a long time ago (e.g., Balona & Stobie 1979; Watson 1988). An additional complication is taking into account the effects of rotation when identifying modes, in particular, the rotational coupling for close-frequency modes (e.g., Daszyńska-Daszkiewicz et al. 2002).

A big advantage for seismic modelling is the presence of radial modes, especially two or more. This is because their oscillation spectrum is sparse and the period ratio of radial modes takes specific values from a very narrow range. There is a subgroup of  $\delta$  Sct stars, called high-amplitude  $\delta$  Scuti (HADS) stars, which often exhibit two radial modes. HADS stars change their brightness in the range larger than about 0.3 mag in the Johnson *V* filter and most of them are already in the post-main sequence phase of evolution. Asteroseismology of double-mode radial  $\delta$  Sct stars provides strong constraints on the parameters of the model and theory (Daszyńska-Daszkiewicz et al. 2020, 2022). Besides, their seismic models are extremely sensitive to adopted opacity data (Daszyńska-Daszkiewicz et al. 2023).

As pointed out by Breger (2000), HADS stars are rather slow

<sup>\*</sup> E-mail: daszynska@astro.uni.wroc.pl

rotators with  $V_{\text{rot}} \sin i \lesssim 40 \text{ km s}^{-1}$ . This paper concerns the HADS star V2367 Cygni which is suspected of having a surprisingly high rotation (Balona et al. 2012). The effect of rotation on the period ratio of radial modes was studied by Suarez et al. (2006). Then, Suarez et al. (2007) included the effect of near-degeneracy. In both papers, the authors limited their computation to the rotation up to  $50 \text{ km s}^{-1}$ . Here, we consider the rotational velocity up to the half of critical velocity.

The paper is organized as follows. Sect. 2 gathers the information on V2367 Cygni. In Sect. 3, we present the frequency analysis of the whole light curves from the two space missions: *Kepler* and *TESS*. Sect. 4 is devoted to the mode identification for the three main frequencies using the multi-colour photometry. In Sect. 5, we study the effects of rotation on radial modes, including the effect of mode coupling. Extensive asteroseismic modelling of V2367 Cyg with Monte Carlo-based Bayesian analysis, taking into account the rotational mode coupling, is presented in Sect. 6. A summary is given in the last section.

## 2 V2367 CYGNI

V2367 Cygni is a high-amplitude  $\delta$  Scuti star with the average visual brightness of  $V = 11.48$  mag. It was identified for the first time as a  $\delta$  Scuti variable from the ROTSE-I All-Sky Surveys (Akerlof & et al. 2000). Subsequently, Jin et al. (2003) classified V2367 Cyg as HADS based on the two-passband *VI* photometry. One periodicity  $P = 0.176617$  d was detected. This classification was confirmed by Pigulski et al. (2009) who analysed the ASAS data.

The Gaia DR3 parallax of V2367 Cyg amounts to  $\pi = 0.7859 \pm 0.0147$  mas, which corresponds to the distance  $d = 1272.43 \pm 23.80$  pc (Gaia Collaboration, 2020). According to Frasca et al. (2016), the spectral type of this HADS is F0III and their classification was based on the low-resolution spectra from LAMOST (The Large Sky Area Multi-Object Fibre Spectroscopic Telescope). Using the medium-resolution spectra from NOT (the Nordic Optical Telescope), Niemczura et al. (2017) assigned a spectral type F0IVs+, where *s* indicates narrow (sharp) absorption lines. These authors mentioned also that V2367 Cyg is a member of binary system but they did not provide any justification for this statement. Besides, the Gaia DR3 RUWE parameter equal to 0.948 does not reveal that V2367 Cyg is part of a binary system.

The star was also observed in the framework of the *Kepler* and *TESS* missions. Uytterhoeven et al. (2011) analysed the first two quarters of Kepler data, i.e., Q0 (short cadence, SC) and Q1 (long cadence, LC). They detected the main frequency  $\nu_1 = 5.661 \text{ d}^{-1}$  and suggested many more frequency peaks in the range  $(4.3, 80.0) \text{ d}^{-1}$ . Moreover, using the Strömgren photometry, Uytterhoeven et al. (2011) derived the effective temperature  $T_{\text{eff}} = 6810 \pm 130$  K and the surface gravity  $\log g = 3.80 \pm 0.19$  dex.

Subsequently, Balona et al. (2012) used a longer set of *Kepler* data, i.e., Q0, Q6, Q7 (SC) and Q1, Q2, Q5 (LC), and extracted three main frequencies  $\nu_1 = 5.6611 \text{ d}^{-1}$ ,  $\nu_2 = 7.1490 \text{ d}^{-1}$  and  $\nu_3 = 7.7756 \text{ d}^{-1}$ . They also detected a dozen other frequencies, but most of the signals could be explained by harmonics and combinations of the three main frequencies. Moreover, using a single, low resolution ( $R \sim 5000$ ) spectrum, Balona et al. (2012) derived basic parameters,  $T_{\text{eff}} = 7300 \pm 150$  K,  $\log g = 3.5 \pm 0.1$  (in cgs), and concluded that V2367 Cyg has a solar abundance. Besides, the authors announced an unusual fast rotation with the projected value of  $V_{\text{rot}} \sin i = 100 \pm 10 \text{ km s}^{-1}$ , what made V2367 Cyg the fastest rotating HADS (more than twice that of other HADS stars).

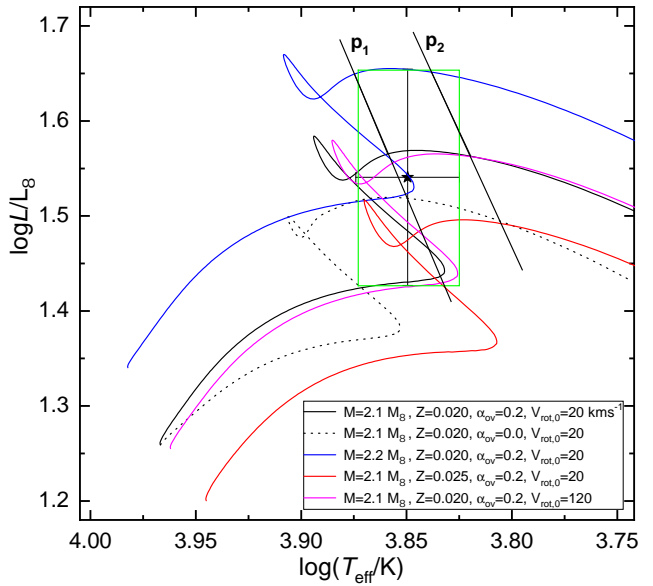


**Figure 1.** The position of V2367 Cyg in the HR diagram. Evolutionary tracks were computed with the OPAL opacity tables, the solar mixture from AGSS09, initial hydrogen abundance  $X_0 = 0.70$  and the MLT parameter  $\alpha_{\text{MLT}} = 0.5$ . There is shown the effect of mass  $M$ , metallicity  $Z$ , overshooting from the convective core  $\alpha_{\text{ov}}$  and the initial value of rotation. For  $Z = 0.020$ ,  $\alpha_{\text{ov}} = 0.2$ ,  $V_{\text{rot},0} = 20 \text{ km s}^{-1}$ , the line of constant frequency  $\nu_1 = 5.66106 \text{ d}^{-1}$  are indicated for the radial fundamental ( $p_1$ ) and first overtone mode ( $p_2$ ) radial modes.

Balona et al. (2012) attempted also to make seismic modelling of V2367 Cyg assuming that  $\nu_1$  and  $\nu_2$  are both radial modes: fundamental & first overtone or first overtone & second overtone. However, the frequency ratio  $\nu_1/\nu_2 = 0.79187$  did not fit to any of these cases and the final conclusion was that higher order effects of rotation, including mode coupling, must be taken into account if  $\nu_2$  were to be a radial mode.

The fast rotation of V2367 Cyg was confirmed by Ulusoy et al. (2013) on the basis of higher resolution spectra ( $R \sim 16000$ ). However, the most recent determination by Niemczura et al. (2017), based on the spectra with  $R \sim 25000$  and  $46000$ , indicates rather a low projected rotational velocity  $V_{\text{rot}} \sin i = 16 \pm 1 \text{ km s}^{-1}$ . Niemczura et al. (2017) also determined abundances of 29 chemical elements, which are similar to the solar abundances within the errors. Using their abundances, we determined the bulk metallicity by mass in the range  $Z \in [0.0134, 0.0356]$ .

Ulusoy et al. (2013) also obtained time-series photometry in the *UBVRI* bands. Their aim was to make the mode identification from the amplitudes and phases for the three main frequencies. Unfortunately, their identification was not successful.

In our analysis, we adopted the whole range of effective temperature from the above mentioned literature, i.e.,  $T_{\text{eff}} \in (6680, 7484)$  K, which corresponds to  $\log(T_{\text{eff}}/\text{K}) = 3.8495 \pm 0.0246$ . To derive the luminosity  $L$ , we adopted a distance determined on the basis of Starhorse2 model (Anders et al. 2022), using the Gaia DR3 observations (Gaia Collaboration et al., 2022). The bolometric corrections were taken from Kurucz model atmospheres for the microturbulent velocity  $\xi_t = 2, 4 \text{ km s}^{-1}$  and metallicity  $[\text{m}/\text{H}] = 0.0, +0.1, +0.3$ . Finally, we got  $\log L/\text{L}_\odot = 1.5407 \pm 0.1138$ . The error in luminosity also includes errors in

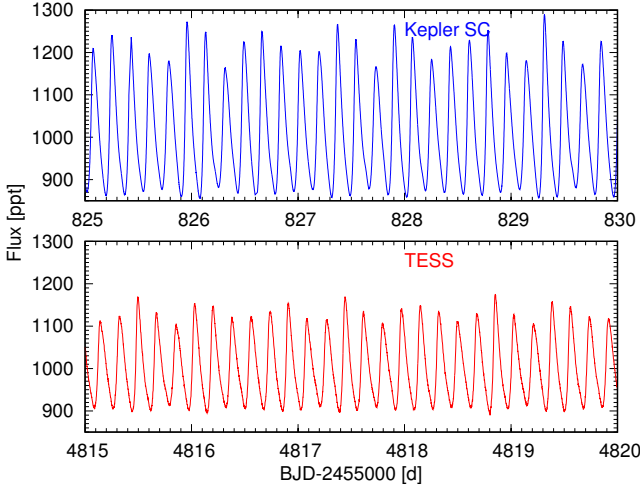


**Figure 2.** Five-days cuts of *Kepler* (top panel) and *TESS* (bottom panel) light curves of V2367 Cyg.

the effective temperature and bolometric correction. Therefore, the relative error of  $L$  is larger than the relative error of the distance  $d$ .

In Fig. 1, we show the position of V2367 Cyg on the Hertzsprung-Russell (HR) diagram. A few evolutionary tracks were depicted, presenting the effect of a mass  $M$ , metallicity  $Z$ , the overshooting zone convective core  $\alpha_{\text{ov}}$  and the initial rotation  $V_{\text{rot},0}$ . The track were computed with Warsaw-New Jersey code for the OPAL opacity tables (Iglesias & Rogers 1996) and the solar chemical mixture of Asplund et al. (2009), hereafter AGSS09. We depicted also lines of the constant frequency  $\nu_1 = 5.66106 \text{ d}^{-1}$  for the fundamental ( $p_1$ ) and first overtone ( $p_2$ ) radial modes, for  $Z = 0.020$ ,  $\alpha_{\text{ov}} = 0.2$ ,  $V_{\text{rot},0} = 20 \text{ km s}^{-1}$ . In this case, the value of  $\nu_1$  as  $p_1$  or  $p_2$  is reached only in the hydrogen-shell burning (HSB) phase.

### 3 ANALYSIS OF SPACE PHOTOMETRY

In this section, we analysed the photometric data delivered by two very successful space missions: *Kepler* (e.g. Borucki et al. 2010; Koch et al. 2010) and *TESS* (e.g. Ricker et al. 2015). *Kepler* observed V2367 Cyg in two modes: a long cadence (LC,  $\sim 30$  min exposure) and short cadence (SC, 1 min exposure). LC data are available for all *Kepler* quarters, i.e. Q0-Q17 from BJD 245 4953.539 to BJD 245 6424.001, whereas SC data are for Q0.1 from BJD 245 4953.529 to BJD 245 4963.255 and for Q6.1-Q10.3 from BJD 245 5372.460 to BJD 245 5833.276. Eight years later the star was observed by *TESS* in its 2 min mode in sectors: S14-S15 from BJD 245 8683.356 to BJD 245 8737.411, S40-S41 from BJD 245 9390.655 to BJD 245 9446.581, and S54-S55 from BJD 245 9769.901 to BJD 245 9824.265.

Light curves from both missions can be downloaded from MAST portal. There are two types of flux data: simple aperture photometry (SAP) and Pre-search Data Conditioning SAP flux (PDCSAP). Five-days cuts of *Kepler* and *TESS* light curves can be seen in Fig. 2, where the normalized and converted to ppt SAP data are shown.

We started with the frequency analysis of the *Kepler* data. The Nyquist frequency for the SC and LC data is  $720 \text{ d}^{-1}$  and  $24.5 \text{ d}^{-1}$ , respectively. Therefore, to circumvent aliasing issues, we first performed analysis on the SC data. Each single part of this data,

i.e.  $Qn.m$ , where  $n$  is the quarter number and  $m$  is one of the three parts in quarter, was normalized by a linear function.

In the case of the *Kepler* data of V2367 Cyg, the SAP and PDCSAP fluxes are almost indistinguishable, thus we decided to analyse only the SAP fluxes. It appeared that amplitudes in Q0.1 are considerably lower than in other *Kepler* quarters. This is reflected in the standard deviation which is lower in Q0.1 than in other data parts (cf. Table 1). Moreover, there is a 400-day gap between Q0.1 and the remaining data. Therefore, the exclusion of Q0.1 seems to be justified and for the further analysis we used data from Q6.1 to Q10.3. This data set consists of 624 096 observational points which span 460.8 d. This range translates into the Rayleigh resolution of  $\Delta\nu_{R,K} = 0.0022 \text{ d}^{-1}$ .

In order to extract frequencies of the periodic light variability, we proceeded the standard pre-whitening procedure. The amplitude Lomb-Scargle periodograms (Lomb 1976; Scargle 1982) were calculated up to  $130 \text{ d}^{-1}$  with the fixed resolution of  $10^{-5} \text{ d}^{-1}$ . Above  $100 \text{ d}^{-1}$ , no signal was detected. We used an algorithm based on the fast Fourier transforms for non-equally spaced data (e.g., Leroy 2012). As a significance criterion of a given frequency peak we chose the signal to noise ratio,  $S/N = 5$ , which corresponds to the estimate made by Baran & Koen (2021) for *TESS* data. The noise  $N$  was calculated as a mean amplitude in a one day window centred at the significant frequency before its extraction. Four periodograms from the *Kepler* SC Q6.1-Q10.3 data are shown in Fig. 3. For a better visibility only frequencies up to  $25 \text{ d}^{-1}$  were depicted.

In the case of *Kepler* data which have a high point-to-point precision, there is a risk of artificially introducing spurious signals in the pre-whitening process. According to Loumos & Deeming (1978), in their most conservative case, frequencies that are separated less than 2.5 times the Rayleigh resolution cannot be resolved properly and may be spurious. Therefore, we excluded all lower-amplitude frequencies from the following range:

$$\nu \in \sum_{i=0}^n \langle \nu_i - 2.5\Delta\nu_{R,K}, \nu_i + \Delta\nu_{R,K} \rangle, \quad (1)$$

where  $n$  is the number of all detected frequencies  $\nu_i$  at a given pre-whitening step. In the bottom panel of Fig. 3, there are residual peaks clearly exceeding the detection threshold. These are the frequencies that fall into the range defined in Eq. 1. This procedure allowed us to detect 958 frequency peaks that met our criteria. However, during the non-linear fit, 13 frequencies drifted into the prohibited range given by Eq. 1. Therefore, they were also excluded from our ultimate frequency list. Our final frequencies, along with their corresponding amplitudes and phases, were determined by the non-linear least-squares fitting function in the form:

$$S(t) = \sum_{i=1}^N A_i \sin(2\pi(\nu_i t + \phi_i)) + c, \quad (2)$$

where  $N = 945$  is the number of sinusoidal components,  $A_i$ ,  $\nu_i$ ,  $\phi_i$  are the amplitude, frequency, and phase of the  $i$ -th component, respectively, while the  $c$  is an offset. Finally, we applied corrections to the formal errors of frequencies according to Schwarzenberg-Czerny (1991), the so-called post-mortem analysis. We got that the formal errors should be multiplied by about 2.7.

In the last step, we looked for harmonics and combinations. A given frequency was considered a harmonic if it satisfied, up to the Rayleigh resolution, the equation:

$$\nu_i = m\nu_j, \quad (3)$$

where  $m$  is an integer from the range  $\langle 2, 20 \rangle$ . The frequency was

**Table 1.** The standard deviation in all available parts of Kepler SC data of V2367 Cyg.

ID	Q0.1	Q6.1	Q6.2	Q6.3	Q7.1	Q7.2	Q7.3	Q8.1	Q8.2	Q8.3	Q9.1	Q9.2	Q9.3	Q10.1	Q10.2	Q10.3
SD	115.8	118.6	118.7	118.5	119.4	119.5	119.7	119.3	119.2	119.1	118.0	118.0	117.8	118.6	118.6	118.4

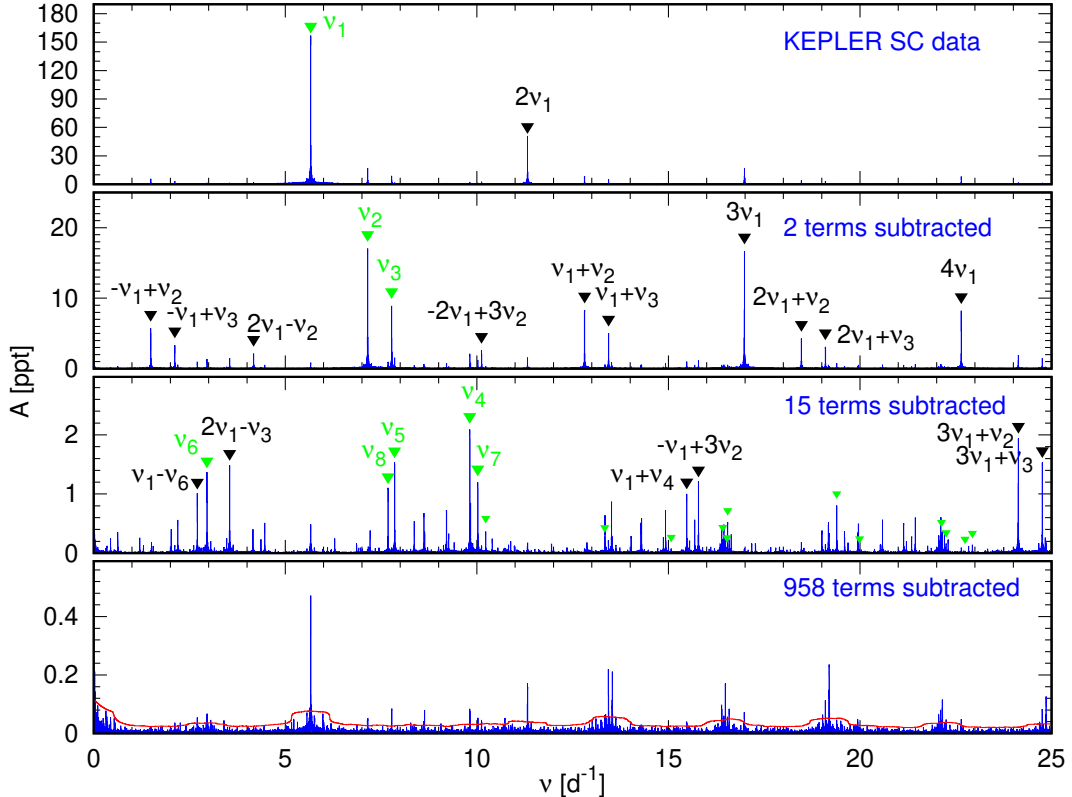


**Figure 3.** Amplitude periodograms for the *Kepler* SC Q6.1-Q10.3 data of V2367 Cyg. Panels from top to bottom show periodograms: for the original data set; after subtraction of 2 terms; after subtraction of 15 terms and after subtraction of 958 terms. Red solid line in the bottom panel indicates the  $5S/N$  level. All frequency peaks above 1 ppt are marked by down-pointing triangles; green for independent signals and black for combinations or harmonics. Independent frequencies with amplitudes smaller than 1 ppt are marked by smaller green triangles.

considered a combination with two parents if it met, up to the Rayleigh resolution, the equation

$$v_i = mv_j + nv_k, \quad (4)$$

where  $m$  and  $n$  are integers from the range  $\langle -10, 10 \rangle$ , except for  $v_1$ , for which we assumed  $m \in \langle -15, 15 \rangle$ . Similarly, the frequency was considered a combination with three parents if it satisfied the equation

$$v_i = mv_j + nv_k + ov_l, \quad (5)$$

where  $m, n, o$  are integers from the range  $\langle -2, 2 \rangle$ , except for  $v_1$ , for which we used  $m \in \langle -5, 5 \rangle$ . Additionally, when searching for combinations and harmonics, we excluded signals with very low frequencies, i.e. less than  $0.1 \text{ d}^{-1}$ , as they are most probably of instrumental origin.

After all steps of selection, we found that only a small part of the numerous signals detected in *Kepler* data are independent frequencies. They are listed in Table 2 and the complete list of frequencies with  $S/N > 5$  are available in Appendix A in Table A1. A smaller part of the *Kepler* data, from Q0.1 and Q6.1-Q7.3, have already been analysed by Balona et al. (2012). We have confirmed all of their frequencies (see Table 1 of Balona et al. (2012)). However,

their  $v_{B,4}, v_{B,11}, v_{B,12}, v_{B,13}$ , and  $v_{B,15}$  were identified by us as combinations. We provide Balona's frequency designations in the last column of Table 2.

High frequencies, which we define as those above  $30 \text{ d}^{-1}$  listed in Table 2 (i.e.,  $v_{15}, v_{18}, v_{23}, v_{24}, v_{25}$ , and  $v_{26}$ ), are of an unclear origin. All of them have very small amplitudes and, most probably, they are higher-order combinations, i.e., with higher  $m, n, o$  integers, than we assumed in our analysis. However, we know that as these integers increase, the probability of Equations 4 and 5 being met by chance also increases. The mentioned six frequencies can be expressed as:  $v_{15} = 9v_1 + 1v_3 - 2v_4$ ,  $v_{18} = 1v_1 - 1v_2 + 4v_4$ ,  $v_{23} = 6v_1 - 2v_2 + 4v_8$ ,  $v_{24} = 10v_1 + 2v_2 - v_5$ ,  $v_{25} = 9v_1 + 1v_2 + 1v_9$ ,  $v_{26} = 5v_1 + 5v_2 + 5v_4$ . Here, we note that  $v_{15}$  and  $v_{18}$  are also present in the LC data, whereas  $v_{23}$ ,  $v_{24}$ ,  $v_{53}$ ,  $v_{26}$  as well as their aliases are absent in these data. Moreover, none of these high frequencies were detected in the *TESS* data. Like Balona et al. (2012), we also detected an independent low-frequency peak  $v_6 = 2.95671 \text{ d}^{-1}$ , which can only be associated with the high-order g mode. On the other hand, including higher-order combinations, we can express this low frequency as  $v_6 = -5v_1 + 3v_2 + 1v_4$ . However, if both, this low frequency and above-mentioned high frequencies, correspond to pulsation modes, then we encounter a problem with their excita-

**Table 2.** Independent frequencies detected in the *Kepler* SC data. The subsequent columns contain: our ID<sub>K</sub> number, frequency, amplitude, phase, signal to noise ratio and ID<sub>B</sub> from Table 1 of Balona et al. (2012).

ID <sub>K</sub>	$\nu$ [d <sup>-1</sup> ]	A [ppt]	$\phi$ [0–1]	S/N	ID <sub>B</sub>
1	5.661058(2)	156.998(2)	0.8725(1)	75.7	$\nu_{1,B}$
2	7.148954(7)	17.051(2)	0.9992(1)	72.6	$\nu_{2,B}$
3	7.775571(9)	8.922(2)	0.9548(1)	67.6	$\nu_{3,B}$
4	9.81587(1)	2.113(2)	0.5615(1)	43.8	$\nu_{5,B}$
5	7.85334(2)	1.528(2)	0.4139(2)	48.3	$\nu_{6,B}$
6	2.95671(2)	1.359(2)	0.3161(2)	42.9	$\nu_{7,B}$
7	10.02421(2)	1.223(2)	0.6596(3)	39.4	$\nu_{8,B}$
8	7.68347(2)	1.092(2)	0.3050(3)	52.8	$\nu_{9,B}$
9	19.39129(2)	0.806(2)	0.8494(4)	28.5	$\nu_{10,B}$
10	16.54373(3)	0.520(2)	0.1694(6)	19.6	$\nu_{14,B}$
11	10.22938(3)	0.388(2)	0.8355(8)	27.6	
12	22.12973(4)	0.321(2)	0.231(1)	18.0	
13	16.42229(4)	0.239(2)	0.966(1)	16.8	
14	13.33679(4)	0.235(2)	0.870(1)	14.9	
15	39.09191(6)	0.168(2)	0.349(2)	23.9	
16	22.24766(6)	0.147(2)	0.743(1)	13.3	
17	22.93256(6)	0.138(2)	0.096(2)	20.9	
18	37.77743(8)	0.109(2)	0.086(3)	18.5	
19	15.0704(1)	0.071(2)	0.066(4)	11.0	
20	16.5302(1)	0.065(2)	0.460(5)	6.3	
21	19.9908(1)	0.047(2)	0.348(7)	7.6	
22	22.7419(2)	0.039(2)	0.935(8)	8.1	
23	50.4010(2)	0.039(2)	0.301(8)	13.4	
24	63.0535(6)	0.011(2)	0.54(2)	7.1	
25	77.4900(9)	0.007(2)	0.50(5)	6.8	
26	91.684(1)	0.006(2)	0.11(5)	7.6	

**Table 3.** The standard deviation SD for the combined adjacent sectors of the TESS SAP and PDCSAP data, i.e., S14+S15, S40+S41, and S54+S55.

	S14+S15	S40+S41	S54+S55
SD(SAP)	76.1	75.0	76.7
SD(PDCSAP)	90.8	85.7	86.2

tion. They would have to be driven by a mechanism other than the classical  $\kappa$  mechanism or some modifications to the mean opacity profile would have to be made.

For the TESS data, we followed the same procedure as with the *Kepler* data. However, this time, the SAP and PDCSAP fluxes showed a significant difference. Furthermore, the amplitudes based on PDCSAP flux in combined sectors S14+S15 are significantly larger than those in combined sectors S40+S41 and S54+S55. This issue is greatly mitigated in the case of SAP data. Therefore, we decided to analyse SAP data. The standard deviations calculated for the three pairs of the TESS sectors are listed in Table 3. Moreover, since there are large time-gaps between data from sectors 14+15, 40+41 and 54+55, we analyzed the combined data as well as data from the adjacent sectors. We started by analysing all combined sectors. This data set consists of 110 891 observational points spanning 1140.9 d what translates into the Rayleigh resolution  $\Delta\nu_{R,T,all} = 0.00088$  d<sup>-1</sup>. The error corrections for this data were of about 1.6. Pre-whitening procedure resulted in 171 frequencies, most of which were combinations or harmonics. All independent frequencies are listed in Table 4. A sample of periodograms are shown in Fig. 4 (only for  $\nu < 25$  d<sup>-1</sup>).

As in case of the *Kepler* data, we excluded frequencies lower

than 0.1 d<sup>-1</sup>. For their accurate determination, a long-term observations are necessary. Therefore, we analysed the three data sets: the combined *Kepler* SC data, the combined LC data and the combined TESS data. We cannot be certain whether frequencies from the LC observations are real or aliases. Such low frequencies are often of instrumental origin. Since none of them agrees within the corresponding Rayleigh resolution in all three data sets, we consider them not intrinsic to the star. All low frequencies are listed in Appendix A in Table A3.

Additionally, we excluded frequencies close to  $\nu_1$ , but exceeding the limit of  $2.5\Delta\nu_{R,T,all}$ , and marked them as spurious. These frequencies may result from small differences in amplitudes in various sectors or imperfect subtraction of  $\nu_1$ , or both. Such frequencies also appeared in the *Kepler* data, but they were identified as combinations (see Table A1 in Appendix A). However, their origin can also be explained in a similar way. All frequencies with  $S/N > 5$  extracted from the six combined TESS sectors are listed in Appendix A in Table A2.

In the next step, we analysed TESS data from combined adjacent sectors, i.e., S14+S15, S40+S41 and S54+S55. Each of these data sets spans about 55 days and have the Rayleigh resolution of about 0.018 d<sup>-1</sup>. Here, we limited  $m$ ,  $n$  in Eq. 4 to the range  $< -10, 10 >$  for all detected frequencies. We found 61, 66 and 68 significant frequencies in S14+S15, S40+S41 and S54+S55, respectively. Independent frequencies are given in Appendix A in Table A4. All significant frequencies (i.e. with  $S/N > 5$ ) are listed in Tables A5–A7 in Appendix A along with a sample of periodograms calculated for the S14+S15 data shown in Fig. A1. We stress that due to the low Rayleigh resolution of the two-sector data, some frequencies identified in the full data set as independent are classified in Tables A5–A7 as combinations.

Subsequently, we looked for possible changes in the three highest-amplitude independent frequencies,  $\nu_1$ ,  $\nu_2$  and  $\nu_3$ . To this end, we analyzed the *Kepler* data for each quarter separately. Whenever possible, we utilized SC data. In quarters where SC data were not available, we used LC data. However, due to a strong aliasing problem (see Fig. A2 in Appendix A), arising from the low Nyquist frequency for the LC data, we limited the pre-whitening process to several frequencies with the highest amplitudes. The results are presented in Fig. 5, where the values of three dominant frequencies are plotted as a function of time. The frequency values from adjacent TESS sectors were also added. As one can see, all three frequencies, within errors, are constant over the time considered. The frequency values are listed in Table A8 in Appendix A.

#### 4 IDENTIFICATION OF THE MODE DEGREE $\ell$ FROM *UBVRI* PHOTOMETRY

Within the linear theory, the local radial displacement of the surface element as a result of a pulsational mode with the angular frequency  $\omega$ , harmonic degree  $\ell$  and azimuthal order  $m$ , can be written as

$$\frac{\delta r}{R} = \text{Re}\{\varepsilon Y_\ell^m(\theta, \varphi) e^{-i\omega t}\}, \quad (6)$$

where  $\varepsilon$  is the intrinsic mode amplitude, that cannot be determined within the linear approach, and  $Y_\ell^m(\theta, \varphi)$  is a spherical harmonic defined as:

$$Y_\ell^m(\theta, \phi) = (-1)^{\frac{m+|m|}{2}} \sqrt{\frac{(2\ell+1)(\ell-|m|)!}{(\ell+|m|)!}} P_\ell^{|m|}(\cos \theta) e^{im\phi}. \quad (7)$$

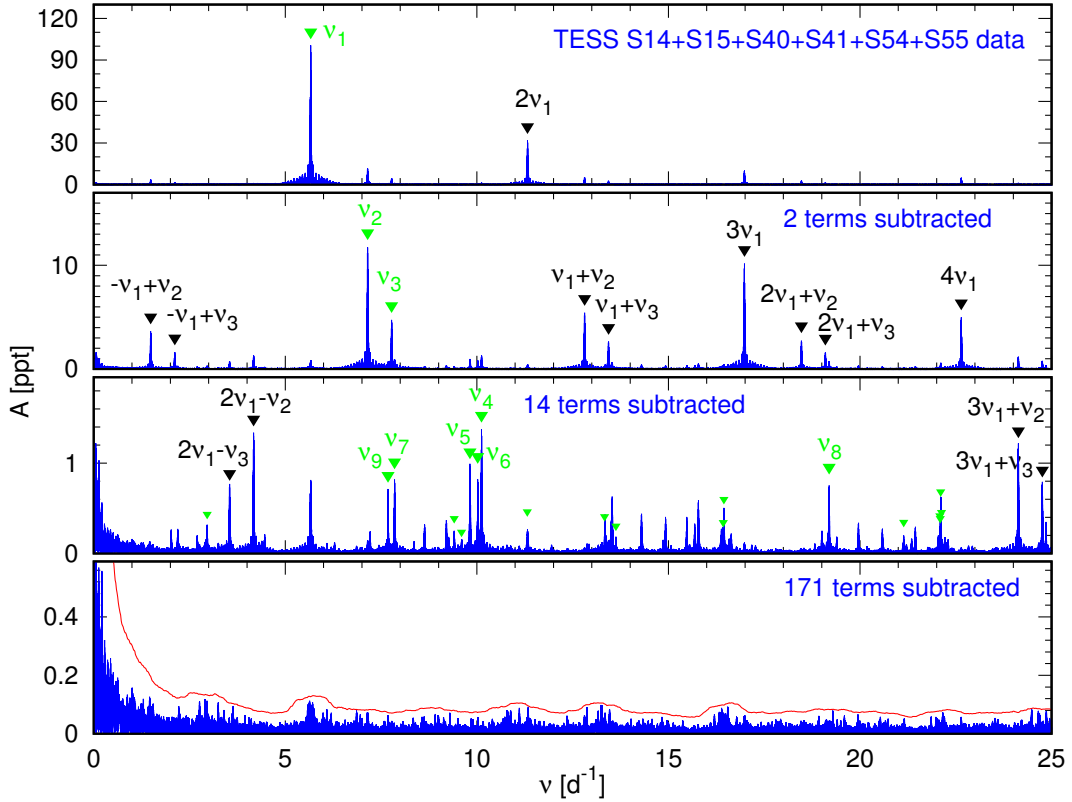


**Figure 4.** Amplitude periodogram for the combined *TESS* data of V2367 Cyg. Panels from top to bottom show periodograms: for the original data; after subtraction of 2 terms; after subtraction of 14 terms and after subtraction of 171 terms. Red solid line in bottom panel indicates the  $5S/N$  level. All frequency peaks above 0.63 ppt (the *TESS* amplitudes are smaller than the *Kepler* amplitudes by about this factor) are marked by down-pointing triangles, green for independent signals, black for combinations or harmonics. Independent frequencies with amplitudes smaller than 0.63 ppt are marked by small green triangles.

**Table 4.** Independent frequencies detected in *TESS* combined data. The subsequent columns contain: our ID<sub>T</sub> number, frequency, amplitude, phase, signal to noise ratio, ID<sub>K</sub> and ID<sub>B</sub>. Tildes in the last and penultimate columns indicate that the difference in frequencies exceeds the Rayleigh resolution of the *Kepler* SC data but it is below 3 times this resolution.

ID <sub>T</sub>	$\nu$ [d <sup>-1</sup> ]	A [ppt]	$\phi$ [0–1]	S/N	ID <sub>K</sub>	ID <sub>B</sub>
1	5.6610574(7)	100.24(1)	0.86115(2)	31.7	$\nu_{1,K}$	$\nu_{1,B}$
2	7.148978(3)	11.76(1)	0.9321(2)	31.3	$\nu_{2,K}$	$\nu_{2,B}$
3	7.775571(3)	4.71(1)	0.9577(4)	28.0	$\nu_{3,K}$	$\nu_{3,B}$
4	10.122796(8)	1.39(1)	0.918(1)	17.3	$-2\nu_{1,K} + 3\nu_{2,K}$	$\nu_{4,B}$
5	9.81861(1)	0.92(1)	0.881(2)	16.7	$\sim \nu_{4,K}$	$\sim \nu_{5,B}$
6	10.02425(1)	0.87(1)	0.513(2)	19.7	$\nu_{7,K}$	$\nu_{8,B}$
7	7.85337(1)	0.81(1)	0.338(2)	16.8	$\nu_{5,K}$	$\nu_{6,B}$
8	19.19308(1)	0.77(1)	0.665(2)	18.0	$9\nu_{4,K} - 9\nu_{8,K}$	
9	7.68344(1)	0.72(1)	0.331(2)	20.3	$\nu_{8,K}$	$\nu_{9,B}$
10	22.10602(1)	0.53(1)	0.288(4)	16.2	$\sim 8\nu_{3,K} - 4\nu_{7,K}$	$\sim \nu_{11,B}$
11	16.44771(2)	0.43(1)	0.067(4)	12.7	$5\nu_{1,K} + 1\nu_{3,K} - 2\nu_{4,K}$	$\nu_{13,B}$
12	2.95974(3)	0.29(1)	0.752(6)	9.6	$\sim \nu_{6,K}$	$\sim \nu_{7,B}$
13	22.12713(3)	0.32(1)	0.162(6)	9.1	$\sim \nu_{12,K}$	
14	9.40935(3)	0.25(1)	0.212(7)	9.0	$4\nu_{7,K} - 3\nu_{11,K}$	
15	22.08397(3)	0.28(1)	0.492(6)	8.9	$1\nu_{1,K} + 1\nu_{13,K}$	
16	13.33399(4)	0.27(1)	0.503(7)	7.0	$\sim \nu_{14,K}$	
17	21.13797(3)	0.21(1)	0.791(8)	11.0	$2\nu_{1,K} + 1\nu_{4,K}$	
18	11.33598(3)	0.22(1)	0.272(9)	8.0	$\sim -2\nu_{14,K} + 1\nu_{17,K} + 1\nu_{19,K}$	
19	13.63011(4)	0.16(1)	0.64(1)	6.9	$8\nu_{6,K} - 1\nu_{7,K}$	
20	22.09581(4)	0.22(1)	0.098(9)	6.5	$-1\nu_{4,K} + 2\nu_{8,K} + 1\nu_{10,K}$	
21	27.96166(6)	0.10(1)	0.35(2)	6.2	$-2\nu_{9,K} + 3\nu_{16,K}$	
22	9.60108(7)	0.10(1)	0.36(2)	6.0	$1\nu_{2,K} - 1\nu_{3,K} + 1\nu_{11,K}$	
23	43.23259(7)	0.09(1)	0.10(2)	7.6	$-8\nu_{1,K} + 4\nu_{12,K}$	
24	32.11376(8)	0.08(1)	0.02(2)	5.6	$\sim -1\nu_{2,K} + 5\nu_{5,K}$	
25	26.18343(9)	0.08(1)	0.24(2)	5.2		

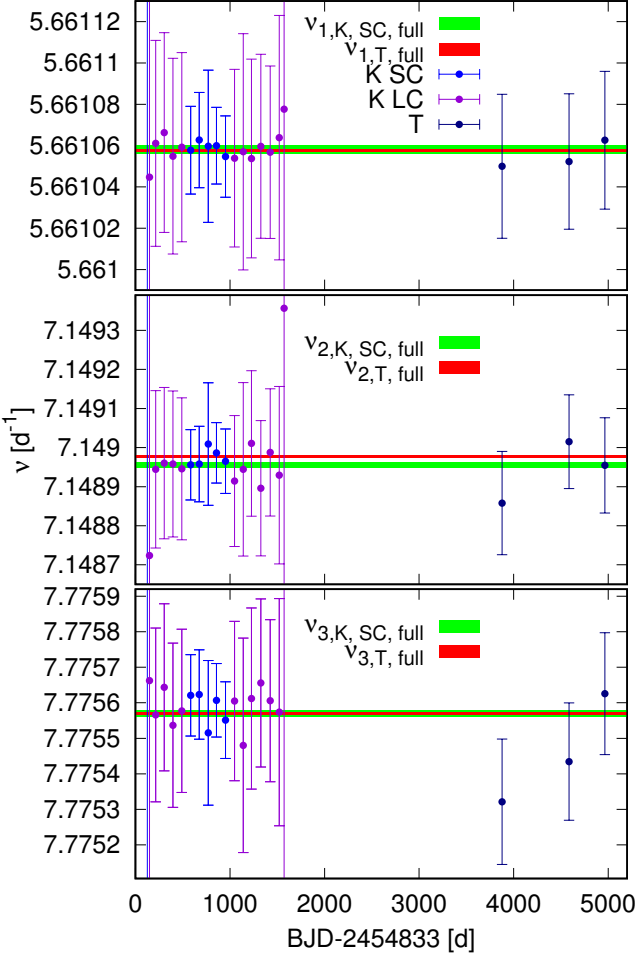


**Figure 5.** The values of  $v_1$  (top panel),  $v_2$  (middle panel), and  $v_3$  (bottom panel) with error bars determined in each *Kepler* quarter and adjacent pairs of the TESS sectors. For a better visibility, the error bars determined from Q0, Q1 and Q17 data are cut. Horizontal green and red lines, whose width corresponds to the error, represent the values of frequencies determined from full *Kepler* and TESS data sets, respectively.

With this normalization,  $|\varepsilon|$  is the rms value of  $\delta r/R$  over the stellar surface. The corresponding changes of the bolometric flux,  $F_{\text{bol}}$ , and the local gravity,  $g$ , are given by

$$\frac{\delta F_{\text{bol}}}{F_{\text{bol}}} = \text{Re}\{\varepsilon f Y_\ell^m(\theta, \varphi) e^{-i\omega t}\}, \quad (8a)$$

and

$$\frac{\delta g}{g} = -\left(2 + \frac{\omega^2 R^3}{GM}\right) \frac{\delta r}{R}. \quad (8b)$$

The parameter  $f$  describes the ratio of the relative flux variation to the relative radial displacement of the surface. Both  $\varepsilon$  and  $f$  have to be regarded complex. Since we can assume that both  $\varepsilon$  and  $f$  are constant in the atmosphere, we can use the static plane-parallel approximation. Then, the complex amplitude of the relative monochromatic flux variation in a passband  $\lambda$  can be expressed as (e.g., Daszyńska-Daszkiewicz et al. 2005):

$$\mathcal{A}_\lambda = \mathcal{D}_\ell^\lambda(\tilde{\varepsilon}f) + \mathcal{E}_\ell^\lambda \tilde{\varepsilon}, \quad (9)$$

where

$$\tilde{\varepsilon} \equiv \varepsilon Y_\ell^m(i, 0), \quad (10a)$$

$$\mathcal{D}_\ell^\lambda = b_\ell^\lambda \frac{1}{4} \frac{\partial \log(\mathcal{F}_\lambda |b_\ell^\lambda|)}{\partial \log T_{\text{eff}}}, \quad (10b)$$

$$\mathcal{E}_\ell^\lambda = b_\ell^\lambda \left[ (2 + \ell)(1 - \ell) - \left( \frac{\omega^2 R^3}{GM} + 2 \right) \frac{\partial \log(\mathcal{F}_\lambda |b_\ell^\lambda|)}{\partial \log g} \right], \quad (10c)$$

and

$$b_\ell^\lambda = \int_0^1 h_\lambda(\mu) \mu P_\ell(\mu) d\mu. \quad (10d)$$

The term  $\mathcal{D}_\ell^\lambda$  describes the temperature effects and  $\mathcal{E}_\ell^\lambda$  combines the geometrical and pressure effect.  $G$ ,  $M$ ,  $R$  have their usual meanings.  $h_\lambda(\mu)$  is the limb darkening law and  $P_\ell(\mu)$  is the Legendre polynomial. The values of  $b_\ell^\lambda$  and the partial derivatives of  $\mathcal{F}_\lambda |b_\ell^\lambda|$  are calculated from model atmospheres. The values of the amplitude and phase are given by  $A_\lambda = |\mathcal{A}_\lambda|$ ,  $\varphi_\lambda = \arg(\mathcal{A}_\lambda)$ , respectively.

The system of  $N$ -passbands complex equations (9) is solved for a given  $\ell$  and  $(T_{\text{eff}}, \log g)$  to determine  $\tilde{\varepsilon}$  and  $f$ . We considered the degree  $\ell$  and associated complex values of  $\tilde{\varepsilon}$  and  $f$  as most probable if there is a clear minimum in the difference between the calculated and observed photometric amplitudes and phases. The goodness of fit is defined as:

$$\chi^2 = \frac{1}{2N - N_p} \sum_{i=1}^N \frac{|\mathcal{A}_{\lambda_i}^{obs} - \mathcal{A}_{\lambda_i}^{cal}|^2}{|\sigma_{\lambda_i}|^2}, \quad (11)$$

where the superscripts  $obs$  and  $cal$  denote the observed and calculated complex amplitude, respectively.  $N_p$  is the number of parameters to be determined and  $N_p = 4$  because there are two complex parameters,  $\tilde{\varepsilon}$  and  $f$ . The observational errors  $\sigma_\lambda$  are computed as

$$|\sigma_\lambda|^2 = \sigma^2(A_\lambda) + A_\lambda^2 \sigma^2(\varphi_\lambda), \quad (12)$$

where  $\sigma(A_\lambda)$  and  $\sigma(\varphi)$  are the errors of the observed amplitude and phase in a passband  $\lambda$ , respectively.

Ulusoy et al. (2013) gathered multi-colour time series photometry of V2367 Cyg in 5 filters,  $UBVRI$ , and determined the amplitudes and phases for the three main frequencies  $v_1$ ,  $v_2$ ,  $v_3$ . Using these data, we applied the above described method to identify the mode degree  $\ell$ . The results are shown in Fig. 6 for the four pairs of  $(\log T_{\text{eff}}, \log L/L_\odot)$ . We used Vienna model atmospheres (Heiter et al. 2002) that include turbulent convection treatment from Canuto et al. (1996). For the limb darkening law,  $h_\lambda(\mu)$ , we computed coefficients assuming the non-linear formula of Claret (2000). Here, we show results for the atmospheric metallicity [m/H] = +0.2 and microturbulent velocity  $\xi_t = 4 \text{ km s}^{-1}$ . For lower metallicity [m/H], the discriminant  $\chi^2$  takes higher values but the dependence  $\chi^2(\ell)$  is qualitatively the same. As one can see the dominant frequency  $v_1 = 5.66106 \text{ d}^{-1}$  is undoubtedly the radial mode. Taking into account the disc averaging effect, the most probable  $\ell$  degrees for  $v_2 = 7.14989 \text{ d}^{-1}$ ,  $v_3 = 7.77557 \text{ d}^{-1}$  are 0 or 2. Because of the values of  $v_2$  and  $v_3$ , it is obvious that both of them cannot correspond to radial modes. The amplitudes of  $v_2$  and  $v_3$  are smaller than the amplitude of  $v_1$  by about 8.5 and 21.2 times, respectively.

Fig. 7 shows the Petersen diagram with the marked values of the observed frequency ratios,  $v_1/v_2 = 0.79187$  and  $v_1/v_3 = 0.72807$ , along with the run of theoretical ratios for the frequencies of radial fundamental and first overtone  $v(p_1)/v(p_2)$  vs  $v(p_1)$  (lower lines) as well as the first and second overtones  $v(p_2)/v(p_3)$  vs  $v(p_2)$  (upper lines).

All evolutionary computations were performed with the

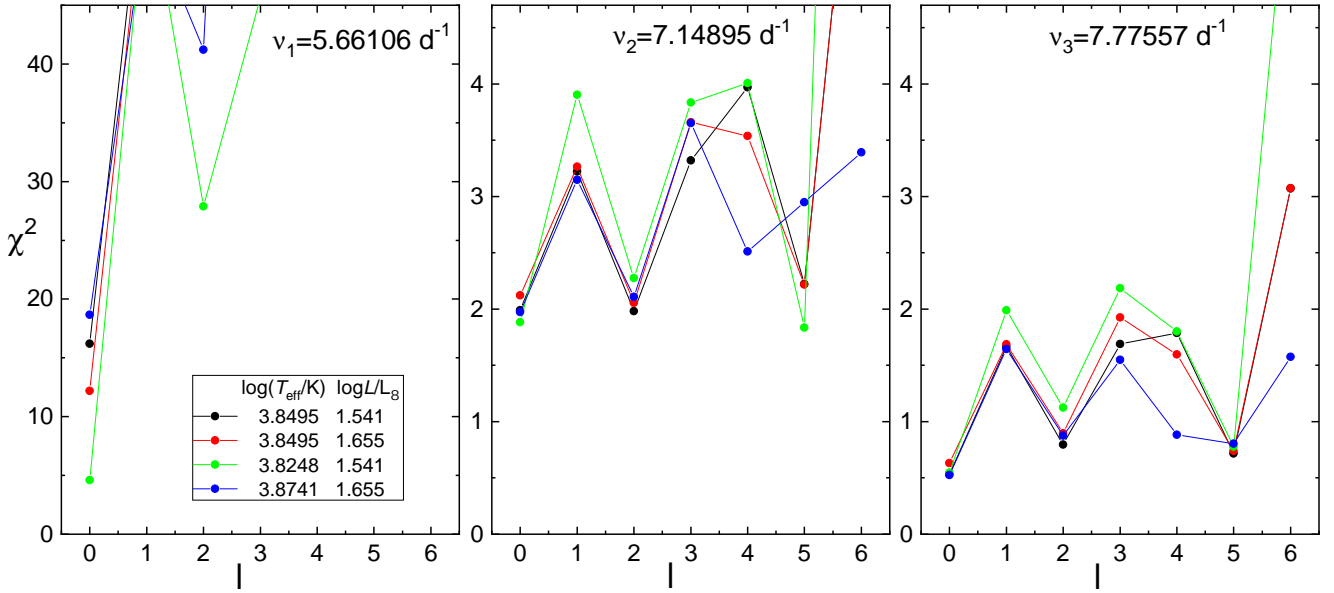


**Figure 6.** Identification of the mode degree  $\ell$  for the three frequencies of V2367 Cyg with the highest amplitudes:  $\nu_1 = 5.66106 \text{ d}^{-1}$  (left panel),  $\nu_2 = 7.14898 \text{ d}^{-1}$  (middle panel) and  $\nu_3 = 7.77558 \text{ d}^{-1}$  (right panel). NEMO model atmospheres were adopted with the metallicity [m/H] = +0.2 and microturbulent velocity  $\xi_t = 4 \text{ km s}^{-1}$ . Results for the four pairs of  $(T_{\text{eff}}, L)$  are presented.

Warsaw-New Jersey code which takes into account the mean effect of the centrifugal force. It assumes the solid-body rotation and conservation of global angular momentum during evolution. Convection in stellar envelope is treated in the framework of standard mixing-length theory (MLT). The OPAL2005 equation of state was used (Rogers et al. 1996; Rogers & Nayfonov 2002), the OPAL opacity tables and AGSS09 chemical mixture. Overshooting from a convective core is treated according to the formula of Dziembowski & Pamyatnykh (2008). In our pulsational computations, we rely on the nonadiabatic code of W. Dziembowski (Dziembowski 1977; Pamyatnykh 1999), which includes the effects of rotation on pulsational frequencies within the perturbation approach taking into account non-spherically symmetric distortion due to the centrifugal force and the second- and third-order effects of the Coriolis force. The convective flux freezing approximation is used, which is justified if convection is not very efficient in the envelope.

In Fig. 7, there is shown the effect of mass ( $M = 2.1$  vs  $2.2 M_{\odot}$ ), metallicity ( $Z = 0.02$  vs  $0.025$ ), initial hydrogen abundance ( $X_0 = 0.70$  vs  $0.74$ ) and overshooting parameter ( $\alpha_{\text{ov}} = 0.2$  vs  $0.0$ ). The mixing length parameter was  $\alpha_{\text{MLT}} = 0.5$  and the initial rotation  $V_{\text{rot},0} = 20 \text{ km s}^{-1}$ .

As one can see, the hypothesis that  $\nu_3$  is a radial mode can be safely rejected because of much too low value of  $\nu_1/\nu_3$ . Changing any parameter (within a reasonable range) will not allow this value to be achieved. On the other hand a ratio of the dominant and second frequency  $\nu_1/\nu_2$  is much closer to the radial frequency ratios, in particular, for the  $p_2 \& p_3$  hypothesis. However, even in that case, we would have to assume high values of metallicity ( $Z > 0.03$ ) and very large overshooting  $\alpha_{\text{ov}} \gtrsim 0.4$ . Moreover, such models have  $M \approx 1.7 M_{\odot}$ ,  $\log T_{\text{eff}} \approx 3.67$  and  $\log L/L_{\odot} \approx 0.9$ , which are far outside the observed error box in the HR diagram. To explain the observed ratio  $\nu_1/\nu_2$  by the fundamental and first overtone (the  $p_1 \& p_2$  hypothesis) we had to assume a very low metallicity ( $Z \lesssim 0.002$ ). In this case, the models have  $M \approx 2.1 - 3.1 M_{\odot}$ ,  $\log T_{\text{eff}} \approx 4.0$  and  $\log L/L_{\odot} \approx 2.1 - 2.6$ , again far outside the observed error box.

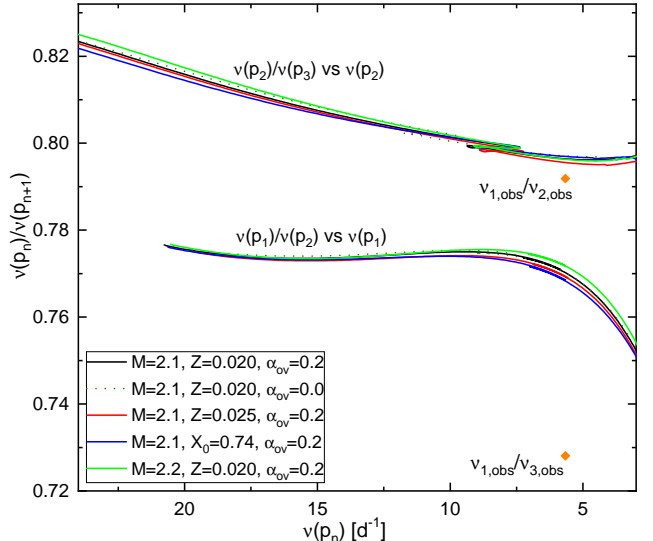


**Figure 7.** The Petersen diagram with a run of the frequency ratio for the two pairs of consecutive radial modes: fundamental and first overtone (lower lines), and the first and second overtone (upper lines). There is shown the effect of a mass  $M$ , initial hydrogen ( $X_0$ ) and metallicity  $Z$  abundances as well as the overshooting parameter  $\alpha_{\text{ov}}$ . The mixing length parameter was  $\alpha_{\text{MLT}} = 0.5$  and the initial rotation  $V_{\text{rot},0} = 20 \text{ km s}^{-1}$ . The OPAL tables and AGSS09 chemical mixture were adopted. The observed ratios of frequencies of V2367 Cyg are marked as orange diamonds.

## 5 THE EFFECTS OF ROTATION

As we mentioned in Sect. 2, there are two different determinations of the projected rotational velocity of V2367 Cyg:  $V_{\text{rot}} \sin i \approx 100 \text{ km s}^{-1}$  (Balona et al. 2012; Ulusoy et al. 2013) and  $V_{\text{rot}} \sin i \approx 16 \text{ km s}^{-1}$  (Niemczura et al. 2017). In any case, this is the lower limit of rotation. Therefore, in our modelling, we will consider

the whole range up to the half of critical rotation, which amounts to about  $V_{\text{rot}}^{\text{crit}} = 340 \text{ km s}^{-1}$ , if  $M \approx 2.2 M_{\odot}$  and  $R \approx 3.7 R_{\odot}$ . The corresponding critical value of rotational frequency is about  $\nu_{\text{rot}}^{\text{crit}} \approx 1.7 \text{ d}^{-1}$ . If the correct value of the projected rotational velocity is  $100 \text{ km s}^{-1}$  then the minimum value of the rotation frequency is approximately  $\nu_{\text{rot}}^{\text{min}} \approx 0.53 \text{ d}^{-1}$ , if it is  $16 \text{ km s}^{-1}$  then  $\nu_{\text{rot}}^{\text{min}} \approx 0.08 \text{ d}^{-1}$ . So, even at half the critical rotation velocity, the ratio  $\nu_{\text{rot}}/\nu_{\text{puls}}$  reaches the values of about 0.15 and 0.12 for the observed frequencies  $\nu_1$  and  $\nu_2$ , respectively. Therefore, using a perturbation approach is justified.

Let us recall the third order expression for a rotationally splitting frequency (e.g., Gough & Thompson 1990; Soufi et al. 1998; Pamyatnykh 2003)

$$\nu_{n\ell m} = \nu_0 + m(1 - C_{n\ell})\nu_{\text{rot}} + \frac{\nu_{\text{rot}}^2}{\nu_0}(D_0 + m^2 D_1) + m \frac{\nu_{\text{rot}}^3}{\nu_0^2} T, \quad (13)$$

where  $n$  is the radial order, the frequency  $\nu_0$  includes already the effect of rotation on the equilibrium model, the Ledoux constant  $C_{n\ell}$  depends on the mode and model parameters, and the term  $m\nu_{\text{rot}}$  transforms the co-rotating coordinate system to the inertial coordinate system of the observer. The coefficients  $D_0$ ,  $D_1$ ,  $T$  describe non-spherically symmetric distortion due to the centrifugal force as well as the second- and third-order effects of the Coriolis force. In the case of radial mode, this formula reduces to:

$$\nu = \nu_0 + D_0 \frac{\nu_{\text{rot}}^2}{\nu_0}. \quad (14)$$

As was shown long time ago by Simon (1969), the coefficient  $D_0$  amounts to about  $\frac{4}{3}$  independently of the radial order  $n$ . Thus, if  $V_{\text{rot}} \approx 100 \text{ km s}^{-1}$  then  $\nu_{\text{rot}}^{\text{min}} \approx 0.5 \text{ d}^{-1}$  and a correction for the frequencies  $\nu_1$  and  $\nu_2$  is about 0.06 and 0.05, respectively.

In Fig. 8, we compare the run of frequency ratios of radial modes on the Petersen diagrams for three values of the initial rotation:  $V_{\text{rot},0} = 0, 100, 170 \text{ km s}^{-1}$ , where  $V_{\text{rot},0} = 170 \text{ km s}^{-1}$  corresponds to about half the critical rotation. The model parameters are given in the caption and vertical line marks the dominant frequency of V2367 Cyg. The top panel of Fig. 8 shows the frequency ratio of the radial fundamental and first overtone modes,  $\nu(p_1)/\nu(p_2)$ , as a function of the fundamental mode frequency  $\nu(p_1)$ . As one can see, the effect of rotation is huge, in particular, in the main-sequence (MS) phase of evolution. The higher the rotational velocity, the higher the frequency ratio. During the post-main sequence (post-MS) phase the differences in  $\nu(p_1)/\nu(p_2)$  decrease and very quickly all three lines converge. The largest difference in the frequency ratio  $\nu(p_1)/\nu(p_2)$  between the rotational velocity 0 and  $170 \text{ km s}^{-1}$  reaches a value of approximately 0.01. This is well above the observational error and much above the accuracy with which we want to match the theoretical frequencies to the observed ones. Typical fitting accuracy is at least to the fourth decimal place in the frequency ratio.

In the bottom panel of Fig. 8, we depicted the frequency ratio of the first and second overtone modes,  $\nu(p_2)/\nu(p_3)$ , as a function of the first overtone frequency  $\nu(p_2)$ . Again, the effect of rotation is huge but the situation is opposite to the previous one. During most of the MS phase, all three lines  $\nu(p_2)/\nu(p_3)(V_{\text{rot}})$  nearly converge, whereas the differences between various  $V_{\text{rot}}$  start to increase at the end of MS and becomes larger and larger in the post-MS phase. The largest difference in  $\nu(p_2)/\nu(p_3)$  between 0 and  $170 \text{ km s}^{-1}$  is about 0.008. Again, this is well above the observational error and above our requirements in seismic modelling.

The same effects of rotation on the Petersen diagram,

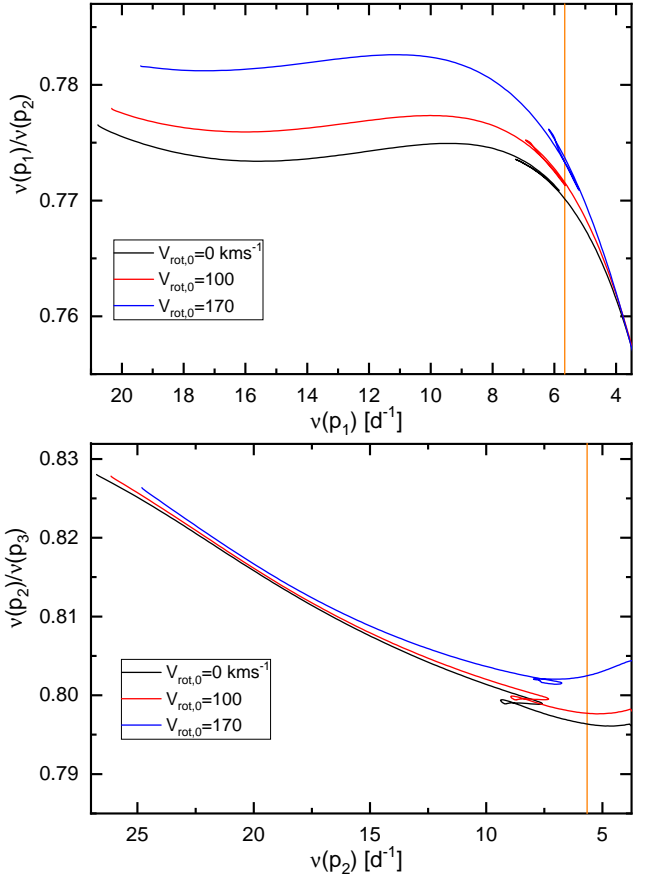


**Figure 8.** The Petersen diagrams for the two pairs of radial modes: fundamental and first overtone (top panel), first and second overtone (bottom panel). The model parameters are:  $M = 2.1 M_{\odot}$ ,  $X_0 = 0.70$ ,  $Z = 0.02$ ,  $\alpha_{\text{MLT}} = 0.5$  and  $\alpha_{\text{ov}} = 0.2$ . The OPAL tables and AGSS09 chemical mixture were adopted. There is shown the effect of rotation (up to the second order) on pulsational frequencies. Models were computed for the three values of the initial rotational velocity  $V_{\text{rot},0} = 0, 100, 170 \text{ km s}^{-1}$ .

$\nu(p_1)/\nu(p_2)$  vs  $\nu(p_1)$ , have already been studied by Suarez et al. (2006) for the rotational velocity up to  $V_{\text{rot}} = 50 \text{ km s}^{-1}$ . Even at such low rotation, the authors obtained differences in  $\nu(p_1)/\nu(p_2)$  on the third decimal place.

One more important effect of rotation, that is not included in Eq. 13, is the rotational coupling of pulsation modes (Chandrasekhar & Lebovitz 1962; Soufi et al. 1998). This effect occurs for the close-frequency modes with the degrees  $\ell$  differing by 2 and with the same azimuthal order  $m$ , i.e.,  $\ell_j = \ell_i + 2$  and  $m_i = m_j$ . Two (or more) modes have close frequencies if their difference is of the order of rotational frequency or less.

In Fig. 9, we show the evolution of frequencies of the pulsational modes with  $\ell = 0$  and  $\ell = 2$ , for the model with parameters:  $M = 2.1 M_{\odot}$ ,  $X_0 = 0.70$ ,  $Z = 0.02$ ,  $\alpha_{\text{MLT}} = 0.5$ ,  $\alpha_{\text{ov}} = 0.2$  and the initial rotation of  $V_{\text{rot},0} = 120 \text{ km s}^{-1}$ . Three phases of evolutions are presented separately: MS (top panel), overall contraction (OC) (middle panel) and hydrogen shell burning (HSB) (bottom panel). We indicated also the value of the rotational frequency on the right-hand Y axis. The three dominant frequencies of V2367 Cyg ( $\nu_1 = 5.66106 \text{ d}^{-1}$ ,  $\nu_2 = 7.14898 \text{ d}^{-1}$ ,  $\nu_3 = 7.77557 \text{ d}^{-1}$ ) are marked with horizontal lines. As one can see, a close encounter of radial and quadrupole modes occurs very often, in particular during

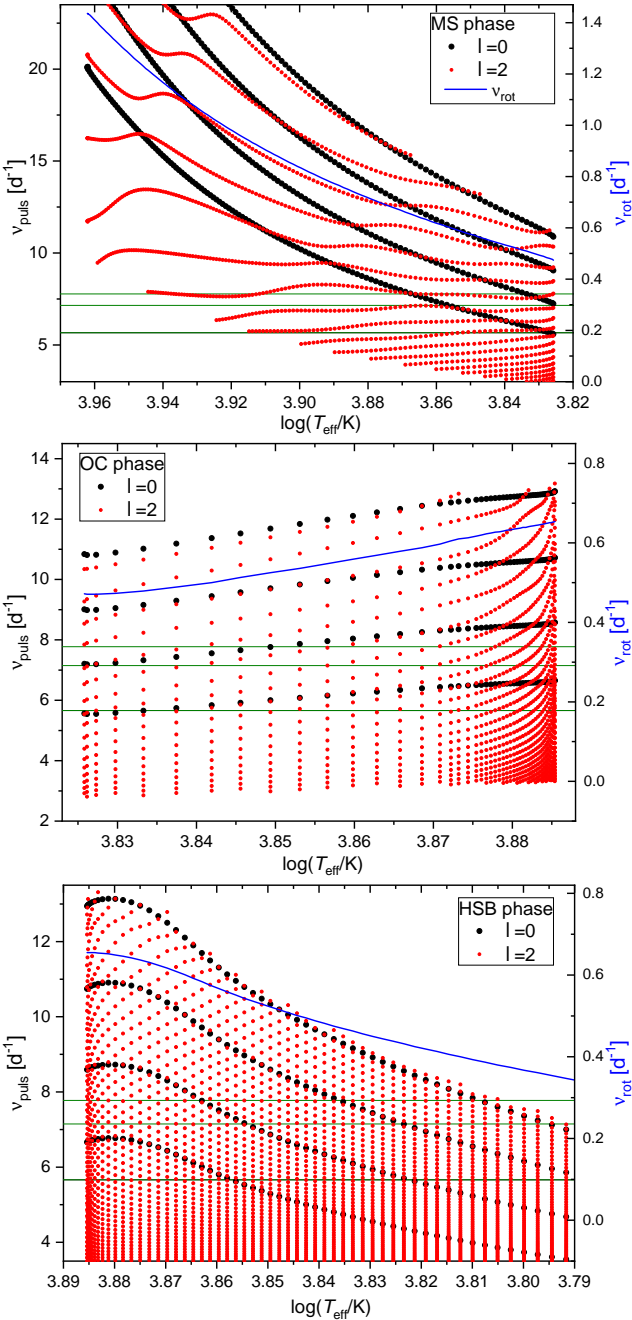


**Figure 9.** The evolution of pulsational frequencies of modes with  $\ell = 0$  and  $\ell = 2$  for the model with the same parameters as in Fig. 8 except for the initial rotation which is here  $V_{\text{rot},0} = 120 \text{ km s}^{-1}$ . Each phases of evolution is presented separately: MS (top panel), OC (middle panel) and HSB (bottom panel). The value of rotational frequency is given on the right-hand Y axis. The horizontal lines mark the values of the three dominant frequencies of V2367 Cyg.

the HSB phase, because of very dense spectrum of nonradial modes.

Using the extended version of W.Dziembowski code (e.g., Daszyńska-Daszkiewicz et al. 2002), which relies on the third order formalism of Soufi et al. (1998), we computed eigenfrequencies of radial modes coupled with the nearest quadrupole mode. In Fig. 10, we show the effect of rotational mode coupling for the first three ra-

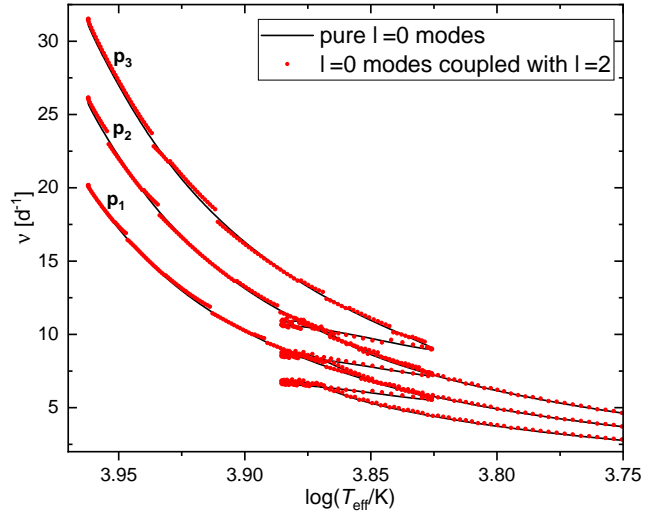


**Figure 10.** The evolution of pulsational frequencies of the pure (solid lines) and coupled (dots) radial modes. The following modes are shown: fundamental ( $p_1$ ), first overtone ( $p_2$ ) and second overtone ( $p_3$ ). The same model as in Fig. 9 was considered.

dial modes. The frequency evolution of pure radial modes and those coupled with the nearest  $\ell = 2$  mode was compared. The same model as before is considered with the initial rotation  $V_{\text{rot},0} = 120 \text{ km s}^{-1}$ . In the case of the MS phase, it is clearly visible that the frequencies of coupled radial modes follow the avoided crossing phenomenon of the  $\ell = 2$  modes. In the HSB phase, the frequencies of coupled radial modes are systematically higher. This comparison suggests rather a small effect of the  $\ell = 0\&2$  rotational coupling on the frequencies of radial modes. However, these small differences produce a huge effect on the Petersen diagrams presented in Fig. 11. The top panel shows the effect of rotational mode coupling if only one radial mode, i.e., the higher overtone, is rotationally coupled with the nearest quadrupole mode. Solid lines represent the frequency ratios of pure radial modes; the lower line corresponds to  $\nu(p_1)/\nu(p_2)$  vs  $\nu(p_1)$  and the upper line corresponds to  $\nu(p_2)/\nu(p_3)$  vs  $\nu(p_2)$ . Red dots correspond to the frequency ratio  $\nu(p_1)/\nu(p_2)$  if the first overtone is coupled and should be compared with the lower solid line. Green dots correspond to the frequency ratio  $\nu(p_2)/\nu(p_3)$  if the second overtone is coupled and should be compared with the upper solid line. In the bottom panel of Fig. 11, we show a similar comparison but if both radial modes are rotationally coupled. As one can see, the second frequency  $\nu_2$  can be easily associated with a radial mode if the effect of rotational mode coupling is taken into account.

## 6 SEISMIC MODELLING OF V2367 CYG

Using the Bayesian analysis based on Monte Carlo simulations, we made an extensive seismic modelling of V2367 Cyg assuming that  $\nu_1$  and  $\nu_2$  are both radial modes and including the rotational mode coupling between the radial and quadrupole modes. Because of the very unique identification of  $\ell = 0$  for the dominant mode  $\nu_1$  (cf. the left panel of Fig. 6) and its high amplitude (about 10 times larger than the amplitude of  $\nu_2$ ), we made the assumption that only the frequency  $\nu_2$  is coupled with the nearest  $\ell = 2$  mode. The same approach was adopted by Balona et al. (2012), who made the first attempt to explain  $\nu_2$  as radial mode through the rotational

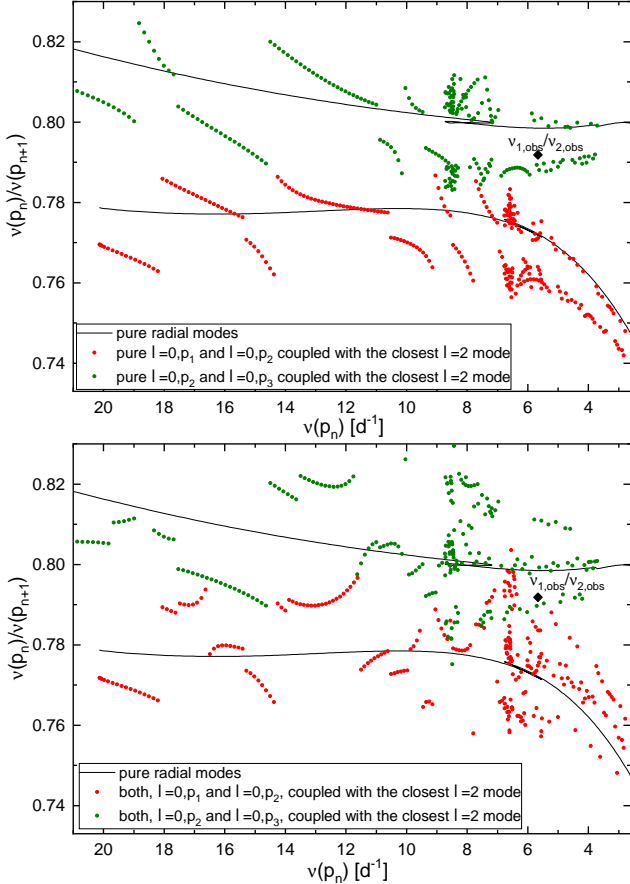


**Figure 11.** The Petersen diagrams for the two pairs of radial modes: fundamental and first overtone (lower solid lines), first and second overtone (upper solid lines). The model parameters are the same as in the case of Fig. 9 with  $V_{\text{rot},0} = 120 \text{ km s}^{-1}$ . The top panel shows the case if one radial mode (a higher overtone) is coupled by rotation with the nearest  $\ell = 2$  mode, whereas in the lower panel both radial modes are coupled.

mode coupling. They provided a sample model which had the radial fundamental mode with the frequency  $v_1$  and the first overtone with the frequency  $7.138 \text{ d}^{-1}$ , which is 0.01 lower than the observed value  $v_2 = 7.14898 \text{ d}^{-1}$ .

It is worth to mention that in the oscillation spectrum of V2367 Cyg, we detected two close-frequency triplets that are nearly equidistant. According to the analysis of the Kepler data these are  $(v_3, v_5, v_8) = (7.77557, 7.85334, 7.68347) \text{ d}^{-1}$  and  $(v_4, v_7, v_{11}) = (9.81587, 10.02421, 10.22938) \text{ d}^{-1}$ . Comparing with pulsational models, these two sequences could be consecutive overtones of  $\ell = 2$  and  $\ell = 1$  modes, respectively. However, without unique identification of the angular numbers ( $\ell, m$ ) of these modes, we cannot include them in seismic modelling. Such modes would provide a very strong selection of parameters and evolutionary stage.

### 6.1 Frequency uncertainty from rotational mode coupling

When two modes are coupled by rotation then the distance between their frequencies increases; in other words, the modes repel each other. This distance becomes larger the closer the frequencies of the two modes are before coupling and the higher the rotational velocity. As a consequence, the frequency of a radial mode can significantly

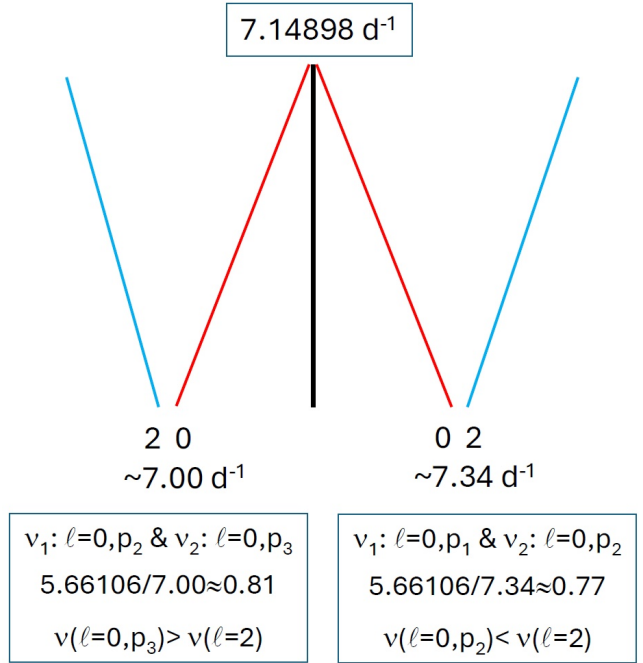


**Figure 12.** A schematic sketch showing the repulsion of modes  $\ell = 0$  and  $\ell = 2$  due to rotational coupling. The observed frequency  $v_2$  is given in the upper box. To the right of a vertical black line, a hypothesis of the radial fundamental mode and first overtone ( $p_1$  &  $p_2$ ) is presented. To the left - a hypothesis of the first and second overtone.

differ from the value given by Eq. (14), hereafter  $v_{\text{Eq14}}$ . Here, we assumed that for the closest approach of  $\ell = 0$  and  $\ell = 2$  modes, the average difference  $\bar{\Delta}v(\ell = 0) = v_{\text{coup}} - v_{\text{Eq14}}$  can be approximated by a linear function of the rotational velocity, i.e.,  $\bar{\Delta}v = a \cdot V_{\text{rot}}$ .

In case of the frequencies  $v_1$  and  $v_2$ , we have to consider two scenarios: 1) they correspond to the radial fundamental and first overtone mode, respectively, (the  $p_1$  &  $p_2$  hypothesis), 2) they correspond to the radial first and second overtone mode, respectively (the  $p_2$  &  $p_3$  hypothesis). A schematic sketch of these two scenarios is presented in Fig. 12. Depending on the scenario a coefficient  $a$  can be positive (first case) or negative (second case) to reach the observed frequency  $v_2$ . We limited our calculations up to the rotational velocity equal to half the critical value, i.e., to  $V_{\text{rot},0} \approx 170 \text{ km s}^{-1}$ .

In case of the  $p_1$  &  $p_2$  hypothesis, the theoretical frequency of the first overtone has to be greater than the observed value  $v_2 = 7.14808 \text{ d}^{-1}$  to give the frequency ratio  $v(p_1)/v(p_2)$  of about 0.77–0.78 as in the case of non-coupling. Moreover,  $v(p_2)$  has to be less than the nearest  $\ell = 2$  mode to be repelled in the right direction, i.e., towards  $v_2$ . In this case, we got the allowed range  $v(p_2) \in (7.14898, v_{\text{max}}) \text{ d}^{-1}$ , where  $v_{\text{max}} = +0.0011236 \cdot V_{\text{rot}} + 7.14898$ .

If the  $p_2$  &  $p_3$  hypothesis is considered, then the theoretical frequency of the second overtone has to be less than the observed value  $v_2$  to give the frequency ratio  $v(p_2)/v(p_3)$  of about 0.80–0.81 as in non-coupling case. In turn,  $v(p_3)$  has to be greater than the nearest  $\ell = 2$  mode to be repelled towards the observed value  $v_2$ . Then, the allowed range for the coupled second overtone was  $v(p_3) \in (v_{\text{min}}, 7.14898) \text{ d}^{-1}$ , where  $v_{\text{min}} = -0.0008765 \cdot V_{\text{rot}} + 7.14898$ .

## 6.2 Seismic models for the two hypotheses

In our seismic modelling, we fitted the dominant frequency  $\nu_1$ , its empirical value of the non-adiabatic complex parameter  $f = (f_R, f_I)$  and the frequency  $\nu_2$  allowing its uncertainty due to rotational coupling within the above estimated ranges. Including the parameter  $f$  into seismic modelling is crucial to get constraints on the efficiency of convection in the outer layers, described by the mixing length parameter  $\alpha_{MLT}$  (Daszyńska-Daszkiewicz et al. 2003). An additional constraint was the consistency of effective temperatures and luminosities of the models with the observed values.

Thus, we had six observables ( $\nu_1, \nu_2, f_R(\nu_1), f_I(\nu_1), T_{\text{eff}}, L$ ) and one could expect that at least five parameters could be derived from our seismic modelling based on MC simulations. However, because of a large "uncertainty" in the second frequency due to allowing for the rotational mode coupling with the  $\ell = 2$  mode, we fixed the initial hydrogen abundance at  $X_0 = 0.70$  and the metallicity at three values  $Z = 0.014, 0.020, 0.030$  from the observed range  $Z \in [0.0134, 0.0356]$ . The parameters to be determined were ( $M, V_{\text{rot}}, \alpha_{\text{ov}}, \alpha_{\text{MLT}}$ ). Guided by our recent results from seismic modelling of double-mode radial HADS stars (Daszyńska-Daszkiewicz et al. 2023) that only with the OPAL opacity tables could we match all observables, we performed all computations with these opacity data.

### The $p_2 \& p_3$ hypothesis

In the first step, we considered that  $\nu_1$  is the first overtone and  $\nu_2$  is the second overtone. We searched for models which reproduce the observables ( $\nu_1, f(\nu_1), T_{\text{eff}}, L$ ) within the  $1-\sigma$  error and for the frequency  $\nu_2$ , we accepted all values from the range  $(\nu_{\min}, 7.14898) \text{ d}^{-1}$ , as described in the previous subsection. We found seismic models of V2367 Cyg which reproduce our observables in the HSB and OC phase, for  $Z = 0.020$  and  $Z = 0.030$  in each phase. The seismic models computed with  $Z = 0.014$  have too low effective temperature and luminosity. In the case of MS models, the first overtone mode never reaches the observed value of the dominant frequency  $\nu_1 = 5.66106 \text{ d}^{-1}$ . Both radial modes are excited in all seismic models. In Table 5, we give the median values for the derived parameters ( $M, V_{\text{rot}}, \alpha_{\text{ov}}, \alpha_{\text{MLT}}$ ) and for the three considered metallicities  $Z$ . For a comparison, we gave also the initial values of rotation  $V_{\text{rot},0}$ . The seismic models for  $Z = 0.014$  were added in Table 5 to demonstrate how their ( $T_{\text{eff}}, L$ ) are far from the observed values, i.e., from  $\log(T_{\text{eff}}/\text{K}) = 3.8495 \pm 0.0246$  and  $\log L/L_{\odot} = 1.5407 \pm 0.1138$ . In the last two columns, we put the empirical values of the intrinsic amplitude of the dominant mode  $|\varepsilon|(\nu_1)$ , as defined by Eq. 6, and the difference  $\Delta\nu_2$  between theoretical and observed values of  $\nu_2$ . The median is more informative statistic for non-Gaussian distributions or distributions with outliers, which is the case for some parameters. The histogram for ( $M, V_{\text{rot}}, \alpha_{\text{ov}}, \alpha_{\text{MLT}}$ ) of the seismic models computed for  $Z = 0.02$  and  $0.03$  are shown in the Appendix B. Uncertainties of parameters in Table 5 were calculated as the 0.84 quantile minus the median and the median minus the 0.16 quantile. These quantiles correspond to one standard deviation from the mean value in the case of a normal distribution.

As one can see, the values of  $(\log T_{\text{eff}}, \log L/L_{\odot}, M)$  are, within the errors, very close in both evolutionary phases. As a consequence for the models with the same  $Z$ , we also got the close empirical values of the mixing length parameter  $\alpha_{\text{MLT}}$ , i.e.,  $\alpha_{\text{MLT}} \approx 0.07$  for  $Z = 0.020$  and  $\alpha_{\text{MLT}} \approx 0.20$  for  $Z = 0.030$ . It means that convection in the envelope of V2367 Cyg is hardly efficient. In turn, significant differences are in the overshooting

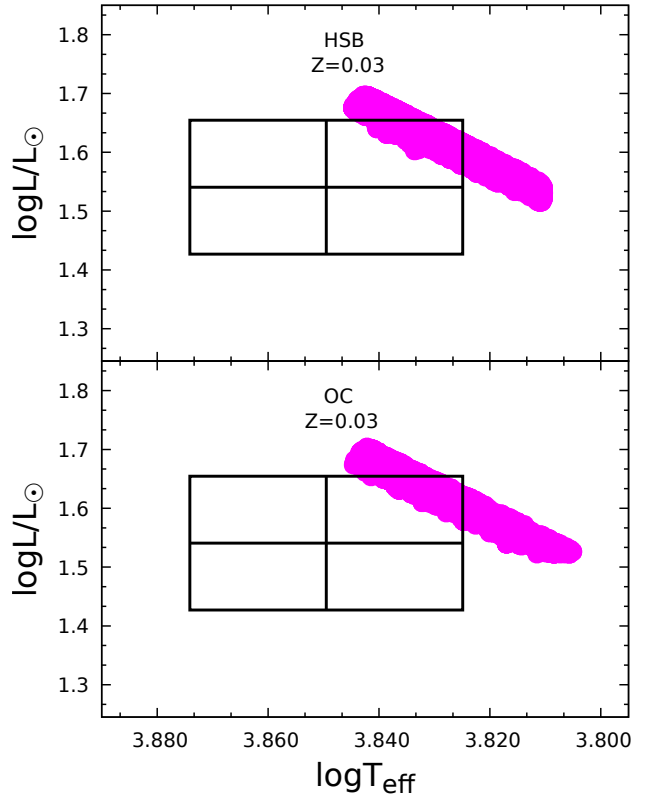


**Figure 13.** The HR diagrams with the position of the HSB (top panel) and OC (bottom panel) seismic models of V2367 Cyg computed with the MC-based Bayesian analysis assuming the  $p_2 \& p_3$  hypothesis. The OPAL table, initial hydrogen abundance  $X_0 = 0.70$  and  $Z = 0.030$  were adopted.

parameter  $\alpha_{\text{ov}}$ , which amounts to  $\alpha_{\text{ov}} \approx 0.15$  for the HSB seismic models and to  $\alpha_{\text{ov}} \approx 0.30$  for the OC models, if  $Z = 0.020$  and  $Z = 0.030$  are considered. The rotational velocity is similar in both phases of evolution with  $V_{\text{rot}} \approx 106 \text{ km s}^{-1}$  for the models with the metallicity  $Z = 0.020$  and  $V_{\text{rot}} \approx 91 \text{ km s}^{-1}$  for models with  $Z = 0.030$ . However, we would like to point out that the uncertainties of  $V_{\text{rot}}$  are of about  $40 \text{ km s}^{-1}$ . The positions of seismic models for  $Z = 0.030$  in the HR diagram along with the error box are shown in Fig. 13. The upper panel contains the seismic models in the HSB phase and the lower panel – in the OC phase.

### The $p_1 \& p_2$ hypothesis

Next, we made seismic modelling assuming that  $\nu_1$  is the radial fundamental mode and  $\nu_2$  is the radial first overtone. All requirements to be fulfilled are the same as above except that for the frequency  $\nu_2$ , we accepted all values from the range  $(7.14898, \nu_{\max}) \text{ d}^{-1}$ . In this case, the number of solutions is much smaller. First of all, only the seismic models with  $Z = 0.030$  reproduce the empirical values of  $f$  (both, the real and imaginary part) within the  $1-\sigma$  error. Such seismic models were found in the OC and HSB evolutionary stages. Their parameters are given in Table 6 and their position on the HR diagram is shown in Fig. 14. As before, the considered radial modes are unstable.

In case of the  $p_1 \& p_2$  hypothesis, the seismic models have much higher rotational velocity, with a median of about  $160 \text{ km s}^{-1}$  in the HSB phase and about  $150 \text{ km s}^{-1}$  in the OC phase. The

**Table 5.** The median of parameters of seismic models of V2367 Cyg from MC simulations assuming the  $p_2\&p_3$  hypothesis. The models were computed with the OPAL opacity tables, initial hydrogen abundance  $X_0 = 0.70$  and the three values of metallicity  $Z = 0.014, 0.020, 0.030$ . Two phases of evolution are possible: HSB and OC. The uncertainties were calculated from quantiles 0.84 and 0.16. The models with  $Z = 0.014$  are outside the error box on the HR diagram and their parameters are given for a comparison.

HSB phase									
$Z$ (fixed)	$\log(T_{\text{eff}}/\text{K})$	$\log L/L_{\odot}$	$M$ [ $M_{\odot}$ ]	$\alpha_{\text{ov}}$	$\alpha_{\text{MLT}}$	$V_{\text{rot},0}$ [km·s $^{-1}$ ]	$V_{\text{rot}}$ [km·s $^{-1}$ ]	$ \varepsilon (\nu_1)$	$\Delta\nu_2$ [d $^{-1}$ ]
0.014	$3.7815^{+0.0030}_{-0.0054}$	$1.352^{+0.009}_{-0.032}$	$1.770^{+0.051}_{-0.024}$	$0.16^{+0.12}_{-0.13}$	$0.08^{+0.06}_{-0.04}$	$140^{+24}_{-17}$	$109^{+21}_{-11}$	$0.0120^{+0.0006}_{-0.0003}$	$-0.092^{+0.008}_{-0.019}$
0.020	$3.8275^{+0.0019}_{-0.0018}$	$1.588^{+0.007}_{-0.008}$	$2.151^{+0.039}_{-0.035}$	$0.15^{+0.13}_{-0.1}$	$0.08^{+0.05}_{-0.05}$	$135^{+42}_{-45}$	$107^{+38}_{-37}$	$0.0126^{+0.0003}_{-0.0002}$	$-0.063^{+0.014}_{-0.024}$
0.030	$3.8324^{+0.0066}_{-0.0077}$	$1.636^{+0.032}_{-0.037}$	$2.370^{+0.048}_{-0.051}$	$0.15^{+0.12}_{-0.10}$	$0.20^{+0.11}_{-0.13}$	$114^{+48}_{-48}$	$91^{+42}_{-39}$	$0.0122^{+0.0003}_{-0.0005}$	$-0.040^{+0.008}_{-0.016}$
OC phase									
$Z$ (fixed)	$\log(T_{\text{eff}}/\text{K})$	$\log L/L_{\odot}$	$M$ [ $M_{\odot}$ ]	$\alpha_{\text{ov}}$	$\alpha_{\text{MLT}}$	$V_{\text{rot},0}$ [km·s $^{-1}$ ]	$V_{\text{rot}}$ [km·s $^{-1}$ ]	$ \varepsilon (\nu_1)$	$\Delta\nu_2$ [d $^{-1}$ ]
0.014	$3.7824^{+0.0021}_{-0.0079}$	$1.357^{+0.009}_{-0.045}$	$1.807^{+0.030}_{-0.085}$	$0.41^{+0.07}_{-0.02}$	$0.11^{+0.02}_{-0.05}$	$151^{+26}_{-14}$	$119^{+13}_{-15}$	$0.0119^{+0.0008}_{-0.0001}$	$-0.099^{+0.009}_{-0.013}$
0.020	$3.8274^{+0.0018}_{-0.0017}$	$1.590^{+0.009}_{-0.010}$	$2.168^{+0.057}_{-0.068}$	$0.34^{+0.06}_{-0.05}$	$0.07^{+0.05}_{-0.05}$	$141^{+42}_{-52}$	$105^{+35}_{-39}$	$0.0126^{+0.0002}_{-0.0002}$	$-0.063^{+0.015}_{-0.021}$
0.030	$3.8326^{+0.0064}_{-0.0078}$	$1.640^{+0.031}_{-0.037}$	$2.398^{+0.082}_{-0.098}$	$0.28^{+0.07}_{-0.05}$	$0.20^{+0.12}_{-0.13}$	$120^{+52.9}_{-49.3}$	$91^{+40}_{-38}$	$0.0122^{+0.0003}_{-0.0005}$	$-0.042^{+0.011}_{-0.015}$

**Table 6.** The median of parameters of seismic models of V2367 Cyg from MC simulations assuming the  $p_1\&p_2$  hypothesis. Two phases of evolution are possible : HSB and OC. Only models computed with  $Z = 0.030$  meet all the requirements described in the text.

$Z = 0.03$ (fixed)									
phase of evolution	$\log(T_{\text{eff}}/\text{K})$	$\log L/L_{\odot}$	$M$ [ $M_{\odot}$ ]	$\alpha_{\text{ov}}$	$\alpha_{\text{MLT}}$	$V_{\text{rot},0}$ [km·s $^{-1}$ ]	$V_{\text{rot}}$ [km·s $^{-1}$ ]	$ \varepsilon (\nu_1)$	$\Delta\nu_2$ [d $^{-1}$ ]
HSB	$3.8420^{+0.0048}_{-0.0061}$	$1.498^{+0.024}_{-0.031}$	$2.237^{+0.030}_{-0.038}$	$0.08^{+0.06}_{-0.05}$	$0.19^{+0.12}_{-0.13}$	$182^{+12}_{-11}$	$162^{+12}_{-11}$	$0.0124^{+0.0006}_{-0.0002}$	$0.161^{+0.006}_{-0.006}$
OC	$3.8426^{+0.0041}_{-0.0059}$	$1.513^{+0.023}_{-0.033}$	$2.31^{+0.087}_{-0.120}$	$0.09^{+0.06}_{-0.05}$	$0.19^{+0.12}_{-0.12}$	$185^{+11}_{-10}$	$152^{+13}_{-11}$	$0.0124^{+0.0005}_{-0.0003}$	$0.152^{+0.016}_{-0.011}$

overshooting parameter  $\alpha_{\text{ov}}$  is lower than in case of the  $p_2\&p_3$  hypothesis, i.e.,  $\alpha_{\text{ov}} \approx 0.1$ . The mixing length parameter  $\alpha_{\text{MLT}}$  has a similar value of about 0.2.

Independent of the adopted hypothesis, the intrinsic mode amplitudes  $|\varepsilon|$  of the dominant frequency  $\nu_1$  is about 0.012.

## 7 SUMMARY

Asteroseismology of moderate and fast rotators is a challenging task. Rotation affects equilibrium stellar models, their pulsation as well as mode identification based on the photometric amplitudes and phases. We cannot also expect equidistant patters resulting from the rotational splitting. Besides the main effects of rotation, i.e., centrifugal and Coriolis forces, we have also to take into account a possibility of mode coupling even if the rotation is not too fast.

In this paper, we presented a comprehensive analysis of the HADS star V2367 Cyg using all available observational data. We analysed the whole space photometry of V2367 Cyg, both from *Kepler* and *TESS* mission. We confirmed all frequencies found by Balona et al. (2012), including the three dominant ones, and found much more.

Then, we performed identification of the mode degree  $\ell$  from the photometric amplitudes and phases using data of Ulusoy et al. (2013) for the three main frequencies. We got an unambiguous iden-

tification for the dominant frequency  $\nu_1$ , i.e., the radial mode. Determination of  $\ell$  was less successful for  $\nu_2$  and  $\nu_3$  but, because of the visibility effect, the most probable degrees were  $\ell = 0$  or  $\ell = 2$ . From a comparison of the theoretical values of frequency ratios, we concluded that only  $\nu_2$  can be a radial mode, but only if the higher order effects of rotation, including mode coupling, are taken into account. It has already been suggested by Balona et al. (2012) who initiated seismic study of V2367 Cyg but in a limited space of parameters. Here we performed the first extensive seismic modelling that takes into account mode coupling by rotation.

Assuming that  $\nu_1$  and  $\nu_2$  are both radial modes and including the non-adiabatic parameter  $f$  of the dominant frequency, we made extended seismic modelling using the Bayesian analysis based on MC simulations. About one million models were computed in total. Two hypotheses had to be considered: 1)  $\nu_1$  and  $\nu_2$  correspond to the radial first and second overtone, respectively (the  $p_2\&p_3$  hypothesis) and 2)  $\nu_1$  and  $\nu_2$  correspond to the radial fundamental and first overtone, respectively (the  $p_1\&p_2$  hypothesis). All models which met our requirements are in the post-MS phase of evolution, either the hydrogen-shell burning (HSB) or overall contraction (OC), regardless of the assumed hypothesis. Besides, all have a moderate or quite fast rotation to account for the frequency ratio of the two radial modes. The rotational velocity is much higher for the seismic models obtained with the  $p_1\&p_2$  hypothesis, with the median value

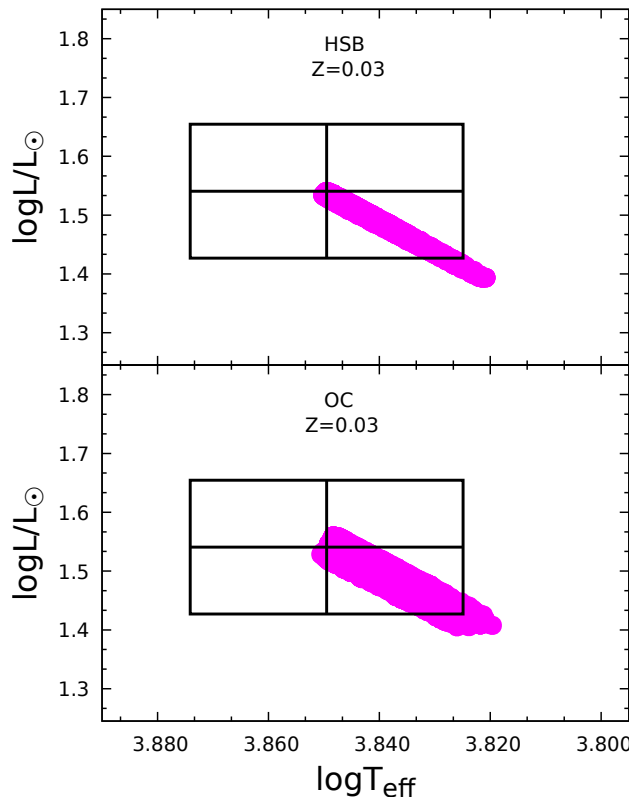


**Figure 14.** The HR diagrams with the position of the HSB (top panel) and OC (bottom panel) seismic models of V2367 Cyg computed with the MC-based Bayesian analysis assuming the  $p_1 \& p_2$  hypothesis. The OPAL table, initial hydrogen abundance  $X_0 = 0.70$  and  $Z = 0.030$  were adopted.

of about  $150 - 160 \text{ km s}^{-1}$ . If the  $p_2 \& p_3$  hypothesis is adopted then the median of  $V_{\text{rot}}$  amounts to  $90 - 110 \text{ km s}^{-1}$ .

Independent of the adopted hypothesis, from our seismic analysis we obtained small values of the mixing length parameter in the total range of  $\alpha_{\text{MLT}} \in (0.01, 0.33)$ . Thus, convective transport of energy in the outer layers of V2367 Cyg is hardly efficient or even completely inefficient.

In the case of the  $p_2 \& p_3$  hypothesis, the value of the overshooting parameter depends on the evolutionary phase. We obtained  $\alpha_{\text{ov}} \in (0.02, 0.29)$  for the HSB models and  $\alpha_{\text{ov}} \in (0.23, 0.40)$  for the OC models. Adopting the  $p_1 \& p_2$  hypothesis, we got similar values of  $\alpha_{\text{ov}}$  for both evolutionary stages (HSB and OC), which amount to about  $\alpha_{\text{ov}} \in (0.03, 0.15)$ .

Our seismic analysis of V2367 Cyg clearly indicates that the star is in a post-MS phase of evolution, either in HSB or in OC. However, it is difficult to say which stage is more preferred and which hypothesis for two radial modes,  $p_2 \& p_3$  or  $p_1 \& p_2$ , is more likely. Perhaps, new time-series multi-colour photometry and spectroscopy would allow for the unambiguous mode identification of a larger number of frequencies. Then, the inclusion of additional modes in seismic modelling would provide additional selection. For example, one could try to incorporate the frequency  $\nu_3$  as a quadrupole mode. However, to make this possible, it would first be necessary to identify its azimuthal order  $m$ .

## ACKNOWLEDGEMENTS

This work has made use of data from the European Space Agency (ESA) mission Gaia (<https://www.cosmos.esa.int/gaia>), processed by the Gaia Data Processing and Analysis Consortium (DPAC; <https://www.cosmos.esa.int/web/gaia/dpac/consortium>). Funding for the DPAC has been provided by national institutions, in particular the institutions participating in the Gaia Multilateral Agreement.

This paper includes data collected by the TESS mission. Funding for the TESS mission is provided by the NASA Explorer Program.

This paper includes data collected by the Kepler mission and obtained from the MAST data archive at the Space Telescope Science Institute (STScI). Funding for the Kepler mission is provided by the NASA Science Mission Directorate. STScI is operated by the Association of Universities for Research in Astronomy, Inc., under NASA contract NAS 5-26555.

Calculations were carried out using resources provided by Wroclaw Centre for Networking and Supercomputing (<http://wcss.pl>), grant no. 265.

## DATA AVAILABILITY

The Kepler and TESS data are available from the NASA MAST portal <https://archive.stsci.edu/>. Theoretical computations will be shared on reasonable request to the corresponding author.

## REFERENCES

- Akerlof C., et al. 2000, AJ, 119, 1901
- Anders F., Khalatyan J., Queiroz A. B. A., et al. 2022, A&A, 658, 91
- Asplund M., Grevesse N., Sauval A. J., Scott P., 2009, Annu.Rev.Astron.Astrophys., 47, 481
- Balona L. A., Stobie P., 1979, MNRAS, 189, 649
- Balona L. A., Lenz P., Antoci V., et al. 2012, MNRAS, 419, 3028
- Baran A. S., Koen C., 2021, Acta Astron., 71, 113
- Bedding T. R., Murphy S. J., Hey D. R., et al. 2020, Nature, 581, 147
- Borucki W. J., et al., 2010, Science, 327, 977
- Breger M., 2000, Delta Scuti and Related Stars, 210, 3
- Canuto V. M., Goldman I., Mazzitelli I., 1996, ApJ, 473, 550
- Chandrasekhar S., Lebovitz N. R., 1962, ApJ, 136, 1105
- Claret A., 2000, A&A, 363, 1081
- Daszyńska-Daszkiewicz J., Dziembowski W. A., Pamyatnykh A. A., Goupil M.-J., 2002, A&A, 392, 151
- Daszyńska-Daszkiewicz J., Dziembowski W. A., Pamyatnykh A. A., 2003, A&A, 407, 999
- Daszyńska-Daszkiewicz J., Dziembowski W. A., Pamyatnykh A. A., 2005, A&A, 441, 641
- Daszyńska-Daszkiewicz J., Pamyatnykh A. A., Walczak P., Szewczuk W., 2020, MNRAS, 499, 3034
- Daszyńska-Daszkiewicz J., Pamyatnykh A. A., Walczak P., Szewczuk W., 2022, MNRAS, 512, 3551
- Daszyńska-Daszkiewicz J., Walczak P., Pamyatnykh A. A., Szewczuk W., Niewiadomski W., 2023, ApJ, 924
- Dziembowski W. A., 1977, Acta Astr., 27, 95
- Dziembowski W. A., Pamyatnykh A. A., 2008, MNRAS, 385, 2061
- Frasca A., Molenda-Zakowicz J., De Cat P., et al. 2016, A&A, 594, 39
- Gough D. O., Thompson M. J., 1990, MNRAS, 242, 25
- Heiter U., Kupka F., van't Veer-Mennen C., et al. 2002, A&A, 392, 619
- Iglesias C. A., Rogers F. J., 1996, ApJ, 464, 943
- Jin H., Kim S., Kwon S., Youn J., et al. 2003, A&A, 404, 621
- Koch D. G., et al., 2010, ApJ, 713, L79
- Leroy B., 2012, A&A, 545, A50
- Lomb N. R., 1976, Ap&SS, 39, 447

- Loumos G. L., Deeming T. J., 1978, Ap&SS, 56, 285  
Niemczura E., Polińska M., Murphy S. J., et al. 2017, MNRAS, 470, 2870  
Pamyatnykh A. A., 1999, Acta Astr., 49, 119  
Pamyatnykh A. A., 2003, Ap&SS, 284, 97  
Pigulski A., Pojmanski G., Pilecki B., Szczygiel D. M., 2009, Acta Astron.,  
59, 33  
Ricker G. R., et al., 2015, Journal of Astronomical Telescopes, Instruments,  
and Systems, 1, 014003  
Rogers F. J., Nayfonov A., 2002, ApJ, 576, 1064  
Rogers F. J., Swenson F. J., Iglesias C. A., 1996, ApJ, 456, 902  
Scargle J. D., 1982, ApJ, 263, 835  
Schwarzenberg-Czerny A., 1991, MNRAS, 253, 198  
Simon R., 1969, A&A, 2, 390  
Soufi F., Goupil M. J., Dziembowski W. A., 1998, A&A, 334, 91  
Suarez J. C., Garrido R., Goupil M. J., 2006, A&A, 447, 649  
Suarez J. C., Garrido R., Moya A., 2007, A&A, 474, 961  
Ulusoy C., Gülmез T., Statyeva I., et al. 2013, MNRAS, 428, 3551  
Uytterhoeven K., Moya A., Grigahcén A., et al. 2011, A&A, 534, 125  
Watson R. D., 1988, Ap&SS, 140, 255

**APPENDIX A: FREQUENCIES FROM THE FOURIER  
ANALYSIS OF THE KEPLER AND TESS LIGHT CURVES**

Table A1: All frequencies detected in *Kepler* SC data with  $S/N > 5$ . Columns contain: number, our  $ID_K$ , frequency, amplitude, phase and signal to noise ratio.

#	$ID_K$	$\nu$ [d $^{-1}$ ]	$A$ [ppt]	$\phi$ [0 – 1]	$S/N$
1	$\nu_1$	5.661058(2)	156.998(2)	0.872513(3)	75.7
2	$2\nu_1$	11.322118(3)	50.863(2)	0.650089(8)	76.0
3	$\nu_2$	7.148954(7)	17.050(2)	0.99924(2)	72.6
4	$3\nu_1$	16.983178(5)	16.695(2)	0.44384(2)	74.6
5	$\nu_3$	7.775571(9)	8.922(2)	0.95486(5)	67.6
6	$1\nu_1 + 1\nu_2$	12.810015(8)	8.300(2)	0.71374(5)	71.4
7	$4\nu_1$	22.644241(7)	8.227(2)	0.19484(5)	73.0
8	$-1\nu_1 + 1\nu_2$	1.487893(9)	5.715(2)	0.4046(1)	70.2
9	$1\nu_1 + 1\nu_3$	13.436644(9)	5.046(2)	0.7212(1)	64.3
10	$2\nu_1 + 1\nu_2$	18.47107(1)	4.282(2)	0.5003(1)	69.1
11	$5\nu_1$	28.30530(1)	3.941(2)	0.9703(1)	71.3
12	$-1\nu_1 + 1\nu_3$	2.11451(1)	3.373(2)	0.3345(1)	65.6
13	$2\nu_1 + 1\nu_3$	19.09770(1)	3.093(2)	0.4674(1)	56.0
14	$-2\nu_1 + 3\nu_2$	10.12259(1)	2.590(2)	0.4603(1)	39.1
15	$2\nu_1 - 1\nu_2$	4.17317(1)	2.160(2)	0.8550(1)	58.6
16	$\nu_4$	9.81587(1)	2.113(2)	0.5615(1)	43.8
17	$6\nu_1$	33.96636(1)	1.943(2)	0.7371(2)	69.2
18	$3\nu_1 + 1\nu_2$	24.13214(1)	1.946(2)	0.2797(2)	65.2
19	$\nu_5$	7.85334(2)	1.528(2)	0.4139(2)	48.3
20	$3\nu_1 + 1\nu_3$	24.75876(2)	1.534(2)	0.2467(2)	50.8
21	$2\nu_1 - 1\nu_3$	3.54655(2)	1.487(2)	0.9810(2)	55.0
22	$\nu_6$	2.95671(2)	1.359(2)	0.3161(2)	42.9
23	$4\nu_1 + 1\nu_2$	29.79320(2)	1.230(2)	0.0559(3)	61.1
24	$-1\nu_1 + 3\nu_2$	15.78366(2)	1.208(2)	0.1664(3)	38.8
25	$\nu_7$	10.02421(2)	1.223(2)	0.6596(3)	39.4
26	$\nu_8$	7.68347(2)	1.092(2)	0.3050(3)	52.8
27	$1\nu_1 + 1\nu_4$	15.47693(2)	1.004(2)	0.2729(3)	44.1
28	$1\nu_1 - 1\nu_6$	2.70434(2)	1.002(2)	0.0026(3)	44.9
29	$7\nu_1$	39.62742(2)	0.974(2)	0.5257(3)	66.6
30	$1\nu_1 + 1\nu_5$	13.51438(2)	0.861(2)	0.2087(4)	33.7
31	$3\nu_1 - 1\nu_2$	9.83422(2)	0.872(2)	0.6075(4)	41.5
32	$4\nu_1 + 1\nu_3$	30.41982(2)	0.865(2)	0.0176(4)	53.0
33	$\nu_9$	19.39129(2)	0.806(2)	0.8494(4)	28.5
34	$3\nu_1 - 1\nu_3$	9.20759(2)	0.754(2)	0.7605(4)	39.0
35	$1\nu_2 + 1\nu_3$	14.92452(3)	0.731(2)	0.8821(4)	44.8
36	$5\nu_1 + 1\nu_2$	35.45426(2)	0.716(2)	0.8316(4)	56.1
37	$1\nu_1 + 1\nu_6$	8.61776(2)	0.677(2)	0.0974(5)	34.3
38	$1\nu_1 + 1\nu_8$	13.34449(3)	0.625(2)	0.0967(5)	30.0
39	$8\nu_3 - 4\nu_7$	22.10873(3)	0.603(2)	0.1350(5)	25.5
40	$3\nu_2$	21.44471(3)	0.593(2)	0.9400(5)	32.3
41	$2\nu_2$	14.29782(3)	0.581(2)	0.9076(5)	36.0
42	$1\nu_1 + 1\nu_7$	15.68529(3)	0.571(2)	0.3542(5)	38.6
43	$-1\nu_1 + 1\nu_5$	2.19229(3)	0.556(2)	0.7936(6)	38.3
44	$1\nu_1 + 1\nu_2 + 1\nu_3$	20.58561(3)	0.560(2)	0.5300(5)	43.7
45	$1\nu_1 + 1\nu_9$	25.05235(3)	0.562(2)	0.6652(5)	31.2
46	$2\nu_1 - 1\nu_6$	8.36541(3)	0.532(2)	0.7869(6)	35.5
47	$\nu_{10}$	16.54373(3)	0.520(2)	0.1694(6)	19.6
48	$2\nu_1 + 1\nu_5$	19.17541(3)	0.500(2)	0.9640(6)	24.4
49	$-3\nu_1 + 3\nu_2$	4.46152(3)	0.506(2)	0.7356(6)	35.7
50	$2\nu_1 + 1\nu_4$	21.13800(3)	0.499(2)	0.0320(6)	36.7
51	$2\nu_1 + 1\nu_6$	14.27881(3)	0.497(2)	0.8934(6)	40.0
52	$8\nu_1$	45.28848(3)	0.492(2)	0.3191(6)	62.3
53	$1\nu_1 + 2\nu_2$	19.95889(3)	0.487(2)	0.6016(6)	31.6
54	$5\nu_1 + 1\nu_3$	36.08089(3)	0.483(2)	0.7887(6)	49.6
55	$5\nu_1 + 1\nu_3 - 2\nu_4$	16.44769(3)	0.489(2)	0.3313(6)	20.7
56	$2\nu_2 + 2\nu_4 - 1\nu_8$	26.24667(3)	0.441(2)	0.2932(7)	41.9
57	$2\nu_3 - 2\nu_5 + 1\nu_{10}$	16.38989(3)	0.444(2)	0.2872(7)	21.0
58	$5\nu_1 + 1\nu_2 - 1\nu_8$	27.76978(3)	0.419(2)	0.8800(7)	26.0

Table A1: continued

#	$ID_K$	$\nu$ [d $^{-1}$ ]	$A$ [ppt]	$\phi$ [0 – 1]	S/N
59	$-1\nu_1 + 1\nu_4$	4.15482(3)	0.414(2)	0.8158(7)	37.9
60	$-1\nu_1 + 1\nu_8$	2.02241(3)	0.404(2)	0.6811(8)	38.4
61	$6\nu_1 + 1\nu_2$	41.11532(3)	0.400(2)	0.6068(8)	52.0
62	instrumental	0.00255(3)	0.350(2)	0.7923(9)	11.6
63	$2\nu_1 + 1\nu_8$	19.00555(3)	0.377(2)	0.8412(8)	23.6
64	$\nu_{11}$	10.22938(3)	0.388(2)	0.8355(8)	27.6
65	$2\nu_1 + 2\nu_6 - 1\nu_7$	7.21331(3)	0.382(2)	0.0601(8)	34.8
66	$-1\nu_7 + 1\nu_9 + 1\nu_{11}$	19.59607(3)	0.378(2)	0.3057(8)	21.5
67	$-1\nu_1 + 2\nu_2$	8.63688(3)	0.361(2)	0.2120(9)	29.7
68	$2\nu_2 + 1\nu_5$	22.14933(4)	0.356(2)	0.8694(9)	16.9
69	$-1\nu_2 + 1\nu_3$	0.62661(3)	0.356(2)	0.3725(9)	26.4
70	$1\nu_1 + 1\nu_{10}$	22.20481(3)	0.345(2)	0.8353(9)	17.2
71	$3\nu_1 + 1\nu_6$	19.93970(3)	0.339(2)	0.8487(9)	35.0
72	instrumental	0.02188(4)	0.324(2)	0.713(1)	11.1
73	$-2\nu_2 + 3\nu_5$	9.26346(3)	0.323(2)	0.234(1)	26.9
74	$9\nu_4 - 9\nu_8$	19.19329(4)	0.343(2)	0.5218(9)	22.6
75	$4\nu_{10} - 4\nu_{11}$	25.25714(4)	0.327(2)	0.0935(9)	22.2
76	$\nu_{12}$	22.12973(4)	0.321(2)	0.231(1)	18.0
77	$2\nu_2 + 1\nu_7 - 1\nu_8$	16.63934(4)	0.320(2)	0.302(1)	17.0
78	$-1\nu_4 + 2\nu_8 + 1\nu_{10}$	22.09576(4)	0.326(2)	0.4784(9)	19.5
79	$1\nu_3 - 1\nu_5 + 1\nu_{12}$	22.05087(4)	0.310(2)	0.035(1)	20.7
80	$-10\nu_1 + 4\nu_{12}$	31.90773(4)	0.282(2)	0.063(1)	33.5
81	$2\nu_1 + 1\nu_7$	21.34637(4)	0.285(2)	0.117(1)	28.6
82	$4\nu_1 - 1\nu_3$	14.86868(4)	0.278(2)	0.551(1)	31.6
83	$3\nu_1 - 1\nu_6$	14.02646(4)	0.278(2)	0.568(1)	22.5
84	$-10\nu_5 + 9\nu_{11}$	13.53223(4)	0.287(2)	0.724(1)	17.8
85	$-1\nu_1 + 1\nu_{12}$	16.46868(4)	0.268(2)	0.442(1)	15.9
86	$2\nu_1 + 2\nu_2$	25.61993(4)	0.269(2)	0.446(1)	30.9
87	$6\nu_1 + 1\nu_3$	41.74195(4)	0.267(2)	0.572(1)	41.3
88	$-1\nu_1 - 1\nu_4 + 1\nu_6$	1.19956(4)	0.265(2)	0.709(1)	28.2
89	$-2\nu_2 + 4\nu_8$	16.43463(4)	0.256(2)	0.722(1)	16.3
90	$3\nu_1 + 1\nu_5$	24.83648(4)	0.251(2)	0.742(1)	23.3
91	$2\nu_5 - 1\nu_7 + 1\nu_{12}$	27.81025(4)	0.253(2)	0.685(1)	17.7
92	$2\nu_1 - 1\nu_5$	3.46878(4)	0.247(2)	0.518(1)	22.3
93	$3\nu_1 - 1\nu_{10}$	0.43970(4)	0.249(2)	0.685(1)	13.1
94	$-3\nu_1 - 3\nu_4 + 2\nu_{10}$	6.28767(4)	0.248(2)	0.979(1)	26.4
95	$9\nu_1$	50.94953(4)	0.245(2)	0.124(1)	55.1
96	$2\nu_3 + 1\nu_5 + 1\nu_7$	33.43083(4)	0.247(2)	0.622(1)	24.2
97	$\nu_{13}$	16.42229(4)	0.238(2)	0.966(1)	16.8
98	$4\nu_1 + 1\nu_2 - 1\nu_9$	10.40196(4)	0.238(2)	0.699(1)	19.7
99	instrumental	0.01577(4)	0.226(2)	0.167(1)	9.0
100	$4\nu_1 + 1\nu_6$	25.60068(4)	0.238(2)	0.712(1)	33.5
101	$-1\nu_2 + 3\nu_4$	22.30043(4)	0.237(2)	0.978(1)	18.3
102	$-1\nu_1 + 1\nu_7$	4.36313(4)	0.239(2)	0.933(1)	30.5
103	$\nu_{14}$	13.33679(4)	0.234(2)	0.870(1)	14.9
104	$1\nu_1 + 1\nu_{13}$	22.08330(5)	0.227(2)	0.835(1)	19.5
105	$1\nu_1 + 1\nu_{12}$	27.79080(4)	0.225(2)	0.965(1)	16.8
106	$1\nu_1 + 3\nu_2$	27.10582(4)	0.227(2)	0.682(1)	22.4
107	$7\nu_3 - 2\nu_{14}$	27.75677(4)	0.229(2)	0.258(1)	17.9
108	instrumental	0.01019(4)	0.213(2)	0.235(1)	8.5
109	$2\nu_1 + 1\nu_{10}$	27.86586(4)	0.216(2)	0.603(1)	19.2
110	$9\nu_6 - 1\nu_7$	16.58671(5)	0.213(2)	0.973(1)	15.5
111	$-8\nu_1 + 9\nu_{11}$	46.77639(4)	0.218(2)	0.395(1)	44.5
112	$2\nu_1 + 1\nu_9$	30.71345(5)	0.216(2)	0.304(1)	24.2
113	$-1\nu_1 + 1\nu_{10}$	10.88236(5)	0.203(2)	0.026(2)	16.1
114	$-9\nu_1 + 4\nu_{12}$	37.56880(5)	0.205(2)	0.835(2)	31.9
115	$3\nu_1 + 1\nu_4$	26.79908(5)	0.201(2)	0.792(2)	22.1
116	$-1\nu_1 + 2\nu_2 + 1\nu_5$	16.48918(5)	0.203(2)	0.489(2)	15.0
117	$3\nu_1 + 1\nu_8$	24.66660(5)	0.190(2)	0.629(2)	19.7

Table A1: continued

#	ID <sub>K</sub>	$\nu$ [d <sup>-1</sup> ]	A [ppt]	$\phi$ [0 – 1]	S/N
118	$1\nu_1 + 2\nu_3$	21.21222(5)	0.192(2)	0.567(2)	25.4
119	$3\nu_1 + 2\nu_2$	31.28099(5)	0.192(2)	0.235(2)	26.9
120	$-9\nu_1 + 6\nu_7$	9.19411(5)	0.193(2)	0.428(2)	18.5
121	instrumental	0.03466(5)	0.199(2)	0.730(2)	8.0
122	$2\nu_3$	15.55120(5)	0.192(2)	0.731(2)	20.8
123	$6\nu_7 - 4\nu_8$	29.41195(5)	0.183(2)	0.684(2)	21.6
124	$2\nu_1 - 1\nu_4$	1.50629(5)	0.184(2)	0.605(2)	24.1
125	$-7\nu_2 + 10\nu_3$	27.71195(5)	0.183(2)	0.771(2)	18.0
126	$-2\nu_2 - 2\nu_6 + 2\nu_{10}$	12.87436(5)	0.180(2)	0.775(2)	17.1
127	$-3\nu_5 + 9\nu_6$	3.05249(5)	0.179(2)	0.854(2)	13.1
128	$4\nu_7 - 3\nu_{11}$	9.40932(5)	0.177(2)	0.405(2)	17.0
129	$4\nu_1 - 1\nu_6$	19.68759(5)	0.175(2)	0.350(2)	16.3
130	$-1\nu_8 + 1\nu_{14}$	5.65355(6)	0.176(2)	0.286(2)	10.6
131	$2\nu_1 - 1\nu_8$	3.63866(5)	0.171(2)	0.632(2)	21.1
132	$5\nu_1 - 3\nu_2$	6.86056(5)	0.170(2)	0.450(2)	19.7
133	$-4\nu_3 + 4\nu_{10}$	35.07300(6)	0.168(2)	0.526(2)	21.7
134	$\nu_{15}$	39.09191(6)	0.168(2)	0.349(2)	23.9
135	$2\nu_8 + 2\nu_{11} - 1\nu_{13}$	19.40417(5)	0.167(2)	0.191(2)	13.8
136	$-2\nu_1 + 4\nu_2$	17.27156(6)	0.164(2)	0.320(2)	19.5
137	$2\nu_6 - 2\nu_{10} + 2\nu_{13}$	5.66864(6)	0.162(2)	0.464(2)	10.1
138	$1\nu_4 + 8\nu_6$	33.47114(6)	0.161(2)	0.527(2)	17.9
139	$1\nu_2 + 1\nu_7$	17.17313(6)	0.163(2)	0.564(2)	20.8
140	$-2\nu_1 + 2\nu_4 + 1\nu_{10}$	24.85434(6)	0.162(2)	0.274(2)	18.0
141	$5\nu_1 + 1\nu_6$	31.26170(6)	0.153(2)	0.556(2)	25.8
142	$7\nu_1 + 1\nu_3$	47.40301(6)	0.153(2)	0.363(2)	36.3
143	$2\nu_1 + 1\nu_{13}$	27.74440(6)	0.149(2)	0.525(2)	16.5
144	$4\nu_1 + 2\nu_2$	36.94206(6)	0.150(2)	0.007(2)	27.7
145	$2\nu_4 - 1\nu_8$	11.94874(6)	0.150(2)	0.740(2)	18.3
146	$\nu_{16}$	22.24766(6)	0.147(2)	0.743(2)	13.3
147	$2\nu_1 + 2\nu_3$	26.87329(6)	0.146(2)	0.300(2)	19.2
148	$-2\nu_9 + 3\nu_{16}$	27.96148(6)	0.145(2)	0.726(2)	17.3
149	$4\nu_1 + 1\nu_5$	30.49754(6)	0.142(2)	0.512(2)	19.8
150	$4\nu_1 - 1\nu_2$	15.49529(6)	0.146(2)	0.415(2)	17.7
151	$2\nu_5 + 2\nu_7 - 2\nu_{13}$	2.91081(6)	0.143(2)	0.866(2)	11.3
152	$5\nu_1 - 1\nu_3$	20.52973(6)	0.142(2)	0.388(2)	20.1
153	$4\nu_1 + 1\nu_9$	42.03551(6)	0.141(2)	0.765(2)	31.0
154	$8\nu_6 - 1\nu_7$	13.63021(6)	0.143(2)	0.842(2)	10.5
155	$5\nu_2 - 1\nu_9$	16.35149(6)	0.144(2)	0.845(2)	11.8
156	$\nu_{17}$	22.93256(6)	0.138(2)	0.096(2)	20.9
157	$-1\nu_2 + 5\nu_5$	32.11634(6)	0.140(2)	0.350(2)	17.7
158	$2\nu_3 + 2\nu_8$	30.91820(6)	0.140(2)	0.792(2)	23.5
159	$-8\nu_1 + 4\nu_{12}$	43.22985(6)	0.136(2)	0.632(2)	31.6
160	$3\nu_1 + 1\nu_9$	36.37450(6)	0.134(2)	0.010(2)	23.9
161	$2\nu_1 + 1\nu_{12}$	33.45188(6)	0.132(2)	0.689(2)	15.8
162	$1\nu_7 - 1\nu_{12} + 1\nu_{17}$	10.82642(7)	0.128(2)	0.878(2)	11.5
163	$2\nu_1 - 1\nu_7$	1.29791(6)	0.132(2)	0.533(2)	19.8
164	$-2\nu_{10} + 2\nu_{12} + 1\nu_{16}$	33.41783(6)	0.134(2)	1.000(2)	16.6
165	$1\nu_1 + 1\nu_{14}$	18.99780(6)	0.131(2)	0.625(2)	11.2
166	$-2\nu_1 + 2\nu_2$	2.97430(7)	0.124(2)	0.224(3)	10.4
167	instrumental	0.05427(7)	0.124(2)	0.856(3)	5.5
168	$-7\nu_1 + 9\nu_{11}$	52.43745(7)	0.123(2)	0.194(3)	35.8
169	$-7\nu_6 + 1\nu_{16}$	1.55226(7)	0.120(2)	0.458(3)	20.9
170	$10\nu_1$	56.61059(7)	0.120(2)	0.927(3)	43.5
171	$3\nu_1 - 1\nu_5$	9.12985(7)	0.116(2)	0.265(3)	14.0
172	$9\nu_8 - 3\nu_9$	10.97828(7)	0.121(2)	0.754(3)	10.2
173	$3\nu_1 + 1\nu_{10}$	33.52696(7)	0.117(2)	0.322(3)	16.0
174	$3\nu_1 - 1\nu_4$	7.16721(7)	0.116(2)	0.429(3)	15.2
175	$-2\nu_4 - 2\nu_9 + 2\nu_{10}$	2.60859(7)	0.115(2)	0.515(3)	9.8
176	$-2\nu_1 + 2\nu_{10}$	21.76584(7)	0.116(2)	0.006(3)	11.2

Table A1: continued

#	ID <sub>K</sub>	$\nu$ [d <sup>-1</sup> ]	A [ppt]	$\phi$ [0 – 1]	S/N
177	$8\nu_4 - 2\nu_{15}$	0.34410(7)	0.110(2)	0.967(3)	6.9
178	$2\nu_4 + 1\nu_6 + 1\nu_{10}$	39.13211(7)	0.114(2)	0.336(3)	18.1
179	$1\nu_3 - 1\nu_4 + 1\nu_8$	5.64280(8)	0.109(2)	0.193(3)	7.0
180	$-1\nu_5 + 3\nu_{11}$	22.83424(7)	0.113(2)	0.174(3)	19.1
181	$-1\nu_1 + 2\nu_3$	9.89006(7)	0.112(2)	0.142(3)	12.5
182	$-2\nu_5 + 1\nu_8 + 2\nu_{10}$	25.06519(7)	0.115(2)	0.028(3)	13.8
183	$5\nu_1 - 1\nu_6$	25.34863(7)	0.111(2)	0.165(3)	16.6
184	$-3\nu_4 + 2\nu_{13}$	3.39704(7)	0.112(2)	0.225(3)	12.5
185	$2\nu_1 + 3\nu_2$	32.76683(7)	0.112(2)	0.471(3)	16.6
186	$1\nu_1 + 1\nu_{15}$	44.75300(7)	0.111(2)	0.089(3)	22.1
187	$4\nu_1 + 1\nu_8$	30.32766(7)	0.107(2)	0.408(3)	17.1
188	$4\nu_1 + 1\nu_4$	32.46018(7)	0.105(2)	0.520(3)	16.6
189	$\nu_{18}$	37.77743(8)	0.109(2)	0.086(3)	18.5
190	$8\nu_3 - 2\nu_{17}$	16.33887(8)	0.105(2)	0.323(3)	9.3
191	$3\nu_1 + 1\nu_7$	27.00747(8)	0.108(2)	0.857(3)	16.1
192	$4\nu_1 - 1\nu_{10}$	6.10067(8)	0.104(2)	0.392(3)	7.0
193	$-2\nu_1 + 1\nu_{18}$	26.45532(7)	0.106(2)	0.592(3)	14.2
194	$-10\nu_1 + 9\nu_3$	13.36791(8)	0.101(2)	0.965(3)	7.7
195	$1\nu_4 - 2\nu_5 + 1\nu_{14}$	7.44524(8)	0.102(2)	0.616(3)	13.6
196	$3\nu_1 + 1\nu_{13}$	33.40545(8)	0.099(2)	0.260(3)	15.3
197	$-1\nu_1 + 3\nu_5$	17.89810(8)	0.102(2)	0.284(3)	13.1
198	$1\nu_1 + 2\nu_3 + 2\nu_8$	36.57931(8)	0.102(2)	0.437(3)	20.1
199	$3\nu_1 + 2\nu_3$	32.53435(8)	0.101(2)	0.060(3)	18.1
200	$1\nu_8 + 2\nu_{13} - 1\nu_{18}$	2.75022(8)	0.101(2)	0.458(3)	9.0
201	$-8\nu_5 + 4\nu_{13}$	2.86117(8)	0.097(2)	0.683(3)	9.6
202	$1\nu_1 + 1\nu_{17}$	28.59363(8)	0.099(2)	0.843(3)	18.3
203	$5\nu_4 - 2\nu_5$	33.37306(8)	0.100(2)	0.486(3)	15.9
204	$1\nu_1 + 1\nu_{11}$	15.89044(8)	0.097(2)	0.566(3)	11.3
205	$14\nu_1 - 9\nu_8$	10.10564(8)	0.098(2)	0.145(3)	11.1
206	$1\nu_6 + 1\nu_{18}$	40.73405(8)	0.098(2)	0.238(3)	19.4
207	$5\nu_2 - 1\nu_{10}$	19.19915(8)	0.101(2)	0.005(3)	8.8
208	$-7\nu_7 + 6\nu_{14}$	9.85336(8)	0.096(2)	0.818(3)	12.0
209	$5\nu_1 + 2\nu_2$	42.60312(8)	0.095(2)	0.776(3)	25.2
210	$1\nu_3 + 1\nu_7$	17.79970(8)	0.098(2)	0.471(3)	13.1
211	$-5\nu_6 + 2\nu_{11}$	5.67576(8)	0.092(2)	0.518(3)	6.1
212	$1\nu_4 + 1\nu_5$	17.66919(9)	0.093(2)	0.810(3)	14.5
213	$-8\nu_4 + 9\nu_{11}$	13.53797(8)	0.098(2)	0.283(3)	7.4
214	$3\nu_1 + 1\nu_{12}$	39.11295(8)	0.091(2)	0.417(3)	15.8
215	$5\nu_1 + 1\nu_9$	47.69659(8)	0.092(2)	0.540(3)	28.6
216	$-7\nu_1 + 4\nu_{12}$	48.89091(8)	0.092(2)	0.429(3)	28.0
217	$6\nu_1 + 1\nu_6$	36.92285(8)	0.092(2)	0.301(3)	23.6
218	$5\nu_1 - 1\nu_2$	21.15635(8)	0.092(2)	0.428(3)	13.9
219	$1\nu_2 - 1\nu_3 + 1\nu_{11}$	9.60098(8)	0.092(2)	0.785(3)	11.8
220	$-2\nu_2 + 1\nu_8 + 1\nu_{12}$	15.51435(9)	0.092(2)	0.654(3)	13.4
221	$-2\nu_2 - 2\nu_8 + 2\nu_{17}$	16.19940(9)	0.091(2)	0.141(3)	8.5
222	$-2\nu_1 - 2\nu_3 + 1\nu_{16}$	3.15042(9)	0.090(2)	0.222(3)	8.5
223	$3\nu_1 - 1\nu_7$	6.95905(8)	0.090(2)	0.179(3)	12.8
224	$10\nu_2 - 3\nu_{10}$	21.86046(9)	0.089(2)	0.984(4)	9.3
225	$6\nu_7 - 5\nu_{11}$	8.99886(9)	0.086(2)	0.081(4)	10.7
226	$3\nu_{10} - 4\nu_{11}$	8.71348(8)	0.089(2)	0.666(3)	10.3
227	$15\nu_1 - 4\nu_9$	7.34951(8)	0.088(2)	0.076(4)	13.2
228	$3\nu_1 - 2\nu_2$	2.68703(9)	0.088(2)	0.946(4)	8.6
229	$-9\nu_6 + 4\nu_{13}$	39.07888(9)	0.089(2)	0.750(3)	16.0
230	$-1\nu_5 + 3\nu_7$	22.21936(9)	0.091(2)	0.588(3)	9.2
231	$8\nu_9 - 8\nu_{13}$	23.75088(8)	0.088(2)	0.621(4)	11.4
232	$8\nu_1 + 1\nu_3$	53.06407(9)	0.087(2)	0.152(4)	30.2
233	$2\nu_{11} - 2\nu_{13} + 1\nu_{17}$	10.54744(9)	0.090(2)	0.668(3)	10.1
234	$5\nu_1 + 1\nu_6 - 1\nu_{10}$	14.71878(9)	0.086(2)	0.981(4)	11.7
235	$10\nu_4 - 6\nu_8$	52.05620(9)	0.087(2)	0.522(4)	25.2

Table A1: continued

#	ID <sub>K</sub>	$\nu$ [d <sup>-1</sup> ]	A [ppt]	$\phi$ [0 – 1]	S/N
236	$-2\nu_6 - 2\nu_7 + 2\nu_{16}$	18.53545(9)	0.086(2)	0.536(4)	11.6
237	$-1\nu_1 + 2\nu_{10}$	27.42694(9)	0.085(2)	0.724(4)	10.4
238	$1\nu_1 + 1\nu_{16}$	27.90874(9)	0.083(2)	0.494(4)	11.2
239	$2\nu_{12} - 1\nu_{16}$	22.01256(9)	0.088(2)	0.519(4)	9.7
240	$5\nu_1 + 1\nu_5$	36.15861(9)	0.083(2)	0.281(4)	19.6
241	$2\nu_5 + 3\nu_{11}$	46.39513(9)	0.085(2)	0.827(4)	21.6
242	$-2\nu_1 + 1\nu_9$	8.06926(9)	0.082(2)	0.441(4)	10.8
243	$-2\nu_9 + 2\nu_{10} + 1\nu_{13}$	10.72880(9)	0.081(2)	0.988(4)	9.5
244	$10\nu_1 - 2\nu_{12}$	12.35066(9)	0.082(2)	0.651(4)	11.4
245	$-2\nu_4 + 1\nu_7 + 2\nu_8$	5.75883(9)	0.082(2)	0.373(4)	5.3
246	$-3\nu_1 + 2\nu_{10}$	16.10476(9)	0.084(2)	0.176(4)	8.0
247	$2\nu_5 + 2\nu_7 - 1\nu_{12}$	13.6243(1)	0.078(2)	0.231(4)	6.4
248	$-5\nu_1 + 2\nu_6 + 2\nu_{10}$	10.69557(9)	0.080(2)	0.883(4)	9.4
249	$-1\nu_1 + 1\nu_9$	13.73044(9)	0.078(2)	0.811(4)	6.5
250	$-1\nu_2 + 1\nu_7$	2.87530(9)	0.084(2)	0.839(4)	8.4
251	$2\nu_2 + 2\nu_{11}$	34.7569(1)	0.076(2)	0.222(4)	12.8
252	$2\nu_1 + 1\nu_{14}$	24.65883(9)	0.079(2)	0.410(4)	10.1
253	$-8\nu_3 + 8\nu_4$	16.3236(1)	0.077(2)	0.780(4)	8.0
254	$15\nu_1 - 9\nu_8$	15.76669(9)	0.078(2)	0.953(4)	12.2
255	$-2\nu_3 + 1\nu_9 + 2\nu_{14}$	30.51540(9)	0.078(2)	0.026(4)	14.7
256	$7\nu_2 - 1\nu_{13}$	33.6225(1)	0.076(2)	0.478(4)	13.3
257	$6\nu_1 - 1\nu_3$	26.19075(9)	0.078(2)	0.255(4)	12.0
258	$12\nu_1 - 2\nu_{10}$	34.8461(1)	0.079(2)	0.683(4)	13.0
259	$-2\nu_{12} + 4\nu_{13}$	21.4277(1)	0.076(2)	0.824(4)	13.4
260	$6\nu_1 - 1\nu_2$	26.8174(1)	0.075(2)	0.260(4)	12.5
261	$2\nu_{10} + 2\nu_{14} - 1\nu_{18}$	21.9848(1)	0.073(2)	0.542(4)	9.1
262	$6\nu_1 - 3\nu_2$	12.5215(1)	0.073(2)	0.355(4)	9.9
263	$2\nu_1 + 1\nu_{15}$	50.4141(1)	0.076(2)	0.873(4)	21.4
264	$9\nu_4 - 6\nu_8$	42.2404(1)	0.075(2)	0.127(4)	20.1
265	$5\nu_3 + 2\nu_6$	44.7931(1)	0.074(2)	0.142(4)	16.5
266	$4\nu_1 - 2\nu_2$	8.3483(1)	0.071(2)	0.549(4)	9.2
267	$\nu_{19}$	15.0704(1)	0.071(2)	0.066(4)	11.0
268	$-1\nu_6 + 1\nu_{16}$	19.2909(1)	0.072(2)	0.770(4)	6.7
269	$1\nu_6 - 2\nu_7 + 1\nu_{15}$	21.9999(1)	0.070(2)	0.006(4)	8.7
270	$13\nu_1 - 5\nu_{14}$	6.9107(1)	0.069(2)	0.726(4)	11.0
271	$2\nu_5 + 1\nu_7 - 1\nu_{17}$	2.7999(1)	0.068(2)	0.686(5)	7.6
272	$6\nu_1 - 7\nu_6$	13.2679(1)	0.067(2)	0.135(5)	5.4
273	$-5\nu_1 + 1\nu_{15}$	10.7865(1)	0.070(2)	0.765(4)	8.4
274	$5\nu_2 - 2\nu_8$	20.3798(1)	0.066(2)	0.723(5)	10.2
275	$4\nu_1 + 1\nu_{10}$	39.1880(1)	0.069(2)	0.040(5)	13.4
276	$-4\nu_5 + 5\nu_8$	7.0054(1)	0.067(2)	0.115(5)	11.7
277	$4\nu_1 + 1\nu_6 - 1\nu_{10}$	9.0578(1)	0.068(2)	0.104(5)	9.3
278	$3\nu_1 - 1\nu_8$	9.3000(1)	0.068(2)	0.225(5)	10.8
279	$-1\nu_3 + 1\nu_7$	2.2487(1)	0.069(2)	0.908(4)	9.5
280	$1\nu_4 - 2\nu_{13} + 1\nu_{15}$	16.0630(1)	0.069(2)	0.528(5)	7.7
281	$1\nu_{10} - 1\nu_{13} + 1\nu_{14}$	13.4587(1)	0.063(2)	0.844(5)	5.8
282	$-9\nu_1 + 9\nu_3$	19.0289(1)	0.066(2)	0.758(5)	6.3
283	$-7\nu_2 + 4\nu_9$	27.5215(1)	0.068(2)	0.754(5)	9.2
284	$4\nu_1 - 1\nu_4$	12.8282(1)	0.066(2)	0.335(5)	9.0
285	$-1\nu_4 - 1\nu_{12} + 2\nu_{17}$	11.5120(1)	0.066(2)	0.836(5)	7.2
286	$-2\nu_5 + 2\nu_{11} + 1\nu_{13}$	21.1754(1)	0.068(2)	0.452(5)	11.8
287	$-2\nu_4 + 1\nu_5 + 2\nu_7$	8.2698(1)	0.066(2)	0.182(5)	8.3
288	$-5\nu_1 - 5\nu_3 + 1\nu_{15}$	3.0090(1)	0.067(2)	0.295(5)	7.3
289	$-2\nu_4 + 2\nu_{10} + 2\nu_{12}$	57.7173(1)	0.066(2)	0.302(5)	21.2
290	$6\nu_1 - 1\nu_6$	31.0097(1)	0.066(2)	0.976(5)	14.5
291	$7\nu_8 - 3\nu_{19}$	8.5718(1)	0.067(2)	0.670(5)	8.9
292	$4\nu_5 - 2\nu_{14}$	4.7409(1)	0.066(2)	0.310(5)	9.9
293	$-6\nu_1 + 9\nu_{11}$	58.0985(1)	0.066(2)	0.997(5)	30.8
294	$4\nu_1 + 2\nu_3$	38.1955(1)	0.065(2)	0.806(5)	13.5

Table A1: continued

#	ID <sub>K</sub>	$\nu$ [d <sup>-1</sup> ]	A [ppt]	$\phi$ [0 – 1]	S/N
295	$-1\nu_2 - 1\nu_5 + 2\nu_{12}$	29.2577(1)	0.067(2)	0.963(5)	9.5
296	$1\nu_1 + 1\nu_{18}$	43.4385(1)	0.065(2)	0.775(5)	16.8
297	$-15\nu_1 + 4\nu_{12}$	3.6025(1)	0.064(2)	0.871(5)	10.4
298	$\nu_{20}$	16.5302(1)	0.065(2)	0.460(5)	6.3
299	$-4\nu_4 + 3\nu_{20}$	10.3263(1)	0.063(2)	0.276(5)	8.2
300	$1\nu_8 - 1\nu_{12} + 1\nu_{18}$	23.3303(1)	0.063(2)	0.481(5)	9.8
301	$4\nu_1 + 1\nu_{12}$	44.7740(1)	0.062(2)	0.173(5)	14.8
302	$1\nu_6 - 2\nu_{10} + 2\nu_{20}$	2.9276(1)	0.064(2)	0.155(5)	7.0
303	$-2\nu_{14} + 1\nu_{17} + 1\nu_{19}$	11.3298(1)	0.060(2)	0.167(5)	6.6
304	$-4\nu_7 + 5\nu_{11}$	11.0481(1)	0.060(2)	0.819(5)	6.5
305	$1\nu_2 + 1\nu_5$	15.0025(1)	0.063(2)	0.155(5)	9.9
306	$4\nu_1 + 1\nu_{13}$	39.0665(1)	0.061(2)	0.984(5)	13.1
307	$2\nu_8 + 2\nu_{13} - 2\nu_{17}$	2.3470(1)	0.060(2)	0.794(5)	8.3
308	$-8\nu_2 + 8\nu_5$	5.6357(1)	0.062(2)	0.038(5)	5.0
309	$-2\nu_1 + 1\nu_{17}$	11.6106(1)	0.059(2)	0.465(5)	7.1
310	$6\nu_1 + 2\nu_2$	48.2642(1)	0.061(2)	0.548(5)	21.8
311	$4\nu_4 - 2\nu_{20}$	6.2026(1)	0.060(2)	0.681(5)	7.1
312	$-1\nu_{11} + 1\nu_{16} + 1\nu_{19}$	27.0888(1)	0.060(2)	0.650(5)	12.2
313	$-1\nu_{11} - 1\nu_{15} + 2\nu_{16}$	23.4608(1)	0.061(2)	0.164(5)	9.5
314	$6\nu_1 + 1\nu_9$	53.3577(1)	0.060(2)	0.358(5)	25.6
315	$-6\nu_1 + 4\nu_{12}$	54.5520(1)	0.060(2)	0.219(5)	23.9
316	$5\nu_1 + 1\nu_8$	35.9887(1)	0.059(2)	0.158(5)	13.6
317	$3\nu_3 + 2\nu_5$	39.0341(1)	0.061(2)	0.219(5)	13.2
318	$-1\nu_3 + 7\nu_6$	12.9233(1)	0.060(2)	0.349(5)	7.1
319	$-8\nu_{12} + 9\nu_{17}$	29.3537(1)	0.059(2)	0.846(5)	8.9
320	$-9\nu_{13} + 10\nu_{19}$	2.9028(1)	0.059(2)	0.060(5)	6.9
321	$10\nu_2 - 2\nu_{20}$	38.4279(1)	0.059(2)	0.272(5)	14.0
322	$11\nu_1$	62.2717(1)	0.059(2)	0.728(5)	31.6
323	$4\nu_1 + 1\nu_7$	32.6685(1)	0.059(2)	0.612(5)	11.5
324	$2\nu_5 + 2\nu_6 - 1\nu_8$	13.9351(1)	0.060(2)	0.102(5)	6.0
325	$1\nu_4 + 1\nu_{17}$	32.7497(1)	0.057(2)	0.547(5)	12.3
326	$1\nu_4 - 1\nu_9 + 2\nu_{16}$	34.9187(1)	0.057(2)	0.715(5)	10.3
327	$5\nu_3 - 7\nu_6$	18.1827(1)	0.058(2)	0.052(5)	8.8
328	$-6\nu_5 + 3\nu_{10}$	2.5106(1)	0.059(2)	0.136(5)	7.0
329	$-10\nu_4 + 8\nu_{14}$	8.5363(1)	0.055(2)	0.614(6)	8.2
330	$-4\nu_{11} + 3\nu_{17}$	27.8804(1)	0.059(2)	0.297(5)	8.3
331	$5\nu_1 - 1\nu_{10}$	11.7619(1)	0.057(2)	0.039(5)	6.8
332	$7\nu_3 - 10\nu_6$	24.8628(1)	0.054(2)	0.249(6)	8.1
333	$-7\nu_6 + 7\nu_8$	33.0880(1)	0.057(2)	0.491(5)	10.1
334	$6\nu_9 - 7\nu_{11}$	44.7399(1)	0.058(2)	0.513(5)	14.2
335	$5\nu_1 + 1\nu_4$	38.1213(1)	0.057(2)	0.259(5)	12.7
336	$1\nu_5 - 2\nu_{19} + 2\nu_{20}$	10.7737(1)	0.057(2)	0.007(5)	7.5
337	$7\nu_1 - 1\nu_2$	32.4785(1)	0.056(2)	0.044(6)	11.7
338	$2\nu_7 + 1\nu_{13} - 2\nu_{20}$	3.4123(1)	0.056(2)	0.415(6)	8.0
339	$1\nu_7 + 1\nu_9 - 1\nu_{11}$	19.1864(1)	0.055(2)	0.399(6)	5.4
340	$4\nu_2 - 1\nu_{19}$	13.5254(1)	0.056(2)	0.584(6)	5.1
341	$-3\nu_{16} + 2\nu_{18}$	8.8115(1)	0.056(2)	0.007(6)	7.9
342	$-2\nu_{13} + 1\nu_{15} + 1\nu_{16}$	28.4953(1)	0.056(2)	0.950(6)	12.0
343	$1\nu_{11} + 1\nu_{17} - 1\nu_{19}$	18.0900(1)	0.056(2)	0.092(6)	8.6
344	$-9\nu_{16} + 10\nu_{17}$	29.0959(1)	0.051(2)	0.400(6)	8.9
345	$1\nu_1 - 1\nu_8 + 1\nu_{14}$	11.3146(1)	0.052(2)	0.057(6)	6.2
346	$-2\nu_1 + 2\nu_{19}$	18.8186(1)	0.055(2)	0.605(6)	5.4
347	$10\nu_3 - 6\nu_7$	17.6098(1)	0.054(2)	0.594(6)	9.5
348	$-6\nu_3 + 7\nu_{11}$	24.9520(1)	0.055(2)	0.546(6)	7.9
349	$9\nu_3 - 4\nu_7$	29.8843(1)	0.052(2)	0.995(6)	10.3
350	$2\nu_9 + 1\nu_{11} - 1\nu_{15}$	9.9219(1)	0.055(2)	0.337(6)	7.9
351	$-5\nu_2 + 5\nu_7$	14.3746(1)	0.054(2)	0.475(6)	8.1
352	$2\nu_1 + 1\nu_{17}$	34.2548(1)	0.053(2)	0.499(6)	12.3
353	$11\nu_1 - 2\nu_{10}$	29.1849(1)	0.056(2)	0.929(6)	8.8

Table A1: continued

#	ID <sub>K</sub>	$\nu$ [d <sup>-1</sup> ]	A [ppt]	$\phi$ [0 – 1]	S/N
354	$-4\nu_3 + 5\nu_4$	17.9759(1)	0.051(2)	0.570(6)	9.2
355	$3\nu_4 - 2\nu_{11}$	8.9894(1)	0.050(2)	0.501(6)	8.2
356	$7\nu_1 + 1\nu_6$	42.5840(1)	0.053(2)	0.044(6)	18.3
357	$7\nu_1 - 1\nu_3$	31.8518(1)	0.052(2)	0.059(6)	9.1
358	$-2\nu_{11} + 1\nu_{19} + 2\nu_{20}$	27.6736(1)	0.053(2)	0.284(6)	8.1
359	$-1\nu_3 + 1\nu_{16}$	14.4725(1)	0.052(2)	0.817(6)	7.9
360	$-8\nu_1 + 6\nu_7$	14.8552(1)	0.052(2)	0.221(6)	9.2
361	$1\nu_3 + 1\nu_9$	27.1669(1)	0.051(2)	0.632(6)	10.5
362	$1\nu_2 + 1\nu_9$	26.5402(1)	0.050(2)	0.728(6)	8.5
363	$2\nu_{11} + 1\nu_{12} - 2\nu_{19}$	12.4467(1)	0.048(2)	0.461(6)	8.0
364	$-1\nu_6 + 1\nu_7 + 1\nu_{20}$	23.5966(1)	0.053(2)	0.164(6)	8.3
365	$1\nu_2 + 1\nu_{10}$	23.6927(1)	0.052(2)	0.127(6)	8.3
366	$1\nu_{12} + 1\nu_{13} - 2\nu_{19}$	8.4113(1)	0.049(2)	0.178(6)	7.5
367	$-2\nu_6 + 1\nu_7$	4.1089(1)	0.051(2)	0.726(6)	9.0
368	$3\nu_1 + 1\nu_{15}$	56.0751(1)	0.051(2)	0.706(6)	19.3
369	$2\nu_2 + 1\nu_3$	22.0733(1)	0.050(2)	0.975(6)	6.5
370	$1\nu_{10} - 2\nu_{14} + 1\nu_{18}$	27.6459(1)	0.048(2)	0.251(6)	8.1
371	$7\nu_2 + 1\nu_{14}$	63.3783(1)	0.050(2)	0.104(6)	21.8
372	$-1\nu_{10} - 1\nu_{16} + 2\nu_{20}$	11.4198(1)	0.049(2)	0.230(6)	5.8
373	$-1\nu_2 + 1\nu_{14} + 1\nu_{17}$	29.1218(1)	0.051(2)	0.953(6)	8.6
374	$-1\nu_{13} - 1\nu_{18} + 2\nu_{19}$	28.9914(1)	0.048(2)	0.216(6)	9.0
375	$-10\nu_1 + 6\nu_7$	3.5331(1)	0.050(2)	0.033(6)	8.3
376	$8\nu_5 - 1\nu_{16}$	40.5798(1)	0.049(2)	0.469(6)	11.8
377	$1\nu_2 + 1\nu_8$	14.8322(1)	0.049(2)	0.326(6)	9.1
378	$-4\nu_6 + 3\nu_8$	11.2242(1)	0.047(2)	0.582(7)	5.3
379	$-5\nu_1 + 7\nu_5$	26.6700(1)	0.049(2)	0.474(6)	8.9
380	$-10\nu_6 + 6\nu_{14}$	50.4541(1)	0.048(2)	0.960(6)	15.2
381	$2\nu_9 - 2\nu_{11} + 1\nu_{19}$	33.3954(1)	0.048(2)	0.326(7)	9.2
382	$5\nu_1 - 1\nu_4$	18.4892(1)	0.047(2)	0.124(7)	8.3
383	$-7\nu_6 + 1\nu_{18}$	17.0807(1)	0.047(2)	0.266(7)	7.3
384	$5\nu_4 - 1\nu_{18}$	11.3038(2)	0.043(2)	0.992(7)	5.5
385	$-1\nu_7 + 1\nu_{14}$	3.3141(1)	0.047(2)	0.571(7)	6.8
386	$-2\nu_4 + 1\nu_8 + 2\nu_9$	26.8365(1)	0.047(2)	0.254(7)	9.8
387	$-4\nu_1 + 7\nu_5$	32.3310(1)	0.046(2)	0.310(7)	9.4
388	$-1\nu_{14} - 1\nu_{18} + 1\nu_{20}$	7.9097(1)	0.047(2)	0.678(7)	7.8
389	$7\nu_5 - 2\nu_{16}$	10.4799(1)	0.048(2)	0.801(6)	6.5
390	$-1\nu_2 + 1\nu_{19} + 2\nu_{21}$	47.9015(1)	0.046(2)	0.920(7)	17.3
391	$9\nu_1 + 1\nu_3$	58.7251(1)	0.046(2)	0.976(7)	21.8
392	$3\nu_1 - 1\nu_9 + 2\nu_{19}$	27.7343(1)	0.047(2)	0.605(7)	7.6
393	$\nu_{21}$	19.9908(1)	0.047(2)	0.348(7)	7.6
394	$1\nu_1 + 1\nu_{20}$	22.1911(1)	0.047(2)	0.267(7)	6.0
395	$-1\nu_5 + 1\nu_7 + 2\nu_{13}$	35.0148(1)	0.046(2)	0.569(7)	8.6
396	$2\nu_1 - 2\nu_8 + 2\nu_9$	34.7391(1)	0.049(2)	0.622(6)	9.2
397	$2\nu_5 - 2\nu_7 + 1\nu_{15}$	34.7484(1)	0.048(2)	0.783(7)	9.8
398	$6\nu_1 + 1\nu_5$	41.8197(1)	0.046(2)	0.034(7)	14.6
399	$1\nu_7 + 2\nu_{12} - 1\nu_{13}$	37.8623(2)	0.046(2)	0.238(7)	9.8
400	$1\nu_8 - 1\nu_{13} + 2\nu_{14}$	17.9355(1)	0.044(2)	0.661(7)	8.3
401	$2\nu_1 + 1\nu_{11}$	21.5515(1)	0.045(2)	0.333(7)	9.0
402	$-2\nu_5 + 1\nu_8 + 1\nu_{10}$	8.5221(1)	0.048(2)	0.568(6)	7.3
403	$2\nu_6 + 1\nu_{11}$	16.1408(1)	0.046(2)	0.695(7)	5.3
404	$2\nu_{10} - 2\nu_{12} + 1\nu_{16}$	11.0746(1)	0.046(2)	0.734(7)	5.3
405	$3\nu_9 - 3\nu_{19}$	12.9640(1)	0.046(2)	0.750(7)	5.1
406	$1\nu_4 + 2\nu_9 - 1\nu_{15}$	9.5079(1)	0.044(2)	0.300(7)	7.0
407	$-1\nu_1 + 1\nu_{11}$	4.5685(1)	0.047(2)	0.335(7)	7.7
408	$4\nu_2 + 1\nu_4$	38.4108(1)	0.045(2)	0.350(7)	12.4
409	$2\nu_1 + 1\nu_{16}$	33.5698(1)	0.045(2)	0.249(7)	8.7
410	$15\nu_1 - 5\nu_{20}$	2.2646(2)	0.045(2)	0.881(7)	6.8
411	$1\nu_4 - 1\nu_8$	2.1324(2)	0.043(2)	0.485(7)	8.1
412	$-1\nu_5 + 1\nu_6 + 1\nu_8$	2.7858(1)	0.045(2)	0.471(7)	5.8

Table A1: continued

#	ID <sub>K</sub>	$\nu$ [d <sup>-1</sup> ]	A [ppt]	$\phi$ [0 – 1]	S/N
413	$-3\nu_7 + 2\nu_{21}$	9.9079(2)	0.043(2)	0.638(7)	6.9
414	$3\nu_6 + 2\nu_{14}$	35.5453(2)	0.044(2)	0.748(7)	10.7
415	$7\nu_1 - 1\nu_6$	36.6707(1)	0.044(2)	0.820(7)	12.9
416	$4\nu_1 - 1\nu_{21}$	2.6521(2)	0.043(2)	0.058(7)	5.8
417	$3\nu_5$	23.5594(2)	0.045(2)	0.875(7)	7.6
418	$5\nu_1 + 1\nu_{13}$	44.7276(2)	0.041(2)	0.745(8)	11.7
419	$-6\nu_6 + 1\nu_{18}$	20.0356(2)	0.042(2)	0.313(7)	7.5
420	$2\nu_5 - 1\nu_{10} + 1\nu_{19}$	14.2330(2)	0.044(2)	0.368(7)	7.5
421	$-1\nu_1 + 2\nu_{19}$	24.4797(2)	0.043(2)	0.198(7)	6.2
422	$-4\nu_1 + 2\nu_{10}$	10.4438(1)	0.044(2)	0.480(7)	6.2
423	$-4\nu_6 + 1\nu_{17}$	11.1073(1)	0.044(2)	0.572(7)	5.1
424	$1\nu_1 + 1\nu_{19}$	20.7314(2)	0.044(2)	0.776(7)	7.4
425	$-8\nu_1 + 9\nu_3$	24.6900(2)	0.042(2)	0.461(7)	6.1
426	$4\nu_1 - 1\nu_5$	14.7909(2)	0.043(2)	0.111(7)	8.0
427	$-2\nu_3 + 3\nu_5$	8.0080(2)	0.043(2)	0.590(7)	7.1
428	$5\nu_1 + 1\nu_{12}$	50.4351(2)	0.043(2)	0.981(7)	14.4
429	$-2\nu_4 - 2\nu_{12} + 2\nu_{16}$	2.7336(2)	0.042(2)	0.017(7)	5.7
430	$5\nu_1 + 2\nu_3$	43.8566(2)	0.042(2)	0.536(7)	12.1
431	$6\nu_3 - 6\nu_6$	28.9146(2)	0.041(2)	0.055(8)	8.2
432	$9\nu_{10} - 7\nu_{20}$	33.1825(2)	0.043(2)	0.553(7)	8.5
433	$-2\nu_1 + 1\nu_6 + 1\nu_{15}$	30.7262(2)	0.042(2)	0.722(7)	9.3
434	$-1\nu_6 + 1\nu_8 + 1\nu_{17}$	27.6611(2)	0.042(2)	0.704(7)	7.2
435	$1\nu_2 - 1\nu_6$	4.1923(1)	0.043(2)	0.084(7)	8.0
436	$-1\nu_{14} - 1\nu_{17} + 2\nu_{18}$	39.2836(2)	0.041(2)	0.197(8)	9.7
437	$10\nu_5 - 6\nu_7$	18.3883(2)	0.042(2)	0.085(7)	7.6
438	$-1\nu_4 + 2\nu_{10}$	23.2708(2)	0.040(2)	0.476(8)	7.9
439	$-3\nu_2 + 2\nu_{10}$	11.6406(2)	0.036(2)	0.472(9)	5.7
440	$-8\nu_{11} + 5\nu_{17}$	32.8279(2)	0.041(2)	0.459(8)	10.9
441	$2\nu_1 + 1\nu_{18}$	49.0996(2)	0.041(2)	0.469(8)	14.2
442	$7\nu_1 + 1\nu_9$	59.0187(2)	0.041(2)	0.155(8)	21.6
443	$\nu_{22}$	22.7419(2)	0.039(2)	0.935(8)	8.1
444	$8\nu_2 - 6\nu_3$	10.5382(2)	0.041(2)	0.664(8)	6.2
445	$4\nu_1 - 1\nu_7$	12.6203(2)	0.040(2)	0.881(8)	6.1
446	$8\nu_2 - 3\nu_{13}$	7.9257(2)	0.042(2)	0.632(7)	7.1
447	$2\nu_{11} + 2\nu_{12} - 2\nu_{19}$	34.5759(2)	0.040(2)	0.627(8)	8.7
448	$-1\nu_3 + 4\nu_5$	23.6362(2)	0.040(2)	0.357(8)	7.2
449	$1\nu_9 + 1\nu_{12} - 2\nu_{20}$	8.4609(2)	0.037(2)	0.502(8)	6.6
450	$2\nu_4 - 1\nu_7$	9.6067(2)	0.039(2)	0.095(8)	6.3
451	$7\nu_1 + 2\nu_2$	53.9253(2)	0.039(2)	0.347(8)	18.3
452	$-1\nu_6 - 1\nu_{20} + 2\nu_{21}$	20.4942(2)	0.038(2)	0.505(8)	7.0
453	$-2\nu_1 + 3\nu_5$	12.2372(2)	0.037(2)	0.527(8)	6.6
454	$1\nu_2 + 1\nu_{15}$	46.2409(2)	0.039(2)	0.216(8)	12.3
455	$7\nu_1 - 5\nu_8$	1.2081(2)	0.038(2)	0.305(8)	7.5
456	$1\nu_3 - 1\nu_6 + 2\nu_{19}$	34.9594(2)	0.038(2)	0.441(8)	8.1
457	$1\nu_4 - 1\nu_{12} + 1\nu_{19}$	2.7583(2)	0.037(2)	0.224(8)	5.2
458	$-2\nu_1 + 1\nu_{12}$	10.8074(2)	0.039(2)	0.969(8)	5.7
459	$5\nu_1 + 1\nu_{10}$	44.8491(2)	0.039(2)	0.800(8)	10.6
460	$2\nu_3 + 1\nu_{16} - 1\nu_{21}$	17.8060(2)	0.037(2)	0.608(8)	7.1
461	$-8\nu_2 + 4\nu_{16}$	31.8004(2)	0.039(2)	0.024(8)	7.0
462	$\nu_{23}$	50.4010(2)	0.039(2)	0.301(8)	13.4
463	$3\nu_2 + 1\nu_5$	29.2987(2)	0.037(2)	0.439(8)	6.8
464	$2\nu_4 - 1\nu_7 + 1\nu_{12}$	31.7382(2)	0.039(2)	0.660(8)	7.0
465	$8\nu_{17} - 7\nu_{21}$	43.5234(2)	0.037(2)	0.923(8)	11.0
466	$3\nu_1 + 1\nu_{14}$	30.3199(2)	0.038(2)	0.158(8)	7.2
467	$-9\nu_4 + 3\nu_{15}$	28.9319(2)	0.037(2)	0.334(8)	7.5
468	$-10\nu_1 + 5\nu_{20}$	26.0410(2)	0.037(2)	0.409(8)	6.2
469	$-2\nu_{19} + 6\nu_{20}$	69.0394(2)	0.037(2)	0.906(8)	21.4
470	$1\nu_8 + 2\nu_{12} - 2\nu_{19}$	21.8021(2)	0.036(2)	0.364(9)	5.2
471	$10\nu_3 - 2\nu_{20}$	44.6952(2)	0.036(2)	0.977(9)	10.4

Table A1: continued

#	ID <sub>K</sub>	$\nu$ [d <sup>-1</sup> ]	A [ppt]	$\phi$ [0 – 1]	S/N
472	$-9\nu_1 + 8\nu_7$	29.2447(2)	0.034(2)	0.311(9)	7.1
473	$1\nu_1 + 2\nu_{10}$	38.7491(2)	0.036(2)	0.260(9)	8.4
474	$1\nu_3 + 2\nu_{13}$	40.6203(2)	0.035(2)	0.293(9)	9.0
475	$9\nu_1 - 5\nu_8$	12.5334(2)	0.035(2)	0.798(9)	5.8
476	$3\nu_3 - 1\nu_6$	20.3706(2)	0.037(2)	0.032(8)	6.0
477	$-2\nu_5 - 2\nu_6 + 2\nu_{13}$	14.1832(2)	0.033(2)	0.335(9)	6.2
478	$-7\nu_6 + 1\nu_{22}$	2.0451(2)	0.034(2)	0.011(9)	6.8
479	$-10\nu_8 + 2\nu_{23}$	23.9657(2)	0.036(2)	0.696(9)	6.3
480	$8\nu_1 - 1\nu_2$	38.1395(2)	0.035(2)	0.926(9)	9.3
481	$-2\nu_{12} + 1\nu_{20} + 2\nu_{21}$	12.2522(2)	0.034(2)	0.158(9)	6.2
482	$-3\nu_{16} + 4\nu_{22}$	24.2232(2)	0.035(2)	0.265(9)	6.6
483	$-5\nu_1 + 9\nu_{11}$	63.7596(2)	0.035(2)	0.790(9)	22.1
484	$2\nu_9 - 2\nu_{10} + 2\nu_{11}$	26.1550(2)	0.034(2)	0.432(9)	6.3
485	$4\nu_3 - 1\nu_{17}$	8.1717(2)	0.034(2)	0.907(9)	5.4
486	$9\nu_1 - 3\nu_7$	20.8790(2)	0.032(2)	0.08(1)	6.2
487	$1\nu_3 + 1\nu_{12}$	29.9058(2)	0.036(2)	0.699(9)	7.1
488	$5\nu_4 - 1\nu_7$	39.0566(2)	0.034(2)	0.061(9)	8.6
489	$6\nu_7 - 3\nu_{14}$	20.1335(2)	0.035(2)	0.651(9)	6.1
490	$-5\nu_1 + 4\nu_{12}$	60.2130(2)	0.035(2)	0.017(9)	17.6
491	$-1\nu_1 + 1\nu_{21}$	14.3304(2)	0.033(2)	0.468(9)	6.2
492	$-1\nu_{16} - 1\nu_{21} + 2\nu_{22}$	3.2473(2)	0.032(2)	0.03(1)	5.0
493	$2\nu_{10} + 1\nu_{20} - 1\nu_{21}$	29.6268(2)	0.034(2)	0.488(9)	6.4
494	$8\nu_3 - 6\nu_7$	2.0587(2)	0.034(2)	0.379(9)	6.6
495	$2\nu_2 - 2\nu_3 + 2\nu_{20}$	31.8059(2)	0.033(2)	0.416(9)	6.7
496	$-6\nu_1 + 7\nu_5$	21.0088(2)	0.036(2)	0.754(8)	6.5
497	$2\nu_8 + 2\nu_{10} - 1\nu_{12}$	26.3247(2)	0.033(2)	0.704(9)	6.3
498	$-4\nu_{10} + 2\nu_{15}$	12.0080(2)	0.035(2)	0.240(9)	6.0
499	$7\nu_5 - 9\nu_6$	28.3612(2)	0.033(2)	0.426(9)	8.3
500	$2\nu_{14} - 2\nu_{21} + 2\nu_{22}$	32.1739(2)	0.033(2)	0.081(9)	6.7
501	$9\nu_3 - 1\nu_{18}$	32.2012(2)	0.033(2)	0.573(9)	7.0
502	$1\nu_2 + 2\nu_3$	22.7000(2)	0.032(2)	0.79(1)	6.6
503	$1\nu_3 + 1\nu_{13}$	24.1964(2)	0.033(2)	0.404(9)	6.4
504	$-1\nu_7 + 3\nu_{11}$	20.6636(2)	0.033(2)	0.949(9)	6.4
505	$3\nu_2 + 1\nu_{14}$	34.7828(2)	0.034(2)	0.747(9)	7.5
506	$-2\nu_1 + 1\nu_{21}$	8.6706(2)	0.032(2)	0.62(1)	5.4
507	$1\nu_1 - 2\nu_8 + 2\nu_9$	29.0780(2)	0.036(2)	0.844(9)	6.8
508	$5\nu_4 - 1\nu_{21}$	29.0873(2)	0.037(2)	0.019(8)	7.2
509	$6\nu_2 - 3\nu_6$	34.0223(2)	0.032(2)	0.14(1)	9.3
510	$8\nu_1 - 1\nu_3$	37.5129(2)	0.032(2)	0.85(1)	7.6
511	$-3\nu_1 + 7\nu_5$	37.9921(2)	0.033(2)	0.10(1)	8.3
512	$-6\nu_3 + 8\nu_7$	33.5415(2)	0.033(2)	0.009(9)	7.0
513	$-7\nu_1 + 5\nu_4$	9.4523(2)	0.032(2)	0.29(1)	5.5
514	$1\nu_2 + 1\nu_{12}$	29.2789(2)	0.033(2)	0.895(9)	6.9
515	$6\nu_1 + 1\nu_8$	41.6498(2)	0.033(2)	0.915(9)	10.0
516	$-1\nu_9 - 1\nu_{12} + 2\nu_{13}$	8.4470(2)	0.033(2)	0.14(1)	5.7
517	$5\nu_{17} - 5\nu_{20}$	32.0108(2)	0.032(2)	0.59(1)	6.8
518	$-2\nu_{10} + 2\nu_{16} + 1\nu_{18}$	49.1844(2)	0.033(2)	0.700(9)	12.3
519	$1\nu_8 + 1\nu_{15} - 1\nu_{17}$	23.8438(2)	0.032(2)	0.83(1)	6.0
520	$-9\nu_{11} + 5\nu_{12}$	18.5843(2)	0.033(2)	0.851(9)	5.4
521	$11\nu_1 - 2\nu_{12}$	18.0115(2)	0.031(2)	0.37(1)	6.2
522	$-7\nu_1 + 7\nu_5$	15.3477(2)	0.033(2)	0.928(9)	5.8
523	$-3\nu_{13} + 7\nu_{14}$	44.0888(2)	0.033(2)	0.08(1)	10.5
524	$4\nu_1 + 1\nu_{15}$	61.7361(2)	0.032(2)	0.54(1)	16.4
525	$-8\nu_1 + 8\nu_7$	34.9058(2)	0.033(2)	0.08(1)	7.3
526	$-6\nu_2 + 10\nu_3$	34.8609(2)	0.032(2)	0.71(1)	7.5
527	$2\nu_8 + 1\nu_{15} - 2\nu_{22}$	8.9752(2)	0.032(2)	0.32(1)	5.5
528	$8\nu_7 - 7\nu_{11}$	8.5885(2)	0.031(2)	0.99(1)	5.5
529	$1\nu_6 + 1\nu_{15}$	42.0483(2)	0.032(2)	0.12(1)	11.3
530	$3\nu_1 + 2\nu_8 + 1\nu_9$	51.7402(2)	0.033(2)	0.22(1)	11.9

Table A1: continued

#	ID <sub>K</sub>	$\nu$ [d <sup>-1</sup> ]	A [ppt]	$\phi$ [0 – 1]	S/N
531	$4\nu_9 - 2\nu_{12}$	33.3069(2)	0.031(2)	0.98(1)	7.2
532	$2\nu_4 + 1\nu_{10}$	36.1764(2)	0.033(2)	0.849(9)	9.2
533	$2\nu_2 + 5\nu_5$	53.5625(2)	0.032(2)	0.77(1)	15.3
534	$4\nu_8 + 1\nu_{14}$	44.0718(2)	0.031(2)	0.16(1)	10.9
535	$-4\nu_{17} + 2\nu_{23}$	9.0736(2)	0.033(2)	0.102(9)	5.8
536	$6\nu_1 + 1\nu_4$	43.7824(2)	0.032(2)	0.00(1)	10.5
537	$5\nu_1 + 1\nu_7$	38.3297(2)	0.032(2)	0.31(1)	10.1
538	$7\nu_2 - 6\nu_8$	3.9400(2)	0.031(2)	0.30(1)	6.1
539	$-8\nu_6 + 2\nu_{18}$	51.9019(2)	0.031(2)	0.99(1)	12.1
540	$1\nu_3 + 1\nu_{10}$	24.3192(2)	0.030(2)	0.07(1)	5.7
541	$-9\nu_3 + 6\nu_{20}$	29.1998(2)	0.034(2)	0.008(9)	7.0
542	$1\nu_1 + 3\nu_5$	29.2203(2)	0.032(2)	0.72(1)	7.5
543	$1\nu_9 + 2\nu_{11} - 1\nu_{14}$	26.5128(2)	0.032(2)	0.37(1)	5.9
544	$2\nu_3 - 1\nu_9 + 2\nu_{12}$	40.4180(2)	0.030(2)	0.92(1)	8.5
545	$-10\nu_{11} + 6\nu_{22}$	34.1564(2)	0.031(2)	0.61(1)	8.9
546	$9\nu_2 - 3\nu_{10}$	14.7095(2)	0.032(2)	0.19(1)	6.0
547	$-2\nu_{12} - 2\nu_{16} + 2\nu_{18}$	9.0485(2)	0.031(2)	0.37(1)	5.6
548	$-2\nu_{11} - 2\nu_{13} + 1\nu_{15}$	2.2104(2)	0.030(2)	0.96(1)	5.6
549	$-5\nu_{14} + 6\nu_{20}$	32.4976(2)	0.031(2)	0.03(1)	8.1
550	$5\nu_{19} - 3\nu_{21}$	15.3777(2)	0.031(2)	0.31(1)	5.6
551	$6\nu_1 + 1\nu_{12}$	56.0961(2)	0.029(2)	0.77(1)	13.0
552	$13\nu_1 - 2\nu_{10}$	40.5071(2)	0.031(2)	0.42(1)	8.3
553	$9\nu_1 - 2\nu_{10}$	17.8630(2)	0.029(2)	0.34(1)	6.1
554	$-5\nu_{10} + 3\nu_{18}$	30.6132(2)	0.031(2)	0.26(1)	7.1
555	$6\nu_5 - 2\nu_6$	41.2064(2)	0.030(2)	0.50(1)	9.8
556	$-3\nu_1 + 1\nu_{18}$	20.7944(2)	0.033(2)	0.397(9)	5.9
557	$2\nu_{19}$	30.1408(2)	0.030(2)	0.96(1)	6.0
558	$2\nu_7 - 2\nu_{16} + 2\nu_{22}$	21.0387(2)	0.030(2)	0.11(1)	6.2
559	$2\nu_9 + 1\nu_{16} - 1\nu_{18}$	23.2534(2)	0.028(2)	0.43(1)	6.3
560	$2\nu_3 - 1\nu_{13} + 1\nu_{19}$	14.1975(2)	0.029(2)	0.34(1)	5.5
561	$-2\nu_{13} + 1\nu_{18} + 1\nu_{19}$	20.0028(2)	0.029(2)	0.82(1)	5.5
562	$-1\nu_3 - 1\nu_8 + 1\nu_{23}$	34.9398(2)	0.031(2)	0.76(1)	7.0
563	$8\nu_4 - 3\nu_{12}$	12.1389(2)	0.030(2)	0.66(1)	5.3
564	$1\nu_1 + 1\nu_{21}$	25.6519(2)	0.029(2)	0.13(1)	6.0
565	$2\nu_1 - 1\nu_7 + 1\nu_{21}$	21.2899(2)	0.029(2)	0.05(1)	6.8
566	$3\nu_8 + 1\nu_{14}$	36.3873(2)	0.029(2)	0.41(1)	9.0
567	$6\nu_1 + 1\nu_{13}$	50.3887(2)	0.028(2)	0.49(1)	11.1
568	$-1\nu_{13} + 2\nu_{14} + 2\nu_{17}$	56.1152(2)	0.029(2)	0.74(1)	13.1
569	$3\nu_1 + 1\nu_{19}$	32.0534(2)	0.029(2)	0.36(1)	6.3
570	$1\nu_3 + 1\nu_5$	15.6288(2)	0.028(2)	0.32(1)	5.5
571	$3\nu_1 + 1\nu_{18}$	54.7606(2)	0.030(2)	0.24(1)	12.9
572	$-3\nu_3 + 6\nu_4$	35.5668(2)	0.029(2)	0.52(1)	7.4
573	$8\nu_1 + 1\nu_6$	48.2450(2)	0.029(2)	0.85(1)	13.1
574	$9\nu_2 - 4\nu_7$	24.2452(2)	0.031(2)	0.65(1)	5.8
575	$1\nu_2 + 2\nu_{10}$	40.2370(2)	0.028(2)	0.31(1)	8.0
576	$2\nu_1 + 1\nu_{19}$	26.3924(2)	0.030(2)	0.59(1)	5.6
577	$-14\nu_1 + 7\nu_{19}$	26.2384(2)	0.028(2)	0.11(1)	5.7
578	$15\nu_1 - 2\nu_{10}$	51.8293(2)	0.030(2)	0.68(1)	11.7
579	$-1\nu_2 + 2\nu_{13}$	25.6965(2)	0.028(2)	0.24(1)	5.8
580	$2\nu_5 + 2\nu_{16} - 1\nu_{22}$	37.4614(2)	0.030(2)	0.81(1)	6.9
581	$-2\nu_2 - 2\nu_6 + 2\nu_{12}$	24.0494(2)	0.028(2)	0.84(1)	6.0
582	$-8\nu_7 + 5\nu_{13}$	1.9164(2)	0.028(2)	0.90(1)	5.7
583	$2\nu_{16} + 2\nu_{19} - 2\nu_{21}$	34.6526(2)	0.028(2)	0.94(1)	7.1
584	$3\nu_1 + 1\nu_{17}$	39.9157(2)	0.027(2)	0.42(1)	9.2
585	$6\nu_2 - 1\nu_{10}$	26.3496(2)	0.026(2)	0.86(1)	5.7
586	$-1\nu_9 + 2\nu_{11} + 1\nu_{18}$	38.8435(2)	0.028(2)	0.34(1)	7.3
587	$12\nu_1$	67.9327(2)	0.028(2)	0.54(1)	20.7
588	$6\nu_1 + 2\nu_3$	49.5176(2)	0.028(2)	0.33(1)	11.3
589	$2\nu_{15} - 1\nu_{21} - 1\nu_{23}$	7.7934(2)	0.026(2)	0.22(1)	5.5

Table A1: continued

#	ID <sub>K</sub>	$\nu$ [d <sup>-1</sup> ]	A [ppt]	$\phi$ [0 – 1]	S/N
590	$5\nu_8 - 2\nu_{11}$	17.9565(2)	0.028(2)	0.78(1)	5.8
591	$1\nu_2 + 3\nu_{11}$	37.8350(2)	0.027(2)	0.83(1)	6.8
592	$2\nu_{16} - 2\nu_{17} + 2\nu_{20}$	31.6928(2)	0.028(2)	0.73(1)	5.9
593	$-2\nu_5 + 1\nu_7 + 1\nu_{23}$	44.7176(2)	0.028(2)	0.87(1)	8.2
594	$4\nu_{18} - 5\nu_{22}$	37.3991(2)	0.028(2)	0.45(1)	6.8
595	$5\nu_1 - 1\nu_7$	18.2812(2)	0.027(2)	0.77(1)	5.6
596	$-2\nu_7 + 3\nu_{20}$	29.5415(3)	0.027(2)	0.88(1)	5.8
597	$7\nu_1 + 1\nu_5$	47.4809(2)	0.027(2)	0.76(1)	11.5
598	$-10\nu_7 + 10\nu_{14}$	33.1244(2)	0.027(2)	0.93(1)	6.2
599	$5\nu_1 + 1\nu_2 + 1\nu_9$	54.8455(2)	0.028(2)	0.49(1)	12.8
600	$10\nu_1 - 2\nu_{10}$	23.5239(2)	0.029(2)	0.83(1)	5.7
601	$15\nu_1 - 6\nu_{11}$	23.5387(2)	0.028(2)	0.30(1)	5.8
602	$-1\nu_{16} + 2\nu_{17}$	23.6178(2)	0.027(2)	0.15(1)	5.9
603	$8\nu_1 - 1\nu_6$	42.3318(2)	0.026(2)	0.61(1)	10.1
604	$-13\nu_1 + 7\nu_{19}$	31.8995(2)	0.026(2)	0.97(1)	6.0
605	$-2\nu_1 + 1\nu_{19}$	3.7486(2)	0.026(2)	0.70(1)	5.4
606	$1\nu_3 + 1\nu_8$	15.4589(3)	0.025(2)	0.27(1)	5.1
607	$-8\nu_7 + 6\nu_{17}$	57.4012(2)	0.027(2)	0.02(1)	12.1
608	$-10\nu_6 + 7\nu_7$	40.6009(2)	0.027(2)	0.51(1)	7.5
609	$-4\nu_7 + 4\nu_{10}$	26.0772(2)	0.028(2)	0.80(1)	5.2
610	$2\nu_1 + 1\nu_{20}$	27.8522(2)	0.028(2)	1.00(1)	5.0
611	$2\nu_9 + 1\nu_{14} - 1\nu_{16}$	29.8713(3)	0.026(2)	0.33(1)	6.0
612	$6\nu_1 - 1\nu_4$	24.1503(2)	0.026(2)	0.89(1)	6.0
613	$10\nu_1 + 1\nu_3$	64.3861(2)	0.026(2)	0.79(1)	16.0
614	$-4\nu_3 + 3\nu_{12}$	35.2879(2)	0.026(2)	0.24(1)	6.3
615	$-8\nu_3 + 9\nu_4$	26.1393(2)	0.027(2)	0.25(1)	5.5
616	$-10\nu_{11} + 9\nu_{19}$	33.3398(2)	0.025(2)	0.23(1)	6.1
617	$8\nu_5 - 1\nu_{10}$	46.2814(2)	0.025(2)	0.05(1)	8.7
618	$-1\nu_5 + 2\nu_6 + 1\nu_{22}$	20.8039(2)	0.026(2)	0.13(1)	5.5
619	$-5\nu_6 + 2\nu_{10}$	18.3045(2)	0.026(2)	1.00(1)	5.4
620	$3\nu_1 + 1\nu_{16}$	39.2309(2)	0.026(2)	0.96(1)	6.8
621	$-2\nu_{11} + 1\nu_{19} + 2\nu_{21}$	34.5930(2)	0.026(2)	0.10(1)	6.9
622	$1\nu_6 - 1\nu_{16} + 2\nu_{21}$	20.6887(2)	0.026(2)	0.96(1)	5.5
623	$2\nu_{18} - 3\nu_{21}$	15.5831(2)	0.025(2)	0.93(1)	5.2
624	$2\nu_9 + 1\nu_{20} - 2\nu_{21}$	15.3315(3)	0.025(2)	0.34(1)	5.1
625	$-3\nu_4 + 3\nu_{21}$	30.5238(3)	0.024(2)	0.05(1)	6.1
626	$-2\nu_{16} + 1\nu_{18} + 2\nu_{20}$	26.3420(3)	0.025(2)	0.52(1)	5.5
627	$8\nu_5 - 2\nu_{13}$	29.9804(2)	0.025(2)	0.70(1)	5.8
628	$-10\nu_1 + 8\nu_7$	23.5836(3)	0.026(2)	0.54(1)	5.8
629	$5\nu_1 - 1\nu_7 + 1\nu_9$	37.6718(2)	0.024(2)	0.41(1)	6.6
630	$-4\nu_7 + 3\nu_{13}$	9.1712(2)	0.025(2)	0.69(1)	5.3
631	$6\nu_1 + 1\nu_{10}$	50.5101(2)	0.025(2)	0.63(1)	9.9
632	$1\nu_1 + 1\nu_{23}$	56.0620(3)	0.025(2)	0.13(1)	11.5
633	$9\nu_3 - 6\nu_8$	23.8804(3)	0.024(2)	0.22(1)	5.5
634	$-7\nu_1 + 8\nu_7$	40.5669(3)	0.026(2)	0.82(1)	7.3
635	$10\nu_4 - 4\nu_{10}$	31.9857(3)	0.025(2)	0.46(1)	5.7
636	$2\nu_{17} + 1\nu_{18} - 2\nu_{22}$	38.1587(3)	0.025(2)	0.82(1)	7.7
637	$6\nu_5 - 8\nu_6$	23.4670(3)	0.023(2)	0.36(1)	5.7
638	$2\nu_1 + 2\nu_{10}$	44.4101(3)	0.025(2)	0.11(1)	7.7
639	$-6\nu_5 + 9\nu_{11}$	44.9447(3)	0.025(2)	0.96(1)	7.8
640	$2\nu_2 - 2\nu_3 + 2\nu_{10}$	31.8331(3)	0.024(2)	0.57(1)	5.6
641	$1\nu_1 + 1\nu_{22}$	28.4028(3)	0.024(2)	0.79(1)	6.3
642	$-1\nu_4 + 3\nu_{10}$	39.8175(3)	0.024(2)	0.40(1)	8.5
643	$1\nu_9 + 1\nu_{16} + 2\nu_{20}$	74.7005(3)	0.024(2)	0.68(1)	18.4
644	$8\nu_1 + 2\nu_2$	59.5863(3)	0.024(2)	0.15(1)	14.0
645	$-2\nu_9 - 2\nu_{14} + 2\nu_{18}$	23.4348(2)	0.025(2)	0.33(1)	5.7
646	$-2\nu_9 + 2\nu_{11} + 2\nu_{16}$	26.1721(3)	0.024(2)	0.70(1)	5.2
647	$4\nu_1 + 1\nu_{18}$	60.4216(3)	0.024(2)	0.04(1)	13.2
648	$-2\nu_2 + 7\nu_5$	40.6760(3)	0.024(2)	0.18(1)	7.0

Table A1: continued

#	ID <sub>K</sub>	$\nu$ [d <sup>-1</sup> ]	A [ppt]	$\phi$ [0 – 1]	S/N
649	$1\nu_1 + 2\nu_6 + 2\nu_9$	50.3563(3)	0.024(2)	0.78(1)	9.6
650	$-2\nu_8 + 1\nu_{19} + 2\nu_{21}$	39.6833(3)	0.024(2)	0.93(1)	8.7
651	$4\nu_6 + 1\nu_{21}$	31.8159(3)	0.023(2)	0.29(1)	5.5
652	$-2\nu_{13} + 2\nu_{17} + 2\nu_{20}$	46.0791(3)	0.024(2)	0.51(1)	8.4
653	$3\nu_{10} - 1\nu_{17}$	26.6999(3)	0.023(2)	0.75(1)	5.5
654	$-10\nu_9 + 10\nu_{17}$	35.4105(3)	0.022(2)	0.37(1)	6.2
655	$1\nu_3 + 1\nu_{15}$	46.8674(3)	0.023(2)	0.26(1)	9.4
656	$8\nu_1 + 1\nu_9$	64.6798(3)	0.023(2)	0.98(1)	15.1
657	$1\nu_{13} + 1\nu_{15} - 1\nu_{19}$	40.4439(3)	0.024(2)	0.49(1)	7.5
658	$2\nu_{18} + 1\nu_{19} - 2\nu_{20}$	57.5630(3)	0.023(2)	0.76(1)	10.9
659	$4\nu_1 + 1\nu_{19}$	37.7145(3)	0.023(2)	0.12(1)	6.2
660	$-7\nu_1 + 9\nu_3$	30.3512(3)	0.023(2)	0.21(1)	5.1
661	$10\nu_5 - 3\nu_{19}$	33.3224(3)	0.022(2)	0.26(1)	5.6
662	$-10\nu_7 + 8\nu_{20}$	31.9974(3)	0.022(2)	0.21(1)	5.5
663	$-4\nu_{19} + 2\nu_{23}$	40.5220(3)	0.023(2)	0.38(1)	7.3
664	$8\nu_3 - 2\nu_{14}$	35.5324(3)	0.022(2)	0.05(1)	6.1
665	$6\nu_4 - 1\nu_{18}$	21.1199(3)	0.021(2)	0.07(1)	5.3
666	$-10\nu_7 + 6\nu_{17}$	37.3538(3)	0.022(2)	0.56(1)	6.1
667	$-2\nu_3 + 2\nu_{20} + 2\nu_{21}$	57.4903(3)	0.023(2)	0.48(1)	11.2
668	$4\nu_1 - 1\nu_{16} + 2\nu_{17}$	46.2619(3)	0.022(2)	0.28(1)	7.8
669	$-8\nu_1 + 3\nu_{17}$	23.5082(3)	0.021(2)	0.94(1)	5.3
670	$9\nu_1 - 1\nu_2$	43.8006(3)	0.022(2)	0.68(1)	7.7
671	$-2\nu_5 + 2\nu_{10} + 1\nu_{17}$	40.3137(3)	0.022(2)	0.69(1)	7.5
672	$1\nu_{14} + 1\nu_{16}$	35.5864(3)	0.022(2)	0.17(1)	6.1
673	$3\nu_2 + 1\nu_8$	29.1282(3)	0.021(2)	0.03(1)	5.5
674	$-1\nu_5 + 1\nu_{18}$	29.9255(3)	0.021(2)	0.36(1)	5.1
675	$2\nu_7 - 1\nu_{22} + 1\nu_{23}$	47.7094(3)	0.022(2)	0.88(1)	9.8
676	$1\nu_{14} + 1\nu_{17} - 1\nu_{19}$	21.1978(3)	0.019(2)	0.43(2)	5.2
677	$-8\nu_2 + 2\nu_{15}$	20.9926(3)	0.021(2)	0.14(1)	5.1
678	$-2\nu_{13} + 1\nu_{16} + 2\nu_{22}$	34.8867(3)	0.021(2)	0.17(1)	5.6
679	$-15\nu_1 + 5\nu_{17}$	29.7462(3)	0.020(2)	0.30(2)	5.2
680	$-2\nu_{13} + 1\nu_{15} + 2\nu_{22}$	51.7313(3)	0.022(2)	0.96(1)	9.2
681	$-1\nu_{11} + 1\nu_{17} + 1\nu_{20}$	29.2324(3)	0.019(2)	0.62(2)	5.3
682	$7\nu_1 - 1\nu_8$	31.9429(3)	0.020(2)	0.82(2)	5.0
683	$-2\nu_1 + 7\nu_5$	43.6531(3)	0.020(2)	0.91(2)	7.1
684	$3\nu_2 + 1\nu_{18}$	59.2236(3)	0.021(2)	0.55(1)	12.0
685	$-1\nu_4 + 1\nu_{11} + 2\nu_{22}$	45.8981(3)	0.020(2)	0.03(2)	7.4
686	$8\nu_3 - 4\nu_6$	50.3787(3)	0.021(2)	0.63(2)	8.5
687	$14\nu_1 - 2\nu_{10}$	46.1681(3)	0.022(2)	0.07(1)	7.8
688	$7\nu_1 + 1\nu_{12}$	61.7572(3)	0.019(2)	0.55(2)	11.3
689	$2\nu_7 - 1\nu_{15} + 1\nu_{23}$	31.3574(3)	0.019(2)	0.23(2)	5.3
690	$4\nu_2 + 3\nu_6$	37.4669(3)	0.020(2)	0.22(2)	5.6
691	$-12\nu_1 + 7\nu_{19}$	37.5604(3)	0.019(2)	0.80(2)	5.8
692	$7\nu_1 + 2\nu_3$	55.1786(3)	0.020(2)	0.15(2)	10.4
693	$7\nu_1 + 1\nu_8$	47.3109(3)	0.020(2)	0.67(2)	8.5
694	$7\nu_1 + 1\nu_{13}$	56.0498(3)	0.019(2)	0.28(2)	9.6
695	$5\nu_4 - 1\nu_{12}$	26.9510(3)	0.019(2)	0.77(2)	5.0
696	$4\nu_3 + 1\nu_8$	38.7851(3)	0.019(2)	0.88(2)	5.4
697	$1\nu_6 + 1\nu_8 + 1\nu_{15}$	49.7330(3)	0.020(2)	0.86(2)	8.7
698	$1\nu_2 + 1\nu_6 + 1\nu_{23}$	60.5066(3)	0.020(2)	0.27(2)	11.9
699	$-6\nu_1 + 8\nu_7$	46.2279(3)	0.020(2)	0.64(2)	7.6
700	$-5\nu_4 + 2\nu_{23}$	51.7223(3)	0.020(2)	0.66(2)	8.7
701	$-13\nu_1 + 5\nu_{17}$	41.0684(3)	0.019(2)	0.83(2)	6.5
702	$5\nu_4 - 1\nu_5$	41.2279(3)	0.019(2)	0.26(2)	6.6
703	$6\nu_1 + 1\nu_7$	43.9908(3)	0.019(2)	0.09(2)	7.7
704	$7\nu_7 - 2\nu_{14}$	43.4960(3)	0.019(2)	0.59(2)	6.6
705	$4\nu_1 + 1\nu_{14}$	35.9809(3)	0.019(2)	0.01(2)	5.4
706	$-4\nu_1 + 4\nu_{12}$	65.8741(3)	0.019(2)	0.81(2)	12.3
707	$5\nu_1 + 1\nu_{18}$	66.0828(3)	0.019(2)	0.80(2)	13.1

Table A1: continued

#	ID <sub>K</sub>	$\nu$ [d <sup>-1</sup> ]	A [ppt]	$\phi$ [0 – 1]	S/N
708	$-6\nu_3 + 6\nu_{20}$	52.5285(3)	0.019(2)	0.02(2)	9.8
709	$-6\nu_{14} + 5\nu_{17}$	34.6412(3)	0.018(2)	0.35(2)	5.1
710	$10\nu_3 - 4\nu_7$	37.6585(3)	0.019(2)	0.91(2)	5.5
711	$-4\nu_1 + 9\nu_{11}$	69.4206(3)	0.019(2)	0.64(2)	14.6
712	$-2\nu_4 + 8\nu_8$	41.8374(3)	0.019(2)	0.57(2)	7.2
713	$3\nu_8 + 3\nu_{14}$	63.0623(3)	0.019(2)	0.79(2)	10.6
714	$5\nu_1 + 1\nu_{15}$	67.3971(3)	0.018(2)	0.39(2)	12.0
715	$2\nu_8 + 1\nu_{12}$	37.4968(4)	0.019(2)	0.85(2)	5.4
716	$-2\nu_8 + 1\nu_{17} + 1\nu_{18}$	45.3445(3)	0.019(2)	0.62(2)	7.7
717	$8\nu_{13} - 4\nu_{22}$	40.4093(4)	0.020(2)	0.58(2)	6.4
718	$-2\nu_4 + 2\nu_7 + 2\nu_{21}$	40.3999(3)	0.019(2)	0.48(2)	6.5
719	$9\nu_7 - 3\nu_{13}$	40.9489(3)	0.018(2)	0.08(2)	6.1
720	$1\nu_{12} - 1\nu_{16} + 2\nu_{20}$	32.9409(3)	0.018(2)	0.02(2)	5.3
721	$6\nu_3 - 1\nu_8$	38.9679(3)	0.017(2)	0.75(2)	5.1
722	$1\nu_1 + 2\nu_{19}$	35.8019(4)	0.018(2)	0.63(2)	5.2
723	$5\nu_2 + 1\nu_{11}$	45.9748(4)	0.018(2)	0.45(2)	7.1
724	$2\nu_6 + 2\nu_{10}$	39.0009(3)	0.018(2)	0.97(2)	5.1
725	$1\nu_9 + 1\nu_{17} + 1\nu_{19}$	57.3924(4)	0.019(2)	0.73(2)	9.5
726	$7\nu_1 + 1\nu_{10}$	56.1712(4)	0.018(2)	0.38(2)	8.9
727	$1\nu_8 + 2\nu_{12}$	51.9426(4)	0.017(2)	0.77(2)	8.1
728	$8\nu_{13} - 3\nu_{22}$	63.1514(4)	0.018(2)	0.28(2)	10.4
729	$4\nu_2 + 3\nu_3$	51.9230(4)	0.018(2)	0.07(2)	8.1
730	$-13\nu_1 + 5\nu_{16}$	37.6466(4)	0.018(2)	0.30(2)	5.2
731	$2\nu_9 + 2\nu_{12} - 2\nu_{21}$	43.0599(4)	0.018(2)	0.31(2)	6.0
732	$4\nu_9 - 2\nu_{20}$	44.5044(4)	0.018(2)	0.25(2)	5.7
733	$10\nu_3 - 5\nu_5$	38.4890(4)	0.017(2)	0.13(2)	6.3
734	$1\nu_{13} + 1\nu_{14} + 1\nu_{21}$	49.7499(4)	0.017(2)	0.88(2)	7.9
735	$-7\nu_6 + 4\nu_{10}$	45.4787(4)	0.017(2)	0.08(2)	7.6
736	$3\nu_3 + 1\nu_{22}$	46.0702(4)	0.018(2)	0.28(2)	7.1
737	$9\nu_1 - 1\nu_3$	43.1740(4)	0.016(2)	0.63(2)	6.1
738	$-5\nu_1 + 9\nu_2$	36.0366(4)	0.015(2)	0.71(2)	5.1
739	$-10\nu_2 + 8\nu_{14}$	35.2027(3)	0.018(2)	0.46(2)	5.0
740	$9\nu_1 + 1\nu_6$	53.9061(4)	0.017(2)	0.70(2)	9.3
741	$8\nu_1 + 1\nu_5$	53.1420(4)	0.017(2)	0.53(2)	9.0
742	$-2\nu_{15} + 5\nu_{17}$	36.4810(4)	0.015(2)	0.84(2)	5.3
743	$6\nu_6 + 2\nu_{22}$	63.2241(4)	0.016(2)	0.57(2)	10.1
744	$-1\nu_2 + 2\nu_3 + 2\nu_{13}$	41.2473(4)	0.016(2)	0.02(2)	5.9
745	$-1\nu_4 + 2\nu_8 + 2\nu_{12}$	49.8110(4)	0.017(2)	0.71(2)	7.5
746	$1\nu_6 + 1\nu_{14} + 2\nu_{22}$	61.7762(4)	0.016(2)	0.58(2)	9.4
747	$7\nu_1 + 1\nu_4$	49.4434(4)	0.017(2)	0.86(2)	7.3
748	$2\nu_1 + 1\nu_{23}$	61.7231(4)	0.017(2)	0.94(2)	9.5
749	$-9\nu_6 + 5\nu_{20}$	56.0398(4)	0.016(2)	0.41(2)	8.3
750	$-1\nu_9 + 2\nu_{21} + 1\nu_{22}$	43.3329(4)	0.015(2)	0.17(2)	5.9
751	$-1\nu_9 + 2\nu_{10} + 2\nu_{16}$	58.1895(4)	0.016(2)	0.80(2)	9.9
752	$-4\nu_{11} + 5\nu_{13}$	41.1936(4)	0.016(2)	0.70(2)	5.9
753	$9\nu_2 - 3\nu_6$	55.4721(4)	0.016(2)	0.46(2)	8.6
754	$1\nu_7 + 2\nu_{11} + 1\nu_{14}$	43.8197(4)	0.016(2)	0.62(2)	6.4
755	$11\nu_1 - 2\nu_7$	42.2220(4)	0.015(2)	0.34(2)	6.3
756	$2\nu_9 + 1\nu_{10} - 1\nu_{19}$	40.2540(4)	0.016(2)	0.93(2)	5.8
757	$3\nu_1 + 2\nu_{10}$	50.0712(4)	0.015(2)	0.85(2)	6.9
758	$-9\nu_3 + 5\nu_{17}$	44.6805(4)	0.015(2)	0.98(2)	5.3
759	$-1\nu_{11} + 1\nu_{12} + 2\nu_{22}$	57.3833(4)	0.016(2)	0.45(2)	8.6
760	$1\nu_8 + 1\nu_{17} + 1\nu_{21}$	50.6056(4)	0.016(2)	0.84(2)	6.8
761	$13\nu_1$	73.5938(4)	0.015(2)	0.31(2)	13.3
762	$4\nu_3 + 2\nu_{11}$	51.5593(4)	0.015(2)	0.76(2)	7.3
763	$5\nu_1 + 1\nu_{19}$	43.3756(4)	0.015(2)	0.86(2)	5.7
764	$10\nu_2 + 3\nu_6$	80.3615(4)	0.015(2)	0.55(2)	14.1
765	$9\nu_1 - 1\nu_6$	47.9929(4)	0.015(2)	0.40(2)	7.0
766	$4\nu_2 + 6\nu_6$	46.3371(4)	0.015(2)	0.86(2)	6.0

Table A1: continued

#	ID <sub>K</sub>	$\nu$ [d <sup>-1</sup> ]	A [ppt]	$\phi$ [0 – 1]	S/N
767	$7\nu_5 - 3\nu_6$	46.1049(4)	0.015(2)	0.32(2)	6.5
768	$5\nu_{16} - 3\nu_{22}$	43.0149(4)	0.014(2)	0.28(2)	5.5
769	$-2\nu_{17} + 2\nu_{18} + 1\nu_{19}$	44.7597(4)	0.015(2)	0.39(2)	5.0
770	$1\nu_9 - 1\nu_{13} + 1\nu_{23}$	53.3704(4)	0.015(2)	0.76(2)	8.3
771	$4\nu_{10} - 1\nu_{21}$	46.1831(4)	0.015(2)	0.11(2)	6.4
772	$2\nu_{17} + 2\nu_{19} - 1\nu_{21}$	56.0173(4)	0.015(2)	0.58(2)	7.8
773	$9\nu_2 - 1\nu_{14}$	51.0054(4)	0.014(2)	0.49(2)	7.7
774	$11\nu_1 + 1\nu_3$	70.0472(4)	0.014(2)	0.62(2)	10.7
775	$4\nu_1 + 1\nu_{17}$	45.5764(4)	0.014(2)	0.42(2)	6.5
776	$-2\nu_{11} - 2\nu_{13} + 2\nu_{23}$	47.4984(4)	0.014(2)	0.36(2)	6.8
777	$-9\nu_7 + 9\nu_{13}$	57.5841(4)	0.014(2)	0.84(2)	7.9
778	$-3\nu_2 + 7\nu_7$	48.7210(5)	0.014(2)	0.98(2)	6.0
779	$4\nu_1 + 1\nu_{16}$	44.8921(4)	0.014(2)	0.64(2)	5.0
780	$-7\nu_{17} + 9\nu_{22}$	44.1500(4)	0.014(2)	0.92(2)	6.0
781	$2\nu_{12} + 2\nu_{15} - 2\nu_{18}$	46.8890(5)	0.014(2)	0.97(2)	6.2
782	$-5\nu_1 + 8\nu_7$	51.8890(5)	0.014(2)	0.38(2)	7.0
783	$-8\nu_9 + 10\nu_{12}$	66.1677(4)	0.014(2)	0.04(2)	10.4
784	$1\nu_5 + 2\nu_{11} + 1\nu_{15}$	67.4040(5)	0.013(2)	0.22(2)	9.4
785	$3\nu_2 + 7\nu_6$	42.1421(5)	0.013(2)	0.55(2)	5.6
786	$-3\nu_5 + 5\nu_{14}$	43.1226(5)	0.014(2)	0.45(2)	5.3
787	$6\nu_1 + 1\nu_{18}$	71.7438(4)	0.014(2)	0.61(2)	11.3
788	$2\nu_5 - 2\nu_7 + 1\nu_{23}$	46.0612(4)	0.014(2)	0.93(2)	6.4
789	$-4\nu_1 + 9\nu_2$	41.6975(5)	0.013(2)	0.54(2)	5.2
790	$9\nu_1 + 2\nu_2$	65.2473(5)	0.013(2)	0.01(2)	9.5
791	$1\nu_2 + 2\nu_3 + 2\nu_{11}$	43.1582(5)	0.013(2)	0.37(2)	5.3
792	$-12\nu_1 + 5\nu_{16}$	43.3077(5)	0.013(2)	0.04(2)	5.4
793	$2\nu_8 + 1\nu_{16} + 1\nu_{21}$	57.6037(5)	0.013(2)	0.52(2)	7.7
794	$3\nu_5 + 3\nu_8$	46.6099(5)	0.013(2)	0.94(2)	5.6
795	$3\nu_3 + 1\nu_{21}$	43.3194(5)	0.012(2)	0.77(3)	5.5
796	$2\nu_{15} - 1\nu_{16} - 2\nu_{19}$	25.7945(3)	0.023(2)	0.47(1)	5.0
797	$10\nu_1 - 1\nu_2$	49.4617(5)	0.013(2)	0.43(2)	6.1
798	$-12\nu_1 + 5\nu_{17}$	46.7295(5)	0.013(2)	0.61(2)	5.9
799	$-5\nu_2 + 5\nu_{20}$	46.9083(5)	0.013(2)	0.87(2)	6.1
800	$-1\nu_1 + 7\nu_5$	49.3141(5)	0.012(2)	0.74(2)	6.0
801	$-2\nu_5 + 2\nu_9 + 2\nu_{11}$	43.5365(5)	0.012(2)	0.12(3)	5.5
802	$9\nu_1 + 1\nu_9$	70.3408(5)	0.013(2)	0.81(2)	10.5
803	$-1\nu_{12} - 1\nu_{14} + 2\nu_{23}$	51.9981(5)	0.013(2)	0.61(2)	6.5
804	$-2\nu_7 + 1\nu_{21} + 1\nu_{23}$	50.3416(5)	0.013(2)	0.74(2)	5.8
805	$8\nu_1 + 2\nu_3$	60.8399(5)	0.013(2)	0.81(2)	8.5
806	$3\nu_3 + 2\nu_{22}$	68.8125(5)	0.013(2)	0.06(2)	9.5
807	$1\nu_4 + 4\nu_8$	40.5478(4)	0.014(2)	0.94(2)	5.0
808	$2\nu_9 + 2\nu_{13} - 1\nu_{21}$	51.6359(5)	0.013(2)	0.14(2)	6.6
809	$2\nu_{10} - 1\nu_{11} + 2\nu_{17}$	68.7234(5)	0.013(2)	0.59(2)	9.8
810	$5\nu_{17} - 4\nu_{19}$	54.3821(5)	0.013(2)	0.77(2)	6.5
811	$-11\nu_1 + 7\nu_{19}$	43.2215(5)	0.011(2)	0.54(3)	5.3
812	$3\nu_3 + 5\nu_8$	61.7430(5)	0.013(2)	0.38(2)	7.6
813	$3\nu_2 + 2\nu_{21}$	61.4304(5)	0.013(2)	0.66(2)	7.6
814	$8\nu_1 + 1\nu_{13}$	61.7109(5)	0.011(2)	0.07(3)	8.0
815	$9\nu_{20} - 5\nu_{21}$	48.8195(5)	0.012(2)	0.90(3)	5.4
816	$4\nu_{21} - 1\nu_{22}$	57.2205(5)	0.012(2)	0.45(3)	7.1
817	$9\nu_{11} - 3\nu_{19}$	46.8545(5)	0.011(2)	0.55(3)	5.7
818	$2\nu_{12} - 2\nu_{16} + 1\nu_{23}$	50.1654(5)	0.012(2)	0.04(3)	5.5
819	$-8\nu_5 + 3\nu_{15}$	54.4499(5)	0.011(2)	0.34(3)	6.4
820	$7\nu_1 + 1\nu_7$	49.6519(5)	0.012(2)	0.78(3)	6.2
821	$-2\nu_9 + 2\nu_{18} + 1\nu_{19}$	51.8443(5)	0.012(2)	0.79(3)	6.5
822	$-6\nu_{12} + 8\nu_{22}$	49.1571(5)	0.012(2)	0.31(3)	5.4
823	$-6\nu_4 + 5\nu_{17}$	55.7695(6)	0.011(2)	0.79(3)	6.3
824	$2\nu_9 + 2\nu_{12} - 1\nu_{17}$	60.1109(5)	0.012(2)	0.16(3)	7.4
825	$2\nu_{13} - 1\nu_{17} + 2\nu_{22}$	55.3941(5)	0.012(2)	0.64(3)	6.9

Table A1: continued

#	ID <sub>K</sub>	$\nu$ [d <sup>-1</sup> ]	A [ppt]	$\phi$ [0 – 1]	S/N
826	$10\nu_9 - 6\nu_{12}$	61.1332(5)	0.012(2)	0.20(3)	8.2
827	$10\nu_3 - 3\nu_6$	68.8851(5)	0.011(2)	0.40(3)	9.1
828	$-2\nu_{12} + 2\nu_{15} + 1\nu_{22}$	56.6666(5)	0.011(2)	0.18(3)	7.2
829	$1\nu_{17} + 2\nu_{19} + 1\nu_{21}$	73.0652(5)	0.011(2)	0.90(3)	9.2
830	$-2\nu_3 + 8\nu_8$	45.9151(5)	0.011(2)	0.71(3)	5.3
831	$-2\nu_6 + 1\nu_{12} + 2\nu_{22}$	61.7008(6)	0.011(2)	0.19(3)	7.5
832	$-1\nu_{12} - 1\nu_{15} + 2\nu_{24}$	64.8846(6)	0.011(2)	0.38(3)	7.5
833	$-3\nu_1 + 9\nu_{11}$	75.0818(6)	0.011(2)	0.37(3)	10.0
834	$1\nu_{11} + 2\nu_{18} - 1\nu_{22}$	63.0445(6)	0.012(2)	0.14(3)	7.1
835	$-2\nu_{12} + 2\nu_{15} + 1\nu_{19}$	48.9941(6)	0.011(2)	0.92(3)	5.0
836	$2\nu_{17} - 2\nu_{19} + 2\nu_{20}$	48.7836(6)	0.011(2)	0.12(3)	5.0
837	$2\nu_4 + 10\nu_6$	49.1976(6)	0.010(2)	0.80(3)	5.4
838	$\nu_{24}$	63.0535(6)	0.011(2)	0.54(3)	7.1
839	$-4\nu_1 + 8\nu_7$	57.5499(6)	0.011(2)	0.26(3)	6.6
840	$-2\nu_8 + 2\nu_{12} + 1\nu_{16}$	51.1397(6)	0.011(2)	0.90(3)	5.9
841	$7\nu_2 - 1\nu_6$	47.0842(6)	0.009(2)	0.46(3)	5.0
842	$2\nu_{11} + 1\nu_{12} + 1\nu_{19}$	57.6592(6)	0.011(2)	0.41(3)	6.5
843	$8\nu_1 + 1\nu_{12}$	67.4183(6)	0.010(2)	0.32(3)	7.4
844	$4\nu_{11} + 1\nu_{17}$	63.8506(6)	0.010(2)	0.57(3)	7.7
845	$-3\nu_1 + 4\nu_{12}$	71.5352(6)	0.010(2)	0.59(3)	8.8
846	$-5\nu_3 + 7\nu_{14}$	54.4807(6)	0.010(2)	0.57(3)	5.6
847	$8\nu_1 + 1\nu_{10}$	61.8321(6)	0.010(2)	0.29(3)	7.0
848	$-7\nu_5 + 5\nu_{16}$	56.2664(6)	0.010(2)	0.77(3)	6.0
849	$-11\nu_1 + 5\nu_{17}$	52.3906(6)	0.010(2)	0.27(3)	5.6
850	$9\nu_4 - 5\nu_8$	49.9239(7)	0.009(2)	0.32(3)	5.2
851	$3\nu_2 + 4\nu_3$	52.5500(6)	0.010(2)	0.80(3)	5.5
852	$6\nu_1 + 1\nu_{15}$	73.0582(6)	0.010(2)	0.20(3)	8.1
853	$9\nu_1 + 1\nu_5$	58.8029(6)	0.009(2)	0.39(3)	6.2
854	$-2\nu_3 + 7\nu_4$	53.1596(6)	0.010(2)	0.05(3)	5.6
855	$1\nu_{17} - 1\nu_{22} + 1\nu_{24}$	63.2451(6)	0.010(2)	0.66(3)	6.7
856	$2\nu_{13} - 1\nu_{16} + 2\nu_{22}$	56.0820(7)	0.009(2)	0.66(3)	5.6
857	$2\nu_{13} - 1\nu_{14} + 2\nu_{20}$	52.5692(7)	0.009(2)	0.73(3)	5.5
858	$2\nu_6 + 2\nu_7 + 2\nu_{17}$	71.8288(6)	0.010(2)	0.83(3)	8.4
859	$-1\nu_5 + 3\nu_{16}$	58.8892(7)	0.010(2)	0.08(3)	6.2
860	$1\nu_{11} + 1\nu_{12} + 2\nu_{14}$	59.0314(6)	0.010(2)	0.56(3)	6.4
861	$1\nu_{13} + 2\nu_{20}$	49.4808(6)	0.009(2)	0.44(3)	5.1
862	$2\nu_4 + 1\nu_6 + 1\nu_{15}$	61.6784(6)	0.009(2)	0.36(3)	6.7
863	$3\nu_1 + 1\nu_{23}$	67.3841(7)	0.009(2)	0.79(3)	6.7
864	$-3\nu_{17} + 8\nu_{19}$	51.7661(7)	0.009(2)	0.94(3)	5.3
865	$10\nu_1 + 1\nu_6$	59.5673(7)	0.009(2)	0.36(3)	6.1
866	$8\nu_1 + 1\nu_8$	52.9721(7)	0.009(2)	0.39(3)	5.4
867	$3\nu_3 + 5\nu_{11}$	74.4736(7)	0.009(2)	0.83(3)	8.4
868	$-9\nu_5 + 6\nu_{22}$	65.7719(7)	0.009(2)	0.02(3)	6.9
869	$-1\nu_2 + 2\nu_{12} + 1\nu_{17}$	60.0432(7)	0.009(2)	0.47(3)	5.9
870	$15\nu_1 - 2\nu_7$	64.8661(7)	0.009(2)	0.30(3)	6.5
871	$2\nu_6 + 2\nu_9 + 1\nu_{22}$	67.4373(7)	0.009(2)	0.36(3)	6.7
872	$-1\nu_8 + 2\nu_9 + 1\nu_{12}$	53.2282(7)	0.009(2)	0.25(3)	5.4
873	$10\nu_3 - 2\nu_{11}$	57.2970(7)	0.009(2)	0.96(3)	5.7
874	$4\nu_1 + 2\nu_{10}$	55.7323(7)	0.009(2)	0.63(4)	5.2
875	$6\nu_1 + 2\nu_7$	54.0164(8)	0.008(2)	0.14(4)	5.2
876	$2\nu_{13} + 1\nu_{22}$	55.5849(7)	0.009(2)	0.08(4)	5.3
877	$8\nu_2 + 1\nu_{14}$	70.5273(7)	0.009(2)	0.98(4)	7.2
878	$1\nu_{11} + 1\nu_{16} + 1\nu_{17}$	55.4109(7)	0.009(2)	0.66(3)	5.5
879	$14\nu_1 - 2\nu_7$	59.2052(7)	0.008(2)	0.44(4)	5.9
880	$12\nu_1 + 1\nu_3$	75.7080(7)	0.009(2)	0.61(4)	7.5
881	$8\nu_1 + 1\nu_4$	55.1043(7)	0.009(2)	0.78(3)	5.0
882	$2\nu_7 + 1\nu_{10} + 2\nu_{14}$	63.2647(7)	0.009(2)	0.34(4)	6.1
883	$10\nu_1 + 2\nu_2$	70.9083(7)	0.009(2)	0.85(4)	7.7
884	$10\nu_1 - 1\nu_6$	53.6538(7)	0.009(2)	0.29(4)	5.2

Table A1: continued

#	ID <sub>K</sub>	$\nu$ [d <sup>-1</sup> ]	A [ppt]	$\phi$ [0 – 1]	S/N
885	$1\nu_{10} + 1\nu_{11} + 1\nu_{18}$	64.5502(7)	0.009(2)	0.91(4)	6.3
886	$6\nu_{12} - 4\nu_{13}$	67.0913(7)	0.008(2)	0.50(4)	6.2
887	$1\nu_{15} - 1\nu_{16} + 2\nu_{22}$	62.3275(7)	0.008(2)	0.13(4)	6.3
888	$7\nu_1 + 1\nu_{18}$	77.4049(7)	0.009(2)	0.40(4)	8.0
889	$2\nu_4 + 3\nu_{12}$	86.0226(7)	0.008(2)	0.37(4)	9.4
890	$-1\nu_6 + 2\nu_{13} + 2\nu_{16}$	74.3844(8)	0.008(2)	0.44(4)	7.6
891	$2\nu_{14} - 1\nu_{17} + 1\nu_{24}$	66.7942(8)	0.008(2)	0.04(4)	6.6
892	$9\nu_1 + 1\nu_{13}$	67.3719(7)	0.008(2)	0.82(4)	6.2
893	$9\nu_1 + 2\nu_3$	66.5009(8)	0.008(2)	0.67(4)	6.5
894	$-10\nu_4 + 4\nu_{15}$	58.2109(8)	0.008(2)	0.65(4)	5.2
895	$-1\nu_8 + 1\nu_{14} + 1\nu_{24}$	68.7056(8)	0.008(2)	0.96(4)	6.5
896	$1\nu_1 + 1\nu_{24}$	68.7146(8)	0.008(2)	0.30(4)	6.7
897	$-2\nu_7 + 2\nu_{16} + 2\nu_{20}$	57.5056(8)	0.008(2)	0.37(4)	5.2
898	$2\nu_8 - 2\nu_{21} + 2\nu_{23}$	76.1883(8)	0.008(2)	0.82(4)	6.9
899	$2\nu_{15} - 1\nu_{18} + 2\nu_{19}$	70.5455(8)	0.008(2)	0.26(4)	6.5
900	$1\nu_{14} + 2\nu_{22}$	58.8207(8)	0.007(2)	0.84(4)	5.2
901	$-8\nu_8 + 2\nu_{24}$	64.6392(9)	0.007(2)	0.46(4)	5.7
902	$5\nu_3 + 3\nu_8$	61.9277(8)	0.008(2)	0.43(4)	5.4
903	$-3\nu_1 + 8\nu_7$	63.2110(8)	0.007(2)	0.03(4)	5.4
904	$1\nu_4 + 2\nu_{18} - 1\nu_{19}$	70.3001(9)	0.007(2)	0.38(4)	6.6
905	$3\nu_2 + 2\nu_{12}$	65.7042(8)	0.007(2)	0.31(4)	5.6
906	$7\nu_1 + 2\nu_7$	59.6774(9)	0.007(2)	0.92(4)	5.1
907	$4\nu_2 + 4\nu_{11}$	69.5118(8)	0.007(2)	0.28(4)	6.3
908	$1\nu_7 - 2\nu_8 + 2\nu_{18}$	70.2113(8)	0.007(2)	0.72(4)	6.5
909	$-1\nu_{12} + 5\nu_{20}$	60.5197(9)	0.007(2)	0.50(4)	5.1
910	$-2\nu_9 + 6\nu_{10}$	60.4791(9)	0.007(2)	0.93(4)	5.2
911	$-1\nu_9 + 2\nu_{16} + 1\nu_{18}$	62.8816(9)	0.007(2)	0.21(4)	5.2
912	$-2\nu_8 - 2\nu_{20} + 2\nu_{23}$	68.9061(9)	0.007(2)	0.46(4)	6.2
913	$-7\nu_7 + 9\nu_{10}$	78.7261(9)	0.007(2)	0.80(5)	6.9
914	$14\nu_1$	79.2547(9)	0.007(2)	0.21(4)	7.1
915	$-1\nu_{12} + 1\nu_{15} + 1\nu_{23}$	67.3617(9)	0.007(2)	0.09(4)	5.4
916	$-2\nu_1 + 4\nu_{12}$	77.1963(9)	0.007(2)	0.43(4)	6.8
917	$\nu_{25}$	77.4900(9)	0.007(2)	0.50(5)	6.8
918	$9\nu_9 - 5\nu_{12}$	63.8722(9)	0.007(2)	0.31(5)	5.2
919	$6\nu_8 + 1\nu_9$	65.493(1)	0.006(2)	0.18(5)	5.2
920	$-1\nu_{13} + 4\nu_{22}$	74.5462(9)	0.007(2)	0.19(5)	6.3
921	$-2\nu_6 + 2\nu_{10} + 2\nu_{12}$	71.433(1)	0.006(2)	0.73(5)	5.7
922	$-2\nu_1 + 9\nu_{11}$	80.743(1)	0.006(2)	0.08(5)	6.9
923	$10\nu_1 + 1\nu_9$	76.0019(9)	0.006(2)	0.58(5)	6.0
924	$13\nu_1 + 1\nu_3$	81.369(1)	0.006(2)	0.29(5)	6.6
925	$\nu_{26}$	91.684(1)	0.006(2)	0.11(5)	7.6
926	$-7\nu_8 + 9\nu_{19}$	81.849(1)	0.006(2)	0.65(5)	6.4
927	$10\nu_6 + 3\nu_{10}$	79.201(1)	0.006(2)	0.23(5)	6.0
928	$-4\nu_8 + 8\nu_{14}$	75.961(1)	0.006(2)	0.01(5)	5.7
929	$-4\nu_3 + 5\nu_{16}$	80.135(1)	0.006(2)	0.68(5)	5.9
930	$1\nu_{10} + 2\nu_{12} + 1\nu_{19}$	75.872(1)	0.005(2)	0.60(6)	5.5
931	$11\nu_1 + 2\nu_2$	76.570(1)	0.006(2)	0.58(5)	5.6
932	$-9\nu_4 + 10\nu_{10}$	77.094(1)	0.006(2)	0.66(5)	5.7
933	$1\nu_2 + 3\nu_{12}$	73.539(1)	0.005(2)	0.52(6)	5.1
934	$1\nu_9 + 1\nu_{19} + 1\nu_{23}$	84.862(1)	0.005(2)	0.86(6)	6.0
935	$8\nu_1 + 1\nu_{18}$	83.066(1)	0.005(2)	0.16(6)	6.1
936	$-2\nu_2 + 5\nu_{19}$	61.0553(9)	0.007(2)	0.38(5)	5.0
937	$9\nu_1 + 2\nu_7$	71.000(1)	0.005(2)	0.42(6)	5.1
938	$2\nu_8 - 1\nu_{14} + 2\nu_{15}$	80.214(1)	0.005(2)	0.69(7)	5.1
939	$7\nu_1 + 1\nu_{15}$	78.719(1)	0.005(2)	0.03(6)	5.0
940	$9\nu_2 + 2\nu_7$	84.387(1)	0.005(2)	0.74(6)	5.5
941	$-7\nu_{10} + 4\nu_{23}$	85.796(1)	0.005(2)	0.32(7)	5.5
942	$12\nu_1 + 2\nu_2$	82.230(1)	0.005(2)	0.44(7)	5.3
943	$11\nu_1 + 1\nu_9$	81.663(1)	0.004(2)	0.32(7)	5.1

Table A1: continued

#	ID <sub>K</sub>	$\nu$ [d <sup>-1</sup> ]	A [ppt]	$\phi$ [0 – 1]	S/N
944	$-5\nu_6 + 10\nu_{11}$	87.510(1)	0.004(2)	0.52(7)	5.0
945	$10\nu_{12} - 2\nu_{24}$	95.191(2)	0.004(2)	0.2(4)	5.1

Table A2: All frequencies detected in six combined *TESS* sectors with S/N > 5. Columns contain: number, our ID<sub>T</sub>, frequency, amplitude, phase, signal to noise ratio.

#	ID <sub>T</sub>	$\nu$ [d <sup>-1</sup> ]	A [ppt]	$\phi$ [0 – 1]	S/N
1	$\nu_1$	5.6610574(7)	100.24(1)	0.86115(2)	31.7
2	$2\nu_1$	11.322115(1)	31.99(1)	0.64295(6)	31.6
3	$\nu_2$	7.148978(3)	11.76(1)	0.9321(2)	31.3
4	$3\nu_1$	16.983173(2)	10.14(1)	0.4398(2)	31.5
5	$1\nu_1 + 1\nu_2$	12.810036(4)	5.42(1)	0.6431(3)	30.3
6	$4\nu_1$	22.644231(4)	4.99(1)	0.1819(4)	30.5
7	$\nu_3$	7.775571(3)	4.71(1)	0.9577(4)	28.0
8	$-1\nu_1 + 1\nu_2$	1.487924(4)	3.63(1)	0.3245(5)	27.7
9	$2\nu_1 + 1\nu_2$	18.471093(5)	2.76(1)	0.4338(6)	29.5
10	$1\nu_1 + 1\nu_3$	13.436619(5)	2.64(1)	0.7809(7)	24.3
11	$5\nu_1$	28.305287(5)	2.37(1)	0.9625(7)	29.6
12	$-1\nu_1 + 1\nu_3$	2.114511(7)	1.61(1)	0.351(1)	24.1
13	instrumental	0.067193(8)	1.50(1)	0.146(1)	7.3
14	$2\nu_1 + 1\nu_3$	19.097675(7)	1.58(1)	0.522(1)	21.3
15	$\nu_4$	10.122796(8)	1.39(1)	0.918(1)	17.3
16	$2\nu_1 - 1\nu_2$	4.173135(8)	1.35(1)	0.924(1)	26.4
17	instrumental	0.055213(9)	1.07(1)	0.943(2)	6.3
18	$3\nu_1 + 1\nu_2$	24.132145(8)	1.22(1)	0.235(1)	27.2
19	$6\nu_1$	33.966346(8)	1.15(1)	0.718(2)	27.6
20	$\nu_5$	9.81861(1)	0.92(1)	0.881(2)	16.7
21	instrumental	0.13889(1)	0.93(1)	0.826(2)	5.8
22	$\nu_6$	10.02425(1)	0.87(1)	0.513(2)	19.7
23	$\nu_7$	7.85337(1)	0.81(1)	0.338(2)	16.8
24	spurious	5.664770(9)	1.06(1)	0.665(2)	15.1
25	$3\nu_1 + 1\nu_3$	24.75872(1)	0.78(1)	0.355(2)	19.4
26	$4\nu_1 + 1\nu_2$	29.79320(1)	0.77(1)	0.012(2)	25.4
27	$2\nu_1 - 1\nu_3$	3.54655(1)	0.74(1)	0.943(2)	21.1
28	$\nu_8$	19.19308(1)	0.77(1)	0.665(2)	18.0
29	$\nu_9$	7.68344(1)	0.72(1)	0.331(2)	20.3
30	$-1\nu_1 + 1\nu_8$	13.53203(1)	0.61(1)	0.875(3)	12.9
31	$\nu_{10}$	22.10602(1)	0.53(1)	0.288(4)	16.2
32	$1\nu_1 + 1\nu_4$	15.78387(1)	0.59(1)	0.566(3)	15.6
33	$7\nu_1$	39.62741(1)	0.59(1)	0.456(3)	24.4
34	spurious	5.65103(1)	0.80(1)	0.767(3)	12.7
35	$\nu_{11}$	16.44771(2)	0.43(1)	0.067(4)	12.7
36	$1\nu_1 + 1\nu_7$	13.51442(2)	0.46(1)	0.124(4)	11.3
37	$5\nu_1 + 1\nu_2$	35.45427(2)	0.45(1)	0.729(4)	21.6
38	$4\nu_1 + 1\nu_3$	30.41980(2)	0.44(1)	0.039(4)	18.4
39	$2\nu_2$	14.29794(2)	0.44(1)	0.781(4)	18.7
40	$1\nu_1 + 1\nu_9$	13.34455(2)	0.41(1)	0.870(4)	12.1
41	$1\nu_1 + 2\nu_2 - 1\nu_4$	9.83695(2)	0.43(1)	0.215(4)	13.4
42	$1\nu_2 + 1\nu_3$	14.92455(2)	0.40(1)	0.822(4)	16.8
43	$1\nu_5 + 1\nu_{10} - 1\nu_{11}$	15.47691(2)	0.41(1)	0.029(4)	14.9
44	$1\nu_1 + 1\nu_{10}$	27.76706(2)	0.36(1)	0.111(6)	15.0
45	$3\nu_1 - 1\nu_3$	9.20758(2)	0.36(1)	0.824(5)	12.2
46	$1\nu_1 + 1\nu_6$	15.68531(2)	0.35(1)	0.204(5)	16.8
47	spurious	5.64737(2)	0.40(1)	0.278(5)	9.2
48	$1\nu_1 + 2\nu_2$	19.95902(2)	0.34(1)	0.402(5)	15.8
49	$-1\nu_6 + 2\nu_7$	5.68226(2)	0.41(1)	0.525(5)	10.1
50	$1\nu_1 + 1\nu_8$	24.85414(2)	0.33(1)	0.451(5)	13.1

Table A2: continued

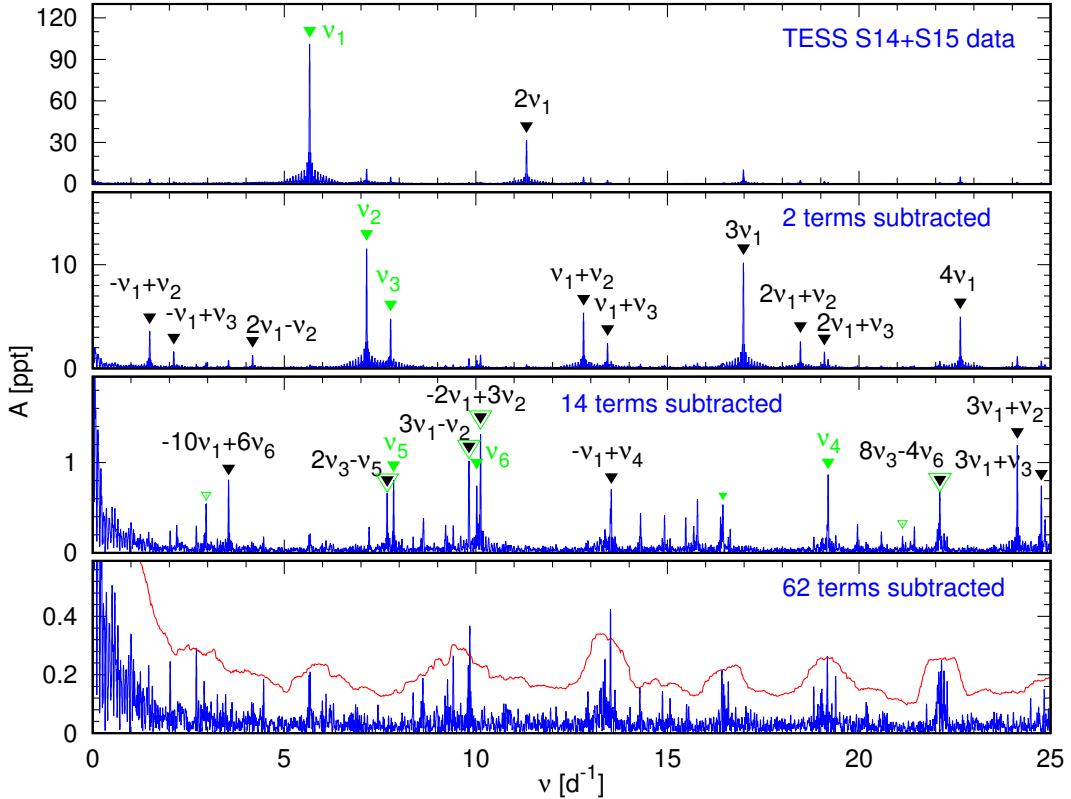
#	ID <sub>T</sub>	$\nu$ [d <sup>-1</sup> ]	A [ppt]	$\phi$ [0 – 1]	S/N
51	$-1\nu_1 + 2\nu_2$	8.63692(2)	0.31(1)	0.049(6)	13.2
52	$\nu_{12}$	2.95974(3)	0.29(1)	0.752(6)	9.6
53	$2\nu_1 + 1\nu_4$	21.44493(3)	0.30(1)	0.317(6)	12.0
54	$8\nu_1$	45.28848(3)	0.29(1)	0.224(6)	17.5
55	$\nu_{13}$	22.12713(3)	0.32(1)	0.162(6)	9.1
56	$2\nu_4 + 2\nu_7 - 2\nu_9$	20.58562(3)	0.28(1)	0.410(6)	14.0
57	$2\nu_1 + 1\nu_7$	19.17551(3)	0.26(1)	0.730(7)	9.0
58	$-1\nu_1 + 1\nu_7$	2.19229(3)	0.26(1)	0.821(7)	8.6
59	$-1\nu_1 + 1\nu_9$	2.02243(3)	0.27(1)	0.492(7)	9.0
60	$6\nu_1 + 1\nu_2$	41.11534(3)	0.27(1)	0.470(7)	16.7
61	$2\nu_1 + 1\nu_9$	19.00559(3)	0.23(1)	0.687(8)	9.5
62	$2\nu_4 - 1\nu_8 + 2\nu_9$	16.42010(3)	0.27(1)	0.342(6)	7.8
63	$\nu_{14}$	9.40935(3)	0.25(1)	0.212(7)	9.0
64	$\nu_{15}$	22.08397(3)	0.28(1)	0.492(6)	8.9
65	$2\nu_1 + 1\nu_2 + 1\nu_3$	26.24667(3)	0.25(1)	0.219(7)	13.2
66	$-10\nu_8 + 9\nu_{13}$	7.21348(3)	0.25(1)	0.630(7)	10.5
67	$-2\nu_3 + 1\nu_8 + 1\nu_9$	11.32587(2)	0.40(2)	0.232(6)	9.8
68	$5\nu_1 + 1\nu_3$	36.08087(3)	0.24(1)	0.729(7)	14.9
69	$2\nu_1 + 1\nu_{10}$	33.42811(3)	0.24(1)	0.824(7)	11.7
70	$2\nu_2 + 1\nu_6 - 1\nu_9$	16.63956(3)	0.23(1)	0.817(8)	6.9
71	$\nu_{16}$	13.33399(4)	0.27(1)	0.503(7)	7.0
72	$1\nu_9 - 1\nu_{11} + 1\nu_{13}$	13.36348(3)	0.25(1)	0.508(7)	8.3
73	spurious	5.67590(2)	0.31(1)	0.031(7)	7.1
74	$6\nu_7 - 4\nu_9$	16.38679(3)	0.23(1)	0.181(8)	7.8
75	$-1\nu_{10} + 1\nu_{11} + 1\nu_{13}$	16.46881(3)	0.23(1)	0.026(8)	7.9
76	$\nu_{17}$	21.13797(3)	0.21(1)	0.791(8)	11.0
77	$2\nu_3 + 2\nu_6 - 2\nu_{11}$	2.70406(4)	0.19(1)	0.179(9)	6.6
78	$2\nu_1 + 2\nu_2$	25.62007(4)	0.20(1)	0.238(9)	11.9
79	$-1\nu_1 + 1\nu_4$	4.46175(4)	0.20(1)	0.112(9)	9.5
80	$\nu_{18}$	11.33598(3)	0.22(1)	0.272(9)	8.0
81	$-2\nu_9 - 2\nu_{15} + 2\nu_{14}$	19.39172(4)	0.18(1)	0.32(1)	7.8
82	$2\nu_5 + 1\nu_{12} - 1\nu_{16}$	9.26349(4)	0.17(1)	0.20(1)	8.0
83	$-1\nu_1 + 1\nu_{20}$	16.43474(3)	0.21(1)	0.415(9)	7.4
84	$2\nu_1 + 1\nu_6$	21.34638(4)	0.18(1)	0.92(1)	11.0
85	$7\nu_3 - 9\nu_{12}$	27.79093(4)	0.19(1)	0.477(9)	7.9
86	$\nu_{19}$	13.63011(4)	0.16(1)	0.64(1)	6.9
87	$7\nu_1 - 3\nu_{18}$	5.61890(4)	0.18(1)	0.69(1)	5.8
88	$3\nu_6 - 1\nu_7$	22.21941(5)	0.14(1)	0.28(1)	6.2
89	$1\nu_{12} + 1\nu_{19}$	16.58941(4)	0.16(1)	0.28(1)	6.5
90	$2\nu_1 + 1\nu_8$	30.51517(4)	0.15(1)	0.29(1)	9.7
91	$1\nu_{10} - 1\nu_{18} + 1\nu_{17}$	31.90772(4)	0.17(1)	1.00(1)	9.8
92	$9\nu_3 - 8\nu_7$	7.15327(5)	0.19(1)	0.02(1)	7.9
93	$1\nu_1 + 1\nu_{15}$	27.74505(5)	0.17(1)	0.10(1)	7.6
94	$-1\nu_7 + 2\nu_{14} + 1\nu_{18}$	22.30067(5)	0.16(1)	0.33(1)	6.3
95	$-4\nu_9 + 2\nu_{15}$	13.43341(7)	0.17(1)	0.52(1)	6.7
96	$3\nu_1 + 1\nu_{10}$	39.08919(5)	0.15(1)	0.49(1)	10.1
97	$9\nu_1$	50.94955(5)	0.15(1)	0.98(1)	11.4
98	$-10\nu_4 + 5\nu_{15}$	9.19148(5)	0.14(1)	0.38(1)	7.2
99	$\nu_{20}$	22.09581(4)	0.22(1)	0.098(9)	6.5
100	$4\nu_{15} - 3\nu_{20}$	22.04787(4)	0.15(1)	0.81(1)	7.7
101	$1\nu_5 + 1\nu_{15} - 1\nu_{20}$	9.80753(4)	0.18(1)	0.91(1)	6.9
102	$6\nu_1 + 1\nu_3$	41.74191(5)	0.14(1)	0.59(1)	10.9
103	$-2\nu_1 - 2\nu_7 + 1\nu_{10}$	2.93054(5)	0.14(1)	0.27(1)	5.1
104	$1\nu_1 + 1\nu_{12}$	8.62080(6)	0.13(1)	0.48(1)	7.0
105	$3\nu_1 + 1\nu_9$	24.66663(5)	0.14(1)	0.53(1)	6.3
106	$4\nu_1 - 1\nu_3$	14.86864(5)	0.13(1)	0.63(1)	8.0
107	$-2\nu_4 + 3\nu_6$	9.82775(5)	0.15(1)	0.97(1)	6.8
108	$3\nu_1 + 2\nu_2$	31.28109(5)	0.13(1)	0.21(1)	9.7
109	$-3\nu_1 + 1\nu_{17}$	4.15481(5)	0.13(1)	0.53(1)	6.8

Table A2: continued

#	ID <sub>T</sub>	$\nu$ [d <sup>-1</sup> ]	A [ppt]	$\phi$ [0 – 1]	S/N
110	$2\nu_8 - 1\nu_{16}$	25.05275(5)	0.12(1)	0.25(1)	6.7
111	$7\nu_1 + 1\nu_2$	46.77639(5)	0.13(1)	0.28(1)	10.6
112	$2\nu_1 - 1\nu_7$	3.46870(5)	0.13(1)	0.83(1)	5.6
113	$10\nu_2 - 3\nu_{11}$	22.14585(6)	0.13(1)	0.54(1)	6.5
114	$3\nu_1 + 1\nu_7$	24.83656(6)	0.12(1)	0.56(1)	6.8
115	$-2\nu_1 - 2\nu_{11} + 2\nu_{13}$	16.48462(5)	0.13(1)	0.38(1)	5.6
116	$3\nu_1 + 1\nu_{11} - 1\nu_{13}$	11.30370(5)	0.14(1)	0.42(1)	5.6
117	$1\nu_1 + 1\nu_{16}$	18.99504(6)	0.16(1)	0.27(1)	5.3
118	$-2\nu_4 + 5\nu_7$	19.02177(5)	0.15(1)	0.71(1)	6.5
119	$1\nu_7 + 1\nu_{18}$	19.18969(7)	0.12(1)	0.65(1)	6.1
120	$-5\nu_1 - 5\nu_9 + 2\nu_{17}$	6.28764(6)	0.11(1)	0.09(2)	6.0
121	$-2\nu_3 - 2\nu_8 + 2\nu_{13}$	9.51061(6)	0.12(1)	0.68(1)	6.6
122	$-2\nu_{11} + 1\nu_{13} + 1\nu_{15}$	11.31553(5)	0.15(1)	1.00(1)	5.7
123	$4\nu_1 + 1\nu_{10}$	44.75023(6)	0.11(1)	0.32(2)	8.5
124	$1\nu_6 - 1\nu_8 + 1\nu_{20}$	12.92612(6)	0.11(1)	0.30(2)	5.2
125	$-1\nu_6 + 3\nu_7$	13.53600(7)	0.12(1)	0.84(2)	5.2
126	$2\nu_1 - 1\nu_{12}$	8.36237(7)	0.10(1)	0.40(2)	6.4
127	$-1\nu_5 + 1\nu_{12} + 1\nu_{17}$	14.27909(7)	0.10(1)	0.74(2)	7.0
128	$2\nu_1 + 1\nu_{15}$	33.40602(6)	0.11(1)	0.21(2)	6.3
129	$2\nu_{10} - 1\nu_{20} + 1\nu_{18}$	33.45204(6)	0.11(1)	0.96(2)	6.5
130	$4\nu_1 - 1\nu_2$	15.49530(6)	0.11(1)	0.25(2)	7.0
131	$4\nu_1 + 2\nu_2$	36.94216(6)	0.10(1)	0.90(2)	8.2
132	$3\nu_1 + 1\nu_4$	27.10600(6)	0.10(1)	0.05(2)	6.4
133	$2\nu_{14}$	18.81875(7)	0.10(1)	0.96(2)	5.7
134	$7\nu_4 - 3\nu_{17}$	7.44535(7)	0.10(1)	0.57(2)	5.7
135	$1\nu_1 + 1\nu_{20}$	27.75683(5)	0.15(1)	0.03(1)	5.4
136	$1\nu_4 + 2\nu_{13} - 2\nu_{16}$	27.70898(6)	0.10(1)	0.32(2)	6.0
137	$\nu_{21}$	27.96166(6)	0.10(1)	0.35(2)	6.2
138	$1\nu_1 + 1\nu_{12} + 1\nu_{19}$	22.25050(7)	0.10(1)	0.84(2)	5.5
139	$-1\nu_3 + 4\nu_{18}$	37.56882(7)	0.10(1)	0.61(2)	7.2
140	$2\nu_4 - 1\nu_{15} + 2\nu_{14}$	16.97953(6)	0.12(1)	0.26(2)	5.2
141	$-1\nu_{11} + 2\nu_{13}$	27.80682(7)	0.10(1)	0.60(2)	6.2
142	$\nu_{22}$	9.60108(7)	0.10(1)	0.36(2)	6.0
143	$-1\nu_1 + 1\nu_6$	4.36321(7)	0.10(1)	0.65(2)	6.0
144	$1\nu_1 + 1\nu_{14}$	15.07043(7)	0.09(1)	0.86(2)	6.4
145	$-4\nu_5 + 5\nu_{14}$	7.7724(1)	0.11(1)	0.75(2)	6.1
146	$1\nu_6 - 1\nu_{14} + 1\nu_{18}$	11.95141(7)	0.09(1)	0.64(2)	6.0
147	$1\nu_1 + 2\nu_3$	21.21219(8)	0.09(1)	0.60(2)	7.0
148	$\nu_{23}$	43.23259(7)	0.09(1)	0.10(2)	7.6
149	$1\nu_2 + 1\nu_6$	17.17319(8)	0.09(1)	0.48(2)	5.5
150	$1\nu_2 + 1\nu_4$	17.27178(7)	0.09(1)	0.67(2)	5.9
151	$-1\nu_5 + 2\nu_6$	10.22971(8)	0.09(1)	0.64(2)	5.2
152	$7\nu_4 - 5\nu_5$	21.76602(8)	0.08(1)	0.44(2)	5.1
153	$2\nu_3$	15.55119(8)	0.08(1)	0.58(2)	6.7
154	$-1\nu_3 + 1\nu_{21}$	20.18693(9)	0.08(1)	0.63(2)	5.2
155	$9\nu_3 - 5\nu_{14}$	22.93281(8)	0.09(1)	0.50(2)	5.4
156	$\nu_{24}$	32.11376(8)	0.08(1)	0.02(2)	5.6
157	$4\nu_1 + 1\nu_7$	30.49757(8)	0.08(1)	0.52(2)	5.6
158	$\nu_{25}$	26.18343(9)	0.08(1)	0.24(2)	5.2
159	$-1\nu_6 - 1\nu_{20} + 2\nu_{18}$	22.83149(9)	0.08(1)	0.57(2)	5.4
160	$1\nu_4 + 6\nu_{12}$	27.88043(9)	0.07(1)	0.19(2)	5.0
161	$1\nu_5 + 1\nu_6 + 1\nu_{14}$	29.25223(9)	0.08(1)	0.52(2)	5.4
162	$5\nu_1 + 1\nu_{10}$	50.41129(9)	0.07(1)	0.08(2)	6.3
163	$8\nu_1 + 1\nu_2$	52.43739(9)	0.08(1)	0.33(2)	6.3
164	$1\nu_1 + 1\nu_{25}$	31.84458(9)	0.07(1)	0.58(2)	5.8
165	$2\nu_1 + 3\nu_2$	32.76980(9)	0.07(1)	0.37(2)	5.4
166	$10\nu_1$	56.61063(9)	0.07(1)	0.63(2)	5.9
167	$2\nu_{12} - 1\nu_{21} + 2\nu_{25}$	30.32497(9)	0.07(1)	0.60(2)	5.1
168	$2\nu_{14} - 1\nu_{24} + 2\nu_{25}$	39.0715(1)	0.07(1)	0.98(3)	5.3

**Table A3.** Low frequencies detected in three data sets, i.e., *Kepler* LC, *Kepler* SC, and *TESS*.

Data set	ID	$\nu$ [d $^{-1}$ ]
<i>Kepler</i> LC	$\nu_{a,K,LC}$	0.10449(4)
<i>Kepler</i> LC	$\nu_{b,K,LC}$	0.00967(3)
<i>Kepler</i> LC	$\nu_{c,K,LC}$	0.09778(5)
<i>Kepler</i> LC	$\nu_{d,K,LC}$	0.02055(5)
<i>Kepler</i> LC	$\nu_{e,K,LC}$	0.03103(5)
<i>Kepler</i> SC	$\nu_{a,K,SC}$	0.00255(3)
<i>Kepler</i> SC	$\nu_{b,K,SC}$	0.02188(4)
<i>Kepler</i> SC	$\nu_{c,K,SC}$	0.01577(4)
<i>Kepler</i> SC	$\nu_{d,K,SC}$	0.01019(4)
<i>Kepler</i> SC	$\nu_{e,K,SC}$	0.03466(5)
<i>Kepler</i> SC	$\nu_{f,K,SC}$	0.05427(7)
TESS	$\nu_{a,T}$	0.067193(8)
TESS	$\nu_{b,T}$	0.055213(9)
TESS	$\nu_{c,T}$	0.13889(1)



**Figure A1.** Amplitude periodogram for the combined S14+S15 *TESS* data of V2367 Cyg. Panels from top to bottom show periodograms: for the original S14+S15 data; after subtraction of 2 terms; after subtraction of 14 terms and after subtraction of 171 terms. Red solid line in bottom panel indicates the 5S/N level. All frequency peaks above 0.63 ppt are marked by down-pointing triangles, green for independent signals, black for combinations or harmonics. Independent frequencies with amplitudes smaller than 0.63 ppt are marked by small green triangles. Additionally, big green open triangles mark frequencies that were identified as independent in the full *TESS* dataset but combinations in S14+S15 dataset, whereas small green open triangles mean the same but for frequencies with amplitudes below 0.63 ppt.

Table A2: continued

#	ID $_T$	$\nu$ [d $^{-1}$ ]	A [ppt]	$\phi$ [0 – 1]	S/N
169	$7\nu_1 + 1\nu_3$	47.4030(1)	0.07(1)	0.21(3)	6.2
170	$9\nu_1 - 4\nu_{12}$	39.1103(1)	0.07(1)	0.41(3)	5.2
171	$5\nu_1 + 2\nu_2$	42.6032(1)	0.06(1)	0.5(3)	5.5

**Table A4.** Independent frequencies detected in the *TESS* data from combined adjacent sectors, i.e., S14+S15, S40+S41 and S54+S55. Columns contain: our ID<sub>T</sub>, frequency, amplitude, phase, signal to noise ratio, ID<sub>K</sub> and ID<sub>B</sub>.

ID <sub>T</sub>	$\nu$ [d <sup>-1</sup> ]	A [ppt]	$\phi$ [0–1]	S/N	ID <sub>K</sub>	ID <sub>B</sub>
S14+S15						
1	5.66105(3)	100.97(3)	0.88792(4)	17.2	$\nu_{1,K}$	$\nu_{1,B}$
2	7.1489(1)	11.63(3)	0.3888(4)	16.4	$\nu_{2,K}$	$\nu_{2,B}$
3	7.7753(2)	4.82(3)	0.9053(9)	15.1	$\nu_{3,K}$	$\nu_{3,B}$
4	19.1940(6)	0.87(3)	0.054(5)	10.7	$9\nu_{4,K} - 9\nu_{8,K}$	
5	10.0244(7)	0.80(3)	0.024(5)	10.3	$\nu_{7,K}$	$\nu_{8,B}$
6	16.447(1)	0.50(3)	0.009(9)	7.2	$5\nu_{1,K} + 1\nu_{3,K} - 2\nu_{4,K}$	$\nu_{13,B}$
S40+S41						
1	5.66105(3)	99.19(2)	0.88294(3)	17.0	$\nu_{1,K}$	$\nu_{1,B}$
2	7.1490(1)	11.55(2)	0.7651(3)	17.3	$\nu_{2,K}$	$\nu_{2,B}$
3	7.7754(2)	4.60(2)	0.5743(7)	14.9	$\nu_{3,K}$	$\nu_{3,B}$
4	10.0243(5)	0.82(2)	0.308(4)	10.7	$\nu_{7,K}$	$\nu_{8,B}$
5	7.8533(5)	0.80(2)	0.581(4)	9.8	$\nu_{5,K}$	$\nu_{6,B}$
6	16.4455(8)	0.45(2)	0.185(7)	6.8	$5\nu_{1,K} + 1\nu_{3,K} - 2\nu_{4,K}$	$\nu_{13,B}$
S54+S55						
1	5.66106(3)	101.55(2)	0.83449(3)	17.1	$\nu_{1,K}$	$\nu_{1,B}$
2	7.1490(1)	11.94(2)	0.0485(3)	17.0	$\nu_{2,K}$	$\nu_{2,B}$
3	7.7756(2)	4.62(2)	0.6908(7)	15.9	$\nu_{3,K}$	$\nu_{3,B}$
4	10.0239(5)	0.94(2)	0.183(3)	11.8	$\nu_{7,K}$	$\nu_{8,B}$
5	7.8534(5)	0.78(2)	0.008(4)	9.0	$\nu_{5,K}$	$\nu_{6,B}$
6	16.4468(7)	0.54(2)	0.473(6)	7.2	$5\nu_{1,K} + 1\nu_{3,K} - 2\nu_{4,K}$	$\nu_{13,B}$

**Table A5:** All frequencies detected in combined *TESS* sectors 14 and 15. Columns contain: number, our ID<sub>T</sub>, frequency, amplitude, phase, signal to noise ratio.

#	ID <sub>T,S14–15</sub>	$\nu$ [d <sup>-1</sup> ]	A [ppt]	$\phi$ [0 – 1]	S/N
1	$\nu_1$	5.66105(3)	100.97(3)	0.88792(4)	17.2
2	$2\nu_1$	11.32210(6)	32.10(3)	0.6850(1)	17.1
3	$\nu_2$	7.1489(1)	11.63(3)	0.3888(4)	16.4
4	$3\nu_1$	16.9831(1)	10.25(3)	0.6458(4)	16.9
5	$1\nu_1 + 1\nu_2$	12.8099(2)	5.37(3)	0.9766(8)	16.0
6	$4\nu_1$	22.6442(2)	5.02(3)	0.2615(9)	16.6
7	$\nu_3$	7.7753(2)	4.82(3)	0.9053(9)	15.1
8	$-1\nu_1 + 1\nu_2$	1.4876(2)	3.59(3)	0.593(1)	14.0
9	$2\nu_1 + 1\nu_2$	18.4710(3)	2.74(3)	0.664(2)	15.3
10	$1\nu_1 + 1\nu_3$	13.4363(3)	2.45(3)	0.975(2)	12.9
11	$5\nu_1$	28.3053(3)	2.38(3)	0.964(2)	16.1
12	$-1\nu_1 + 1\nu_3$	2.1146(4)	1.61(3)	0.848(3)	12.4
13	$2\nu_1 + 1\nu_3$	19.0972(4)	1.54(3)	0.203(3)	10.8
14	$2\nu_1 - 1\nu_2$	4.1725(5)	1.32(3)	0.520(3)	14.2
15	$-2\nu_1 + 3\nu_2$	10.1224(4)	1.37(3)	0.375(3)	8.8
16	$3\nu_1 + 1\nu_2$	24.1323(5)	1.20(3)	0.678(4)	14.1
17	$6\nu_1$	33.9666(5)	1.15(3)	0.775(4)	14.8
18	$3\nu_1 - 1\nu_2$	9.8208(5)	1.04(3)	0.599(4)	9.2
19	$\nu_4$	19.1940(6)	0.87(3)	0.054(5)	10.7
20	$-2\nu_1 + 1\nu_4$	7.8535(7)	0.82(3)	0.668(5)	9.4
21	$-10\nu_1 + 6\nu_5$	3.5457(7)	0.80(3)	0.053(5)	11.4
22	$\nu_5$	10.0244(7)	0.80(3)	0.024(5)	10.3
23	$4\nu_1 + 1\nu_2$	29.7928(7)	0.75(3)	0.542(6)	13.4
24	$3\nu_1 + 1\nu_3$	24.7583(7)	0.74(3)	0.770(6)	10.0
25	$-1\nu_1 + 1\nu_4$	13.5340(7)	0.70(3)	0.404(6)	8.2
26	$8\nu_3 - 4\nu_5$	22.1082(8)	0.68(3)	0.904(6)	9.8
27	$2\nu_1 + 2\nu_3 - 1\nu_4$	7.6836(8)	0.67(3)	0.611(6)	11.0
28	$-1\nu_1 + 3\nu_2$	15.7842(9)	0.60(3)	0.336(7)	8.3
29	$7\nu_1$	39.6273(9)	0.60(3)	0.059(7)	12.8

Table A5: continued

#	ID <sub>T,S14–15</sub>	$\nu$ [d <sup>-1</sup> ]	A [ppt]	$\phi$ [0 – 1]	S/N
30	$\nu_6$	16.447(1)	0.50(3)	0.009(9)	7.2
31	$-2\nu_1 + 2\nu_2$	2.959(1)	0.50(3)	0.395(9)	7.7
32	$5\nu_1 + 1\nu_2$	35.454(1)	0.45(3)	0.51(1)	11.7
33	$2\nu_2$	14.298(1)	0.43(3)	0.35(1)	9.4
34	$1\nu_2 + 1\nu_3$	14.924(1)	0.42(3)	0.73(1)	9.0
35	$4\nu_1 + 1\nu_3$	30.420(1)	0.41(3)	0.94(1)	9.5
36	$2\nu_1 + 1\nu_6$	27.768(1)	0.41(3)	0.62(1)	8.7
37	$-1\nu_1 + 2\nu_2$	8.633(1)	0.39(3)	0.44(1)	8.1
38	$4\nu_1 - 1\nu_2$	15.478(1)	0.41(3)	0.80(1)	7.6
39	$1\nu_1 + 1\nu_4$	24.856(1)	0.37(3)	0.23(1)	7.8
40	$2\nu_3 - 1\nu_4 + 2\nu_5$	16.389(1)	0.36(3)	0.89(1)	6.1
41	$1\nu_1 + 1\nu_5$	15.686(1)	0.33(3)	0.02(1)	8.5
42	$-9\nu_1 + 6\nu_5$	9.210(2)	0.31(3)	0.58(1)	5.6
43	$1\nu_1 + 2\nu_2$	19.961(2)	0.31(3)	0.20(1)	7.4
44	$-3\nu_1 + 1\nu_4$	2.193(2)	0.30(3)	0.45(1)	5.2
45	$-6\nu_2 + 5\nu_5$	7.214(2)	0.28(3)	0.48(2)	7.0
46	$3\nu_2$	21.445(2)	0.28(3)	0.81(2)	6.5
47	$8\nu_1$	45.289(2)	0.27(3)	0.37(2)	9.5
48	$4\nu_4 - 6\nu_5$	16.637(2)	0.25(3)	0.95(2)	5.1
49	$4\nu_1 + 2\nu_5 - 1\nu_6$	26.247(2)	0.24(3)	0.46(2)	6.4
50	$-1\nu_3 - 1\nu_4 + 2\nu_5$	20.584(2)	0.23(3)	0.99(2)	6.4
51	$6\nu_1 + 1\nu_2$	41.116(2)	0.23(3)	0.54(2)	7.8
52	$3\nu_1 + 1\nu_6$	33.429(2)	0.21(3)	0.28(2)	6.0
53	$5\nu_1 + 1\nu_3$	36.081(2)	0.21(3)	0.52(2)	7.5
54	$-10\nu_1 + 10\nu_3$	21.137(3)	0.19(3)	0.14(2)	5.5
55	$2\nu_1 + 1\nu_4$	30.517(3)	0.19(3)	0.09(2)	6.3
56	$-10\nu_1 + 5\nu_6$	25.622(3)	0.18(3)	0.38(2)	5.3
57	$4\nu_1 + 1\nu_6$	39.091(3)	0.16(3)	0.17(3)	5.9
58	$9\nu_1$	50.950(3)	0.15(3)	0.82(3)	5.9
59	$2\nu_1 + 1\nu_5$	21.343(3)	0.15(3)	0.10(3)	5.4
60	$6\nu_1 + 1\nu_3$	41.741(3)	0.14(3)	0.64(3)	6.0
61	$7\nu_1 + 1\nu_2$	46.776(4)	0.13(3)	0.21(3)	5.4
62	$1\nu_1 + 2\nu_3$	21.216(4)	0.11(3)	0(9)	5.0

 Table A6: All frequencies detected in combined *TESS* sectors 40 and 41. Columns contain: number, our ID<sub>T</sub>, frequency, amplitude, phase, signal to noise ratio.

#	ID <sub>T,S40–41</sub>	$\nu$ [d <sup>-1</sup> ]	A [ppt]	$\phi$ [0 – 1]	S/N
1	$\nu_1$	5.66105(3)	99.19(2)	0.88294(3)	17.0
2	$2\nu_1$	11.32209(5)	31.59(2)	0.7505(1)	17.0
3	$\nu_2$	7.1490(1)	11.55(2)	0.7651(3)	17.3
4	$3\nu_1$	16.9831(1)	9.99(2)	0.8321(3)	17.0
5	$1\nu_1 + 1\nu_2$	12.8100(2)	5.38(2)	0.8358(6)	16.7
6	$4\nu_1$	22.6441(2)	4.88(2)	0.5498(7)	16.4
7	$\nu_3$	7.7754(2)	4.60(2)	0.5743(7)	14.9
8	$-1\nu_1 + 1\nu_2$	1.4881(2)	3.59(2)	0.6663(9)	16.1
9	$2\nu_1 + 1\nu_2$	18.4711(2)	2.73(2)	0.292(1)	16.4
10	$1\nu_1 + 1\nu_3$	13.4366(2)	2.68(2)	0.053(1)	13.3
11	$5\nu_1$	28.3052(2)	2.31(2)	0.409(1)	15.9
12	$2\nu_1 + 1\nu_3$	19.0977(3)	1.60(2)	0.317(2)	11.9
13	instrumental	0.0662(4)	1.46(2)	0.539(2)	5.1
14	$-1\nu_1 + 1\nu_3$	2.1139(3)	1.56(2)	0.930(2)	13.9
15	$-2\nu_1 + 3\nu_2$	10.1225(4)	1.37(2)	0.174(2)	9.4
16	$2\nu_1 - 1\nu_2$	4.1727(3)	1.33(2)	0.696(2)	15.1
17	$3\nu_1 + 1\nu_2$	24.1321(4)	1.19(2)	0.466(3)	15.1
18	$6\nu_1$	33.9662(4)	1.14(2)	0.596(3)	15.3
19	$3\nu_1 - 1\nu_2$	9.8206(5)	0.95(2)	0.156(3)	8.9
20	$\nu_4$	10.0243(5)	0.82(2)	0.308(4)	10.7

Table A6: continued

#	ID <sub>T,S40-41</sub>	$\nu$ [d <sup>-1</sup> ]	A [ppt]	$\phi$ [0 – 1]	S/N
21	$3\nu_1 + 1\nu_3$	24.7587(5)	0.80(2)	0.428(4)	10.8
22	$\nu_5$	7.8533(5)	0.80(2)	0.581(4)	9.8
23	$4\nu_1 + 1\nu_2$	29.7932(5)	0.76(2)	0.199(4)	14.2
24	$-10\nu_1 + 6\nu_4$	3.5470(5)	0.75(2)	0.083(4)	12.3
25	$2\nu_1 + 1\nu_5$	19.1926(6)	0.73(2)	0.832(4)	10.4
26	$1\nu_1 + 1\nu_5$	13.5302(6)	0.68(2)	0.279(5)	8.5
27	$2\nu_3 - 1\nu_5$	7.6833(6)	0.70(2)	0.894(5)	11.5
28	$7\nu_1$	39.6275(7)	0.58(2)	0.042(6)	13.7
29	$-1\nu_1 + 3\nu_2$	15.7840(7)	0.56(2)	0.149(6)	8.4
30	$8\nu_3 - 4\nu_4$	22.1051(7)	0.55(2)	0.230(6)	8.2
31	$1\nu_1 + 2\nu_3 - 1\nu_5$	13.3424(7)	0.52(2)	0.740(6)	7.4
32	$4\nu_1 + 1\nu_3$	30.4202(8)	0.45(2)	0.234(7)	10.6
33	$\nu_6$	16.4455(8)	0.45(2)	0.185(7)	6.8
34	$2\nu_2$	14.2967(9)	0.43(2)	0.598(8)	11.0
35	$5\nu_1 + 1\nu_2$	35.4544(9)	0.42(2)	0.197(8)	12.2
36	$-9\nu_1 + 6\nu_4$	9.2040(9)	0.41(2)	0.113(8)	7.6
37	$2\nu_1 + 1\nu_6$	27.765(1)	0.38(2)	0.393(9)	7.8
38	$4\nu_1 - 1\nu_2$	15.479(1)	0.40(2)	0.766(8)	7.5
39	$1\nu_2 + 1\nu_3$	14.924(1)	0.39(2)	0.266(8)	9.4
40	$1\nu_1 + 2\nu_2$	19.958(1)	0.36(2)	0.055(9)	11.0
41	$1\nu_1 + 1\nu_4$	15.686(1)	0.34(2)	0.231(9)	9.2
42	$3\nu_1 + 1\nu_5$	24.854(1)	0.32(2)	0.17(1)	7.4
43	$-4\nu_3 + 5\nu_4$	19.003(1)	0.32(2)	0.97(1)	6.2
44	$-1\nu_1 + 2\nu_2$	8.636(1)	0.31(2)	0.56(1)	8.1
45	$8\nu_1$	45.288(1)	0.29(2)	0.86(1)	10.1
46	$6\nu_1 + 1\nu_2$	41.115(1)	0.28(2)	0.94(1)	10.8
47	$3\nu_2$	21.445(1)	0.28(2)	0.86(1)	6.6
48	$-8\nu_4 + 5\nu_6$	2.023(1)	0.28(2)	0.87(1)	5.7
49	$3\nu_1 + 2\nu_4 - 1\nu_6$	20.586(1)	0.28(2)	0.07(1)	8.5
50	$-1\nu_1 + 1\nu_5$	2.192(1)	0.28(2)	0.45(1)	6.3
51	$4\nu_1 + 2\nu_4 - 1\nu_6$	26.246(1)	0.25(2)	0.11(1)	8.1
52	$-6\nu_2 + 5\nu_4$	7.212(1)	0.25(2)	0.35(1)	6.8
53	$5\nu_1 + 1\nu_3$	36.081(1)	0.24(2)	0.95(1)	8.8
54	$-10\nu_1 + 5\nu_6$	25.619(2)	0.22(2)	0.15(1)	8.1
55	$3\nu_1 + 1\nu_6$	33.426(2)	0.22(2)	0.20(1)	6.8
56	$-3\nu_1 + 3\nu_2$	4.462(2)	0.20(2)	0.05(2)	6.6
57	$-10\nu_1 + 10\nu_3$	21.138(2)	0.20(2)	0.77(2)	6.0
58	$2\nu_1 + 1\nu_4$	21.346(2)	0.19(2)	0.68(2)	6.5
59	$5\nu_1 + 2\nu_4 - 1\nu_6$	31.908(2)	0.16(2)	0.79(2)	5.4
60	$4\nu_1 + 1\nu_5$	30.513(2)	0.14(2)	0.16(2)	5.5
61	$9\nu_1$	50.950(2)	0.14(2)	0.11(2)	6.3
62	$4\nu_1 + 1\nu_6$	39.092(3)	0.12(2)	0.38(3)	5.2
63	$6\nu_1 + 1\nu_3$	41.743(3)	0.12(2)	0.95(3)	5.6
64	$7\nu_1 + 1\nu_2$	46.776(3)	0.12(2)	0.05(3)	6.2
65	$-9\nu_1 + 5\nu_6$	31.281(3)	0.12(2)	0.40(3)	5.4
66	$5\nu_1 + 1\nu_2 + 1\nu_3$	43.229(3)	0.10(2)	1(9)	5.3

Table A7: All frequencies detected in combined TESS sectors 54 and 55. Columns contain: number, our ID<sub>T</sub>, frequency, amplitude, phase, signal to noise ratio.

#	ID <sub>T,S54-55</sub>	$\nu$ [d <sup>-1</sup> ]	A [ppt]	$\phi$ [0 – 1]	S/N
1	$\nu_1$	5.66106(3)	101.55(2)	0.83449(3)	17.1
2	$2\nu_1$	11.32209(6)	32.36(2)	0.7408(1)	17.0
3	$\nu_2$	7.1490(1)	11.94(2)	0.0485(3)	17.0
4	$3\nu_1$	16.9832(1)	10.28(2)	0.4881(3)	16.9
5	$1\nu_1 + 1\nu_2$	12.8100(2)	5.51(2)	0.7926(6)	16.5
6	$4\nu_1$	22.6442(2)	5.05(2)	0.1771(6)	16.5
7	$\nu_3$	7.7756(2)	4.62(2)	0.6908(7)	15.9

Table A7: continued

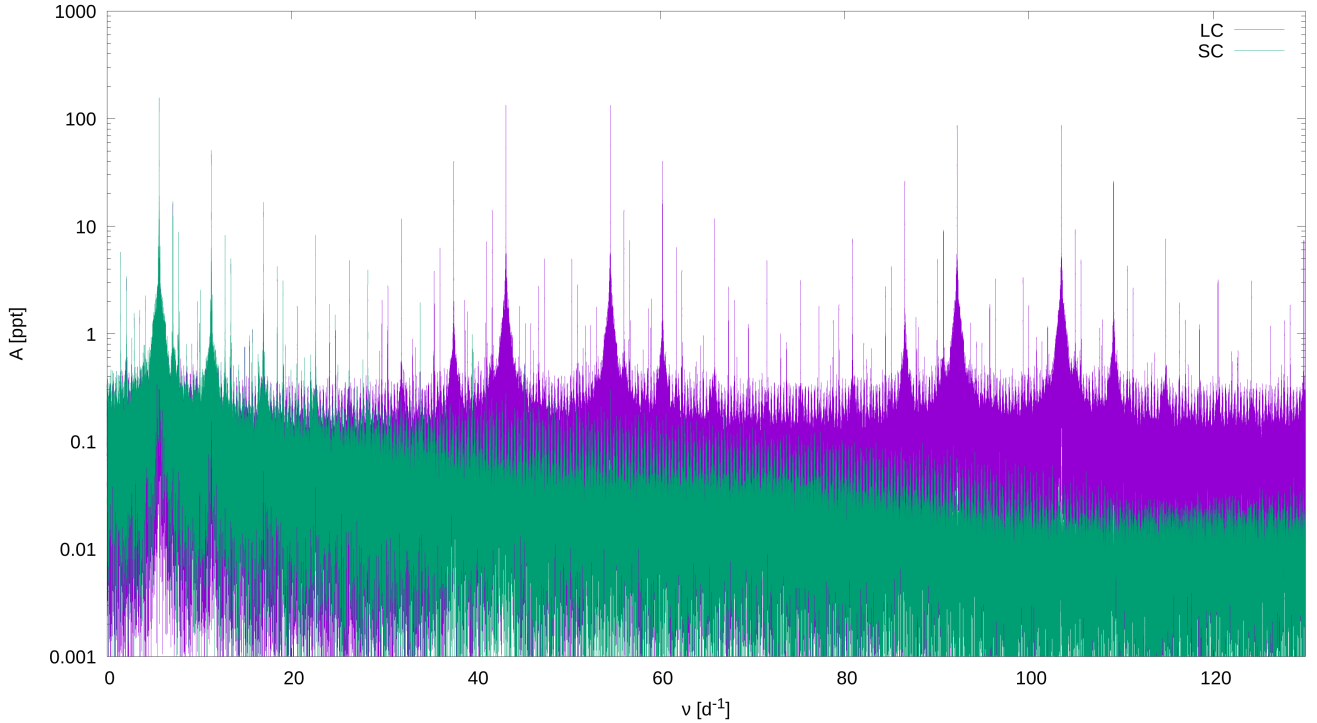
#	ID <sub>T,S54-55</sub>	$\nu$ [d <sup>-1</sup> ]	A [ppt]	$\phi$ [0 – 1]	S/N
8	$-1\nu_1 + 1\nu_2$	1.4881(2)	3.70(2)	0.5804(8)	15.7
9	$2\nu_1 + 1\nu_2$	18.4709(2)	2.82(2)	0.423(1)	16.4
10	$1\nu_1 + 1\nu_3$	13.4362(2)	2.78(2)	0.064(1)	13.7
11	$5\nu_1$	28.3053(2)	2.40(2)	0.841(1)	16.2
12	instrumental	0.0658(3)	1.73(2)	0.076(2)	5.6
13	$-1\nu_1 + 1\nu_3$	2.1144(3)	1.66(2)	0.771(2)	14.3
14	$2\nu_1 + 1\nu_3$	19.0974(3)	1.61(2)	0.760(2)	12.1
15	$-2\nu_1 + 3\nu_2$	10.1225(3)	1.44(2)	0.600(2)	10.2
16	$2\nu_1 - 1\nu_2$	4.1726(3)	1.36(2)	0.308(2)	15.0
17	$3\nu_1 + 1\nu_2$	24.1318(4)	1.25(2)	0.013(2)	15.6
18	$6\nu_1$	33.9662(4)	1.16(2)	0.470(3)	15.1
19	$3\nu_1 - 1\nu_2$	9.8195(4)	1.04(2)	0.276(3)	10.0
20	$\nu_4$	10.0239(5)	0.94(2)	0.183(3)	11.8
21	$\nu_5$	7.8534(5)	0.78(2)	0.008(4)	9.0
22	$3\nu_1 + 1\nu_3$	24.7586(5)	0.80(2)	0.025(4)	11.1
23	$4\nu_1 + 1\nu_2$	29.7931(5)	0.78(2)	0.624(4)	14.5
24	$2\nu_3 - 1\nu_5$	7.6831(5)	0.77(2)	0.098(4)	11.8
25	$-10\nu_1 + 6\nu_4$	3.5464(6)	0.71(2)	0.735(4)	11.7
26	$2\nu_1 + 1\nu_5$	19.1928(6)	0.71(2)	0.026(4)	9.2
27	$8\nu_3 - 4\nu_4$	22.1062(6)	0.68(2)	0.577(5)	9.4
28	$1\nu_1 + 2\nu_3 - 1\nu_5$	13.3428(6)	0.64(2)	0.309(5)	7.2
29	$-1\nu_1 + 3\nu_2$	15.7832(6)	0.62(2)	0.771(5)	8.8
30	$7\nu_1$	39.6269(6)	0.60(2)	0.132(5)	13.8
31	$1\nu_1 + 1\nu_5$	13.5287(7)	0.56(2)	0.284(6)	7.8
32	$\nu_6$	16.4468(7)	0.54(2)	0.473(6)	7.2
33	$5\nu_1 + 1\nu_2$	35.4543(8)	0.48(2)	0.484(6)	12.5
34	$2\nu_2$	14.2970(8)	0.45(2)	0.161(7)	11.4
35	$4\nu_1 + 1\nu_3$	30.4193(8)	0.45(2)	0.701(7)	10.2
36	$4\nu_1 - 1\nu_2$	15.4779(8)	0.42(2)	0.160(7)	9.0
37	$-9\nu_1 + 6\nu_4$	9.2047(8)	0.43(2)	0.085(7)	7.7
38	$2\nu_1 + 1\nu_6$	27.7659(8)	0.44(2)	0.676(7)	8.9
39	$1\nu_2 + 1\nu_3$	14.9253(9)	0.40(2)	0.923(8)	10.6
40	$1\nu_1 + 1\nu_4$	15.6848(9)	0.37(2)	0.802(8)	11.2
41	$1\nu_1 + 2\nu_2$	19.957(1)	0.34(2)	0.765(9)	9.3
42	$-4\nu_3 + 5\nu_4$	19.004(1)	0.34(2)	0.788(9)	6.1
43	$3\nu_1 + 1\nu_5$	24.855(1)	0.33(2)	0.753(9)	7.6
44	$3\nu_1 + 2\nu_4 - 1\nu_6$	20.585(1)	0.32(2)	0.70(1)	8.9
45	$3\nu_2$	21.444(1)	0.32(2)	0.42(1)	7.1
46	$8\nu_1$	45.289(1)	0.29(2)	0.10(1)	10.0
47	$6\nu_1 + 1\nu_2$	41.116(1)	0.27(2)	0.14(1)	9.4
48	$2\nu_2 + 1\nu_3 - 2\nu_4$	2.023(1)	0.28(2)	0.77(1)	5.1
49	$-1\nu_1 + 2\nu_2$	8.638(1)	0.28(2)	0.52(1)	6.8
50	$4\nu_1 + 2\nu_4 - 1\nu_6$	26.245(1)	0.25(2)	0.41(1)	8.3
51	$5\nu_1 + 1\nu_3$	36.081(1)	0.25(2)	0.48(1)	8.9
52	$-6\nu_2 + 5\nu_4$	7.214(1)	0.25(2)	0.96(1)	7.3
53	$3\nu_1 + 1\nu_6$	33.427(1)	0.24(2)	0.90(1)	7.3
54	$-10\nu_1 + 10\nu_3$	21.138(2)	0.21(2)	0.19(1)	6.9
55	$2\nu_1 + 1\nu_4$	21.346(2)	0.19(2)	0.01(2)	7.1
56	$-3\nu_1 + 3\nu_2$	4.462(2)	0.19(2)	0.38(2)	5.5
57	$-10\nu_1 + 5\nu_6$	25.618(2)	0.19(2)	0.34(2)	7.6
58	$3\nu_1 + 2\nu_3 - 1\nu_5$	24.664(2)	0.19(2)	0.24(2)	5.3
59	$5\nu_1 + 2\nu_4 - 1\nu_6$	31.906(2)	0.17(2)	0.92(2)	6.8
60	$6\nu_1 + 1\nu_3$	41.742(2)	0.16(2)	0.32(2)	6.9
61	$9\nu_1$	50.948(2)	0.16(2)	0.48(2)	7.5
62	$-9\nu_1 + 5\nu_6$	31.280(2)	0.16(2)	0.62(2)	6.4
63	$4\nu_1 + 1\nu_6$	39.088(2)	0.15(2)	0.22(2)	6.2
64	$4\nu_1 + 1\nu_5$	30.514(2)	0.15(2)	0.21(2)	5.3
65	$-8\nu_1 + 6\nu_4$	14.866(3)	0.13(2)	0.64(2)	5.2
66	$7\nu_1 + 1\nu_2$	46.777(3)	0.13(2)	0.89(2)	6.8

**Table A8.** The values of three independent frequencies with highest-amplitudes determined separately in each *Kepler* quarter and pairs of adjacent *TESS* sectors. Columns contain: the name of data set, median value of time in each data set, and frequencies of  $\nu_1$ ,  $\nu_2$ , and  $\nu_3$ .

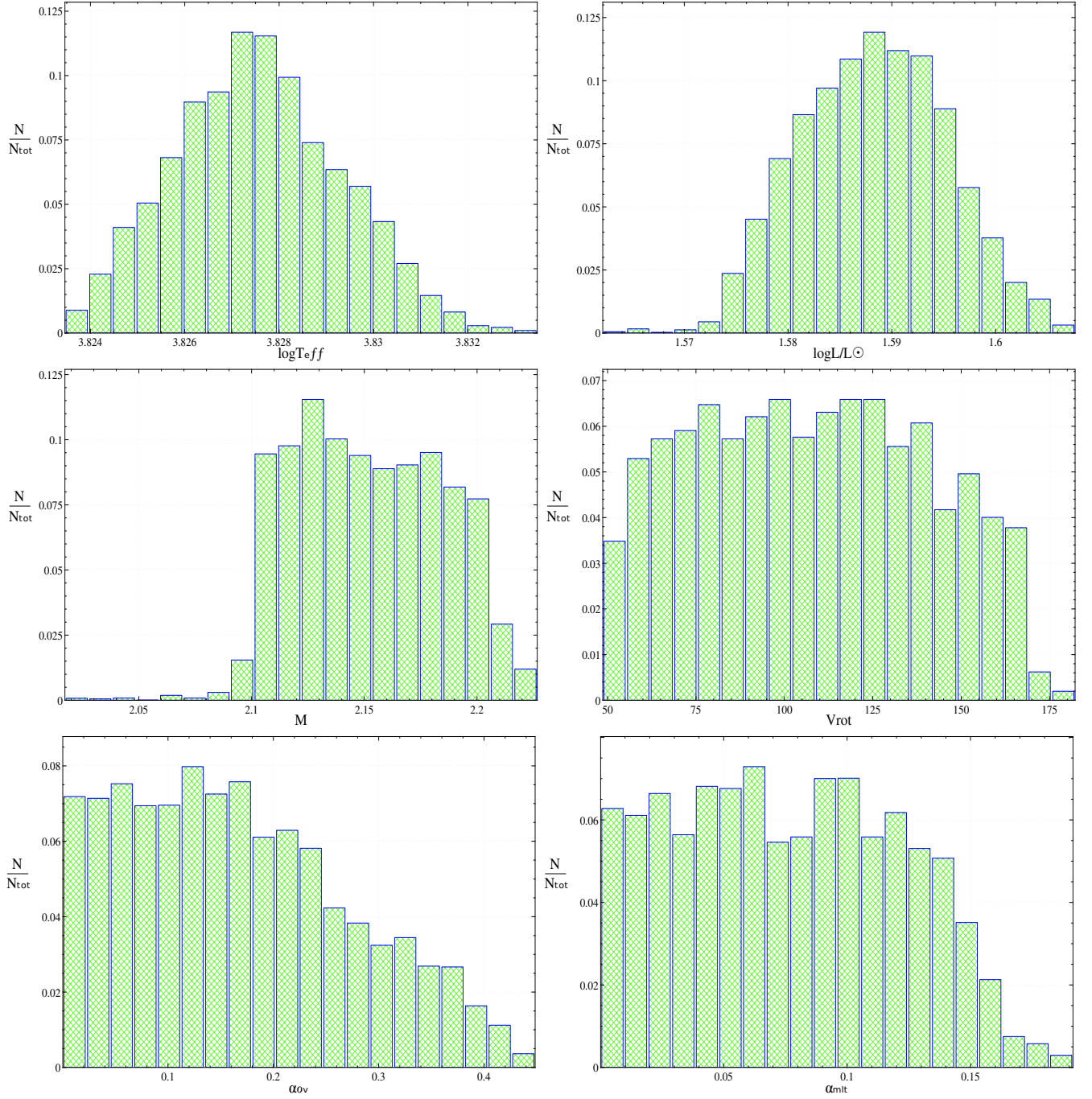
Data set	BJD-2454833 [d]	$\nu_1$ [ $\text{d}^{-1}$ ]	$\nu_2$ [ $\text{d}^{-1}$ ]	$\nu_3$ [ $\text{d}^{-1}$ ]
<i>Kepler</i> Q0SC	125.39	5.661(1)	7.150(4)	7.775(5)
<i>Kepler</i> Q1LC	148.23	5.6610(2)	7.1487(8)	7.7757(9)
<i>Kepler</i> Q2LC	213.98	5.66106(5)	7.1489(2)	7.7756(2)
<i>Kepler</i> Q3LC	304.75	5.66107(5)	7.1490(2)	7.7756(2)
<i>Kepler</i> Q4LC	395.78	5.66105(5)	7.1490(2)	7.7755(2)
<i>Kepler</i> Q5LC	491.14	5.66106(5)	7.1489(2)	7.7756(2)
<i>Kepler</i> Q6SC	584.31	5.66106(2)	7.14896(9)	7.7756(1)
<i>Kepler</i> Q7SC	674.53	5.66106(2)	7.1490(1)	7.7756(1)
<i>Kepler</i> Q8SC	770.20	5.66106(4)	7.1490(2)	7.7755(2)
<i>Kepler</i> Q9SC	857.23	5.66106(2)	7.14899(8)	7.7756(1)
<i>Kepler</i> Q10SC	953.41	5.66105(2)	7.14897(8)	7.7756(1)
<i>Kepler</i> Q11LC	1048.57	5.66105(4)	7.1489(2)	7.7756(2)
<i>Kepler</i> Q12LC	1139.95	5.66106(6)	7.1489(2)	7.7755(3)
<i>Kepler</i> Q13LC	1227.63	5.66105(5)	7.1490(2)	7.7756(3)
<i>Kepler</i> Q14LC	1326.43	5.66106(4)	7.1489(2)	7.7757(2)
<i>Kepler</i> Q15LC	1425.29	5.66106(4)	7.1490(2)	7.7756(2)
<i>Kepler</i> Q16LC	1520.22	5.66106(6)	7.1489(2)	7.7756(3)
<i>Kepler</i> Q17LC	1572.55	5.6611(3)	7.149(1)	7.776(1)
TESS S14S15	3876.74	5.66105(3)	7.1489(1)	7.7753(2)
TESS S40S41	4584.96	5.66105(3)	7.1490(1)	7.7754(2)
TESS S54S55	4964.78	5.66106(3)	7.1490(1)	7.7756(2)

Table A7: continued

#	ID <sub>T,S54–55</sub>	$\nu$ [ $\text{d}^{-1}$ ]	A [ppt]	$\phi$ [0 – 1]	S/N
67	$-8\nu_1 + 5\nu_6$	36.939(3)	0.13(2)	0.36(2)	6.4
68	$5\nu_1 + 1\nu_6$	44.752(3)	0.12(2)	2(8)	5.1



**Figure A2.** Comparison of periodograms calculated for LC (Q0–Q17) and SC (Q6–Q10) *Kepler* data.

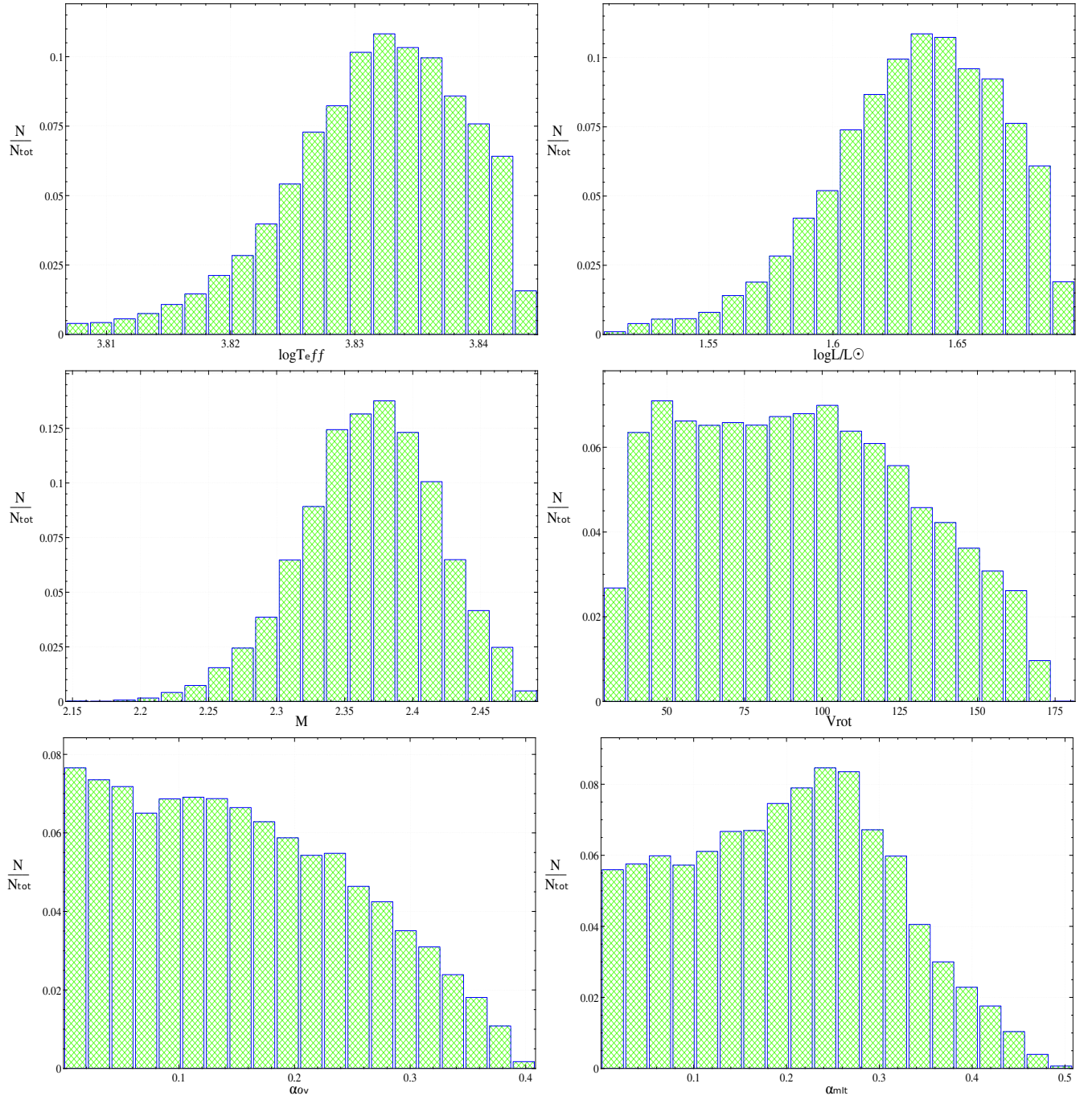


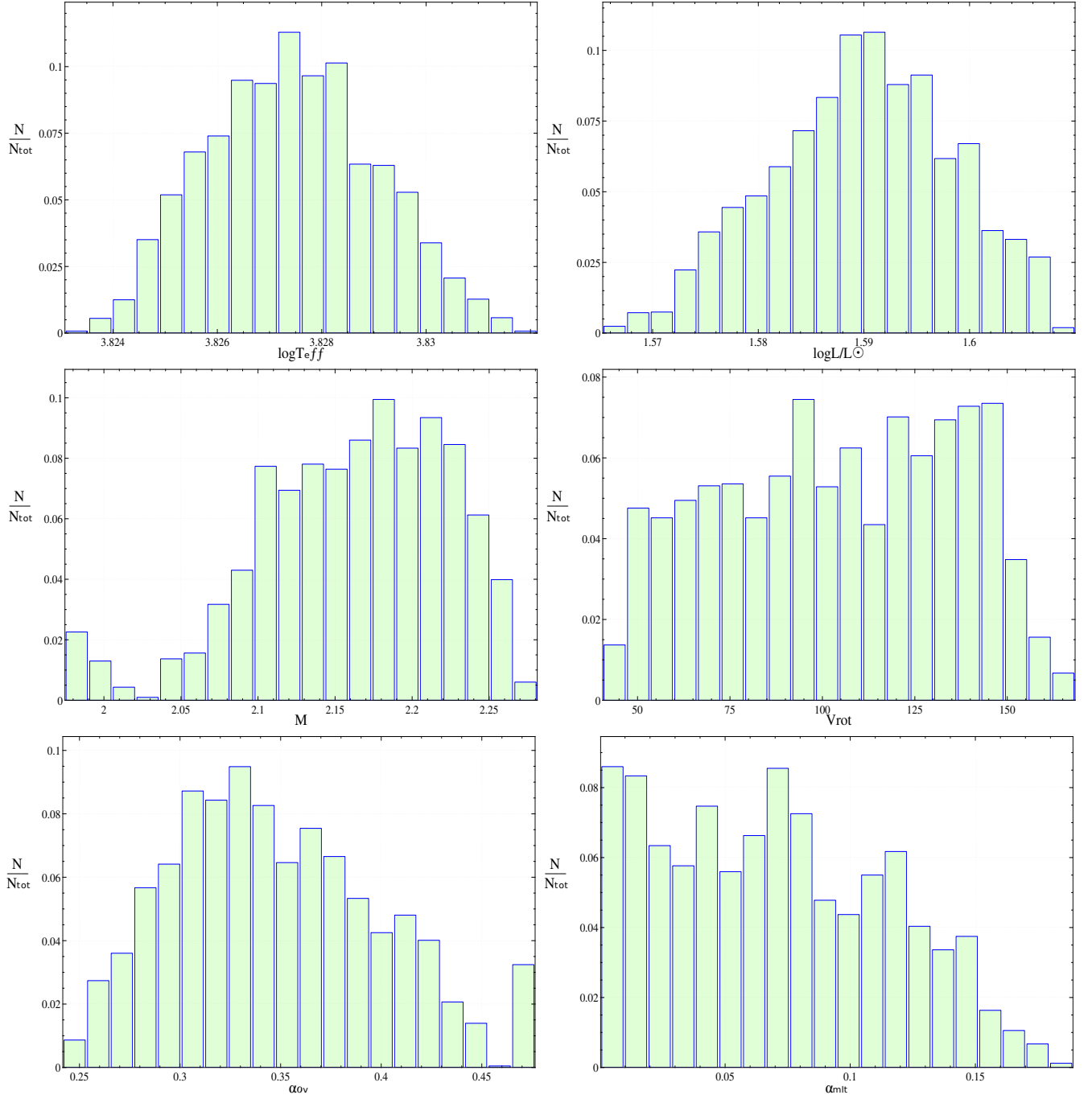
**Figure B1.** The normalized histograms for the parameters of the HSB seismic models of V2367 Cyg, calculated assuming that the observed frequencies  $\nu_1$  and  $\nu_2$  are the first and second radial overtone, respectively (the  $p_2 \& p_3$  hypothesis). The OPAL opacities were adopted and  $X_0 = 0.70$ ,  $Z = 0.020$  were fixed.

## APPENDIX B: ASTEROSEISMIC MODELLING WITH MONTE-CARLO-BASED BAYESIAN ANALYSIS

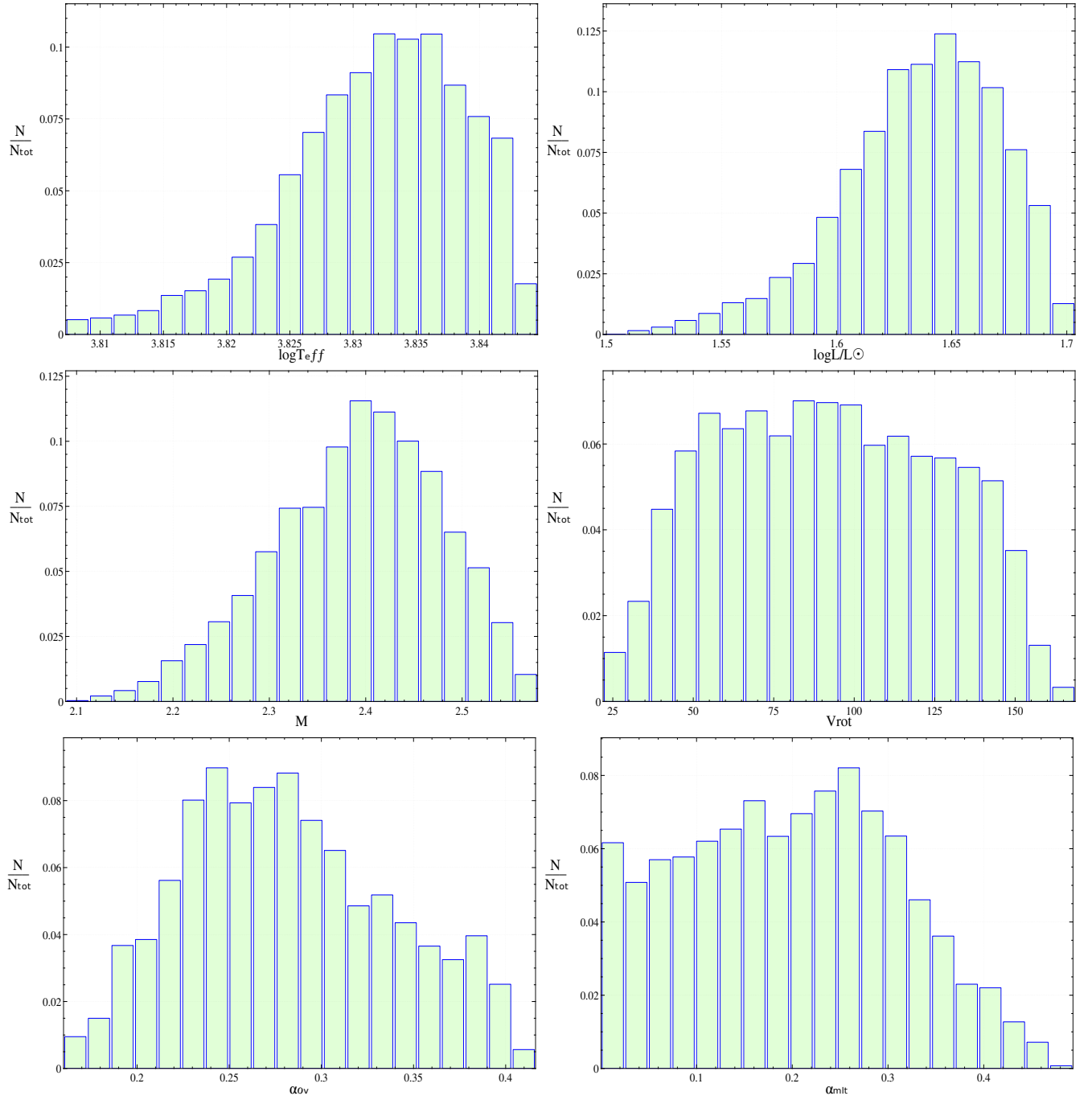
The results of our seismic modelling of V2367 Cyg with the MC-based Bayesian analysis are presented as histograms. In Fig. B1, we show histograms for the parameters ( $\log T_{\text{eff}}$ ,  $\log L/L_{\odot}$ ,  $M$ ,  $V_{\text{rot}}$ ,  $\alpha_{\text{ov}}$  and  $\alpha_{\text{MLT}}$ ) of the HSB seismic models for the  $p_2 \& p_3$  hypothesis and  $Z = 0.020$ . Fig. B2 shows the same but for the seismic models with the metallicity  $Z = 0.030$ . The histograms for parameters of the OC seismic models are presented in Fig. B3 for  $Z = 0.020$  and in Fig. B4 for  $Z = 0.030$ . In case of the  $p_1 \& p_2$  hypothesis, only models with the metallicity  $Z = 0.030$  had the real and imaginary part of the parameter  $f$  consistent within the  $1-\sigma$  error with the empirical counterparts. Histograms for these models are shown in Fig. B5 and Fig. B6 for the parameters of the HSB and OC models, respectively.

This paper has been typeset from a  $\text{\TeX}/\text{\LaTeX}$  file prepared by the author.

**Figure B2.** The same as in Fig. B1 but for  $Z = 0.030$ .



**Figure B3.** The normalized histograms for the parameters of the OC seismic models of V2367 Cyg, calculated assuming that the observed frequencies  $\nu_1$  and  $\nu_2$  are the first and second radial overtone, respectively (the  $p_2 \& p_3$  hypothesis). The OPAL opacities were adopted and  $X_0 = 0.70$ ,  $Z = 0.020$  were fixed.

**Figure B4.** The same as in Fig. B3 but for  $Z = 0.030$ .

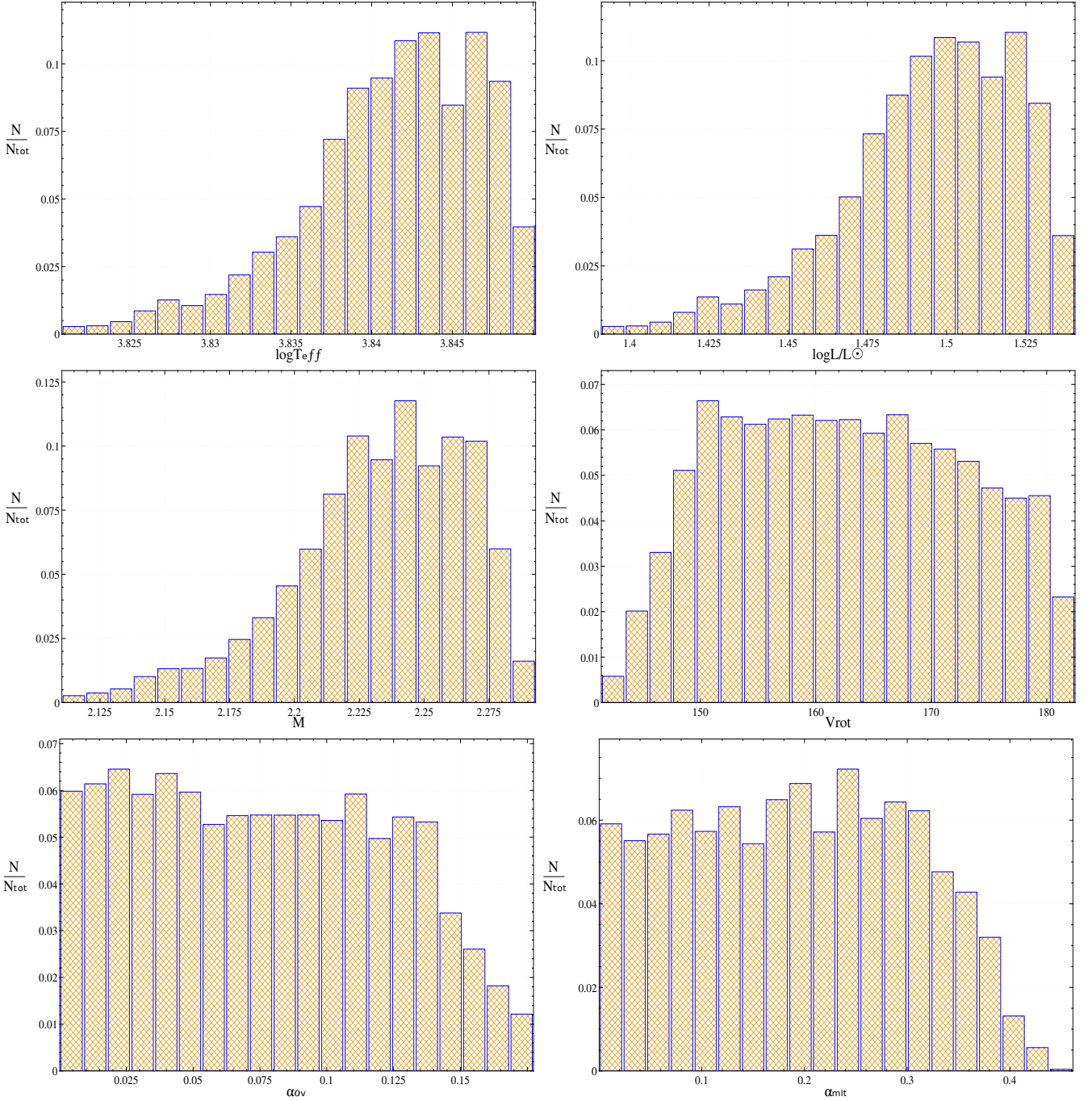


**Figure B5.** The normalized histograms for the parameters of the HSB seismic models of V2367 Cyg, calculated assuming that the observed frequencies  $\nu_1$  and  $\nu_2$  are the fundamental and first overtone radial mode, respectively (the  $p_1 \& p_2$  hypothesis). The OPAL opacities were adopted and  $X_0 = 0.70$ ,  $Z = 0.030$  were fixed.

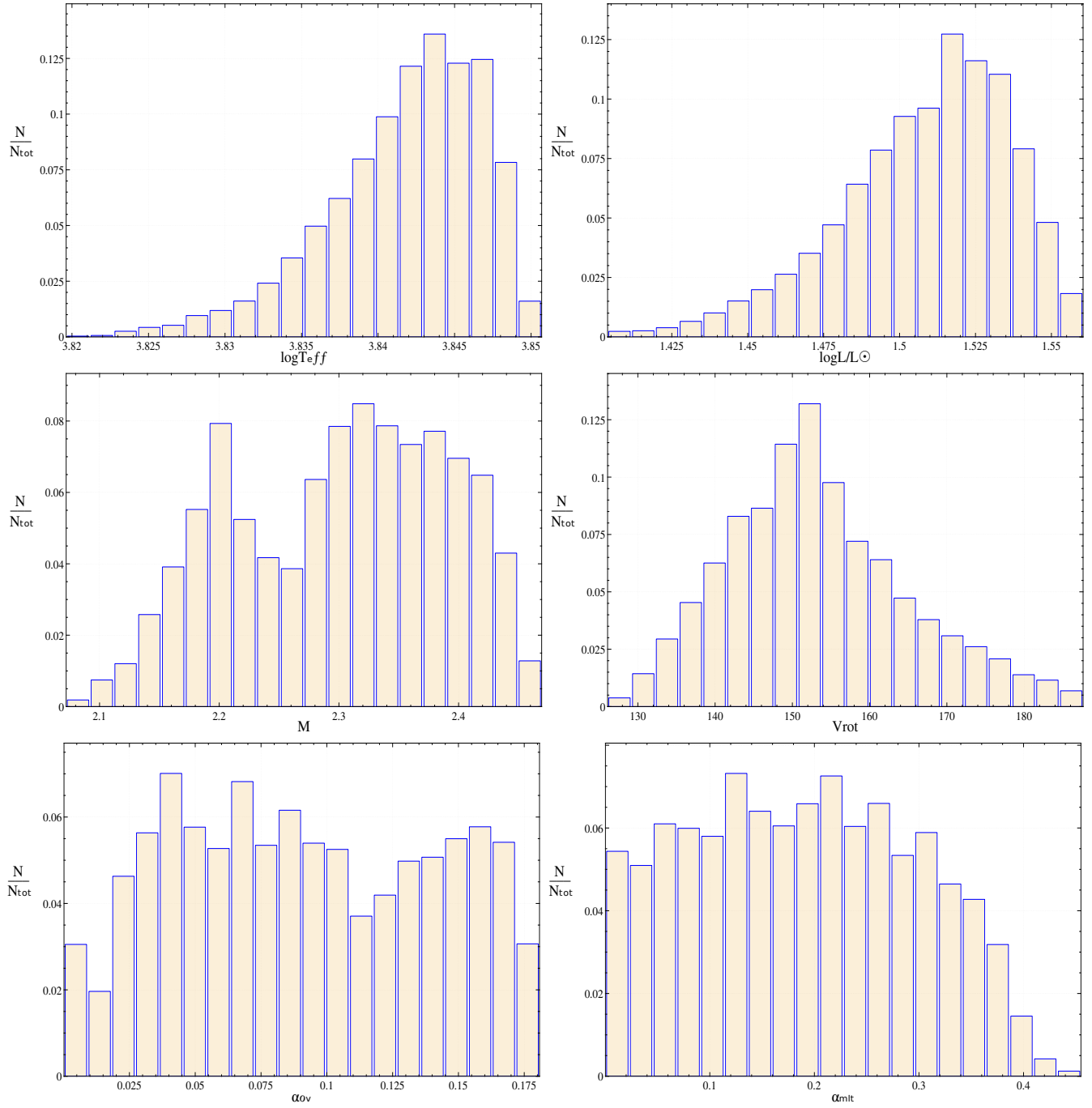


**Figure B6.** The same as in Fig. B5 but for parameters of the OC seismic models.